Preface

In the 20th century, coal played an important role in the development of economics and industry not only in Japan but throughout the world. As raw materials for industrial production such as fuel for the generation of electricity, cokes, tars, gases from coke oven, synthesis gas from coal gasification and liquid fuels from liquefaction, coal has been used extensively in various industries for electric power, iron, tar and gas production, the production of synthetic chemicals and fuel, etc. Although the necessity for coal will change with changing prices of other energy sources such as petroleum and natural gas, the importance of coal as energy and carbon sources will not change in the future.

Coal is more abundant than petroleum and natural gas. Further, coal is not localized but can be used by many more countries than petroleum. Therefore, if we can establish coal utilization technology, coal will bring about a great contribution to human life and society. On the other hand, shortage of petroleum and natural gas are anticipated in the second half of the 21st century. To compensate, the use of coal is expected to gradually increase during the 21st century. In the future, the development of the coal utilization technology will become more and more important to insure the supply of liquid fuels for transportation and carbon sources for the manufacture of chemicals and plastic materials.

In order to develop such technologies, the elucidation of the structure of coal will be a fundamental key study. Further, more efficient coal utilization technology must be established to meet environmental legislation. One of the key technologies for this purpose is catalysis. Given the situation, there is urgent need for a text book which covers both scientific and practical sides of coal utilization with and without catalysts. This volume aims to provide an English description of the basic and practical aspects of the science and technology of coal utilization with and without catalysts. The actual structure of coal, the chemistry included in the reactivity of coal, the methods to elucidate the structure of coal and reaction mechanisms of coal conversion, the most important catalyst for converting coal to liquid and gas, the role of the catalysts in coal conversion, the problems in the process engineering, and how to meet environmental regulations are discussed in detail.

The recent progress in studies on the structure and reactivity of coal made over the last century is summarized and reviewed with emphasis on both fundamental and applied aspects of the science and technology for coal processing in the presence and absence of catalysts. The book consists of six chapters: The first chapter describes the classification and characterization methods of coal. The second chapter describes the chemical and macromolecular structure of coals. The third chapter describes the catalytic and noncatalytic pyrolysis of coal, coal tar, and coal tar pitch. The fourth chapter shows the catalytic and noncatalytic liquefaction of coal. While the fifth chapter introduces the catalytic and noncat-

alytic gasification of coal. The final chapter details the microbial depolymerization of coal which involves catalysis using live organisms.

We would like to express our gratitude to Ms. Cecilia M. Hamagami, and Mr. Ippei Ohta of Kodansha Scientific Ltd. and Dr. Danhong Wang, a postdoctoral fellow at Tokyo Univerisity of Agriculture and Technology, for their invaluable assistance in the preparation of the English manuscript.

April 2004

Toshiaki Kabe
Atsushi Ishihara
Eika Weihua Qian
I Putu Sutrisna
Yaeko Kabe

Studies in Surface Science and Catalysis, volume 149
M. Occelli (Editor)
Published by Elsevier B.V.

New Catalysts May Provide Insights into Role of Nonframework Alumina in Catalytic Cracking Catalysis

Richard W. Fowler[a] and Ruizhong Hu[b]

[a]ExxonMobil Process Research Laboratory, Baton Rouge, Louisiana

[b]Grace Davison, Columbia, Maryland

Catalysts utilized in Fluid Catalytic Cracking (FCC) are typically comprised of zeolite Y in some form of silica-alumina matrix. During the 1980's, much attention was focused on the role of active sites in the zeolite crystal lattice. Reaction pathways were explained in context of the zeolite cell constant or unit cell size. In recent years, more attention has been given to the role of extra-lattice or nonframework aluminum atoms. Several authors have proposed reaction pathways in which nonframework alumina provides an initiation site for olefin formation, thereby enhancing overall reaction rates. Such theories, coupled with unit cell size theory promulgated in the 1980's, provided impetus for development of a new family of FCC catalysts which have recently been introduced to the FCC community. These catalysts provide, among other features, a high intrinsic activity and may offer additional insights into the respective roles of zeolite framework and nonframework alumina in FCC catalysis.

1. INTRODUCTION

Fluid catalytic cracking or FCC is one of the major refining catalyst processes. Its principal products include gasoline, propylene, butenes, isobutane and mid-distillate. A high-boiling bottoms stream is also counted as

an FCC product, although it is generally desired to minimize the yield of this stream. Propylene is a significant feedstock in production of commercial polypropylene plastics.

While various fixed bed catalytic cracking processes were employed as early as 1915 [1,2], the advent of Fluid Catalytic Cracking with the construction of the first "powdered catalyst" unit in Baton Rouge in 1942 revolutionized the refining industry. Early catalysts were acid-treated clays but these were quickly replaced by synthetic silica-alumina catalysts. Then, in 1964, catalyst performance was dramatically enhanced by inclusion of zeolites [3]. These zeolitic FCC catalysts demonstrated both higher activity and improved selectivities. Since that time, volumes have been published about the process, the catalysts, and their postulated chemistries and reaction pathways.

2. UNIT CELL SIZE THEORY AND FRAMEWORK ALUMINA EFFECTS

Notable among these was an article published about 20 years ago by Pine and his co-workers at Exxon Research and Development Laboratories. Their paper dealt with the role of zeolites in determining catalyst activity and selectivity. They convincingly argued that the effect of "various zeolite pretreatments such as cation-exchange, acid extraction, and hydrothermal conditioning can be explained in terms of their effect on the zeolite cell constant" [4] or unit cell size. Since unit cell size is proportional to the number of aluminum atoms per unit cell [5], this broadly accepted argument focuses, then, on the role of aluminum atoms remaining in the crystal lattice. These aluminum atoms remaining in the crystal lattice are referred to as framework aluminum atoms or FA.

3. ROLE OF NONFRAMEWORK ALUMINA IN FCC CATALYSIS

The role of aluminum atoms expulsed from the crystal lattice was largely overlooked in Pine's publication; however, these extra-lattice or nonframework aluminum atoms have received ample press in the intervening years and their role in overall FCC catalyst performance continues to be studied and debated

today. For example, some publications subsequent to that of Pine argued that nonframework alumina was undesirable, contributing to high yields of less desirable products such as coke and gas [6]. The poorer coke selectivity was attributed to alumina debris in the pores of the zeolite. A more recent review of the role of nonframework alumina by Magee [7] found the following performance characteristics attributed to nonframework alumina or NFA:

- NFA reduces gasoline yield;
- NFA increases coke yield;
- NFA may convert HCO to lighter products;
- NFA exhibits strong Lewis acidity;
- NFA catalyzes secondary reactions;
- NFA produces less olefinic and branched C4 and lighter streams; and,
- NFA does not catalyze hydrogen transfer reactions.

Other authors have postulated that nonframework alumina can affect acid site strength by synergistic interactions with framework alumina sites. Such interactions are theorized to result in super acid sites [Ibid].

In parallel with the many studies and articles attempting to elucidate the roles of framework and nonframework alumina, other researchers pursued understanding of chemical pathways. Classic experiments with layered beds of zeolite and matrix [7,8] clearly demonstrated that pre-cracking or initiation occurs on the matrix alumina and products then undergo further reaction on the surface of the zeolite. Studies began appearing which suggested that different mechanisms might be occurring simultaneously on different parts of the catalyst/zeolite. For example, in a departure from conventional thinking at the time, McVicker et al. published studies in the early 1980's suggesting that zeolitic catalysts may promote cracking via both radical-like and carbonium ion routes [9].

More recent work reported by Occelli et al. found that a catalyst containing de-aluminated zeolite but showing no detectable framework alumina by MAS NMR retained substantial cracking activity. The authors suggested that this observation lends "support to the possibility that gas oil cracking is initiated by hydride abstraction on strong [Lewis acid; i.e., nonframework alumina] sites with formation and cracking of carbenium ions" [10].

Beyerlein et al. published a paper in which they described several types of nonframework alumina and suggested the "critical nonframework Al species are (1) highly dispersed, and (2) quite possibly exist as cationic species in the small cages of dealuminated H-Y" zeolite [11]. These researchers also attributed the high catalytic activity of zeolite catalysts to a synergistic interaction between framework (Bronsted) sites and the highly dispersed nonframework (Lewis) sites.

4. NFA/FA SYNERGY AND BIFUNCTIONAL CATALYSIS

Schuette and Schweizer further promulgated this view arguing that this synergy in FCC catalysts between Lewis and Bronsted sites or nonframework and framework alumina was nothing more or less than a manifestation of the bifunctional nature of FCC catalysts and the zeolites incorporated therein. As they described it, "Radical catalytic chemistry...initiates the formation of olefins by dehydrogenation and/or dealkylation of saturates to form olefins. The radical chemistry is catalyzed by Lewis acid electron accepting sites provided by various forms of amorphous alumina. The olefins...diffuse to Bronsted acid

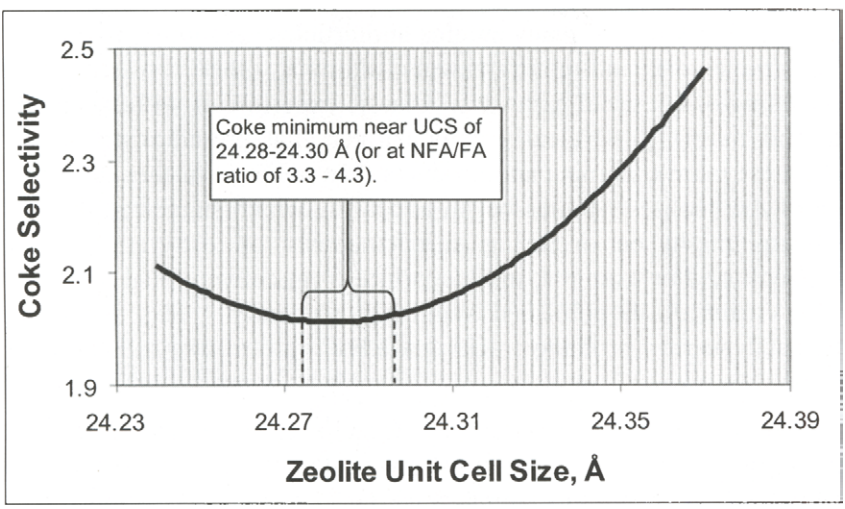

Fig. 1. Typical coke selectivity for FCC catalysts as a function of zeolite unit cell size.

sites where they pick up protons to become carbenium ions [which then] readily convert to low molecular weight carbenium ions." They go on to suggest that "zeolite nonframework alumina is a particularly effective radical catalyst." [12]

One manifestation of the impact of unit cell size is the coke selectivity. Plots such as the one shown in Figure 1 are common in literature dealing with FCC catalysis. While the minimum in coke selectivity has been debated at times, it is certainly accepted that coke selectivity improves as unit cell size shrinks from values of 24.40 Å to values in the range of 24.28-24.30 Å. The curve shown in Figure 1 reflects a minimum in the coke selectivity vs. unit cell size data. Since the number of framework aluminum atoms per unit cell correlates with zeolite unit cell size, Figure 1 could be just as easily represented by plotting coke selectivity vs. the number of aluminum atoms per unit cell. Furthermore, assuming that aluminum atoms rejected from the crystal lattice

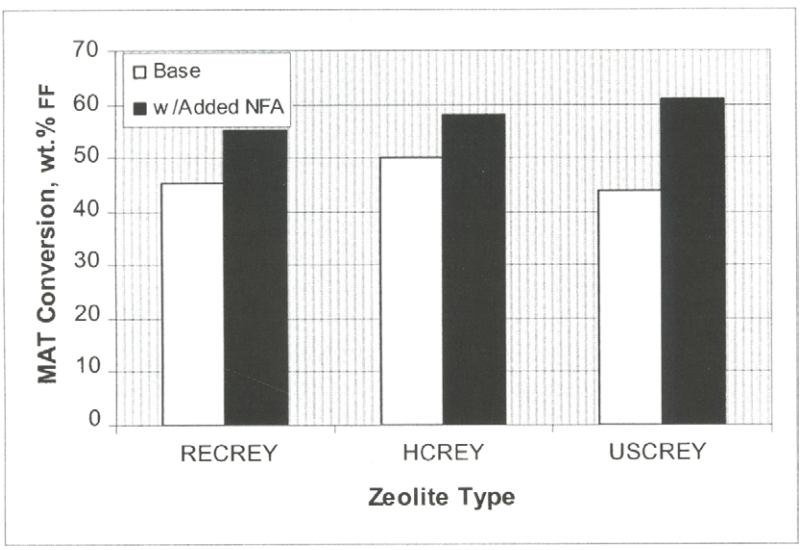

Fig. 2. Laboratory catalysts show significant activity boost with artificial nonframework alumina.

remain in/on the zeolite, the horizontal axis could also be replaced by a ratio of nonframework/framework aluminum atoms or NFA/FA. Thus, it is possible to interpret the minimum in coke selectivity as occurring--not at an optimum unit cell size--but rather, at an optimum ratio of nonframework and framework alumina.

For example, if a fresh zeolite is manufactured with a fresh unit cell size of 24.66 Å, it would have 54 aluminum atoms in the crystal lattice or framework. As the catalyst deactivates over time, the unit cell shrinks to 24.29 Å. Calculations would suggest the zeolite framework now contains only 11.4 aluminum atoms per unit cell. The remaining 42.6 aluminum atoms per unit cell are in extra-lattice or nonframework sites and the ratio of nonframework to framework aluminum atoms is 3.7.

Following Schuette and Schweizer, assuming that framework aluminum provides Bronsted acidity while nonframework alumina contributes Lewis acidity, then one might imagine a zeolite in which artificial nonframework alumina is added. This would increase the number of total acid sites and, in particular, the number of initiation sites, providing higher levels of activity. By increasing the number of framework sites in order to keep the ratio of nonframework and framework aluminum atoms constant, a zeolite is obtained which offers excellent coke selectivity but at higher unit cell size. Such a catalyst would also have higher activity.

To test/demonstrate the role of nonframework alumina as an initiator in FCC catalysis, Schuette and Schweizer prepared several catalysts in which alumina was added to the zeolite via vapor deposition from aluminum acetylacetonate. This "artificial nonframework alumina" resulted in a 20-30% increase in activity of the finished catalyst as illustrated in Figure 2 and was demonstrated to augment the Lewis acidity of the finished catalyst [13]. Coke selectivity was also significantly enhanced.

5. NFA/FA THEORY REDUCED TO COMMERCIAL PRACTICE

Pursuant to the successful demonstration of laboratory scale preparations of catalysts containing zeolites with added nonframework alumina, researchers at ExxonMobil Process Research Laboratories and Davison Catalysts entered

into a joint development program aimed at commercializing this technology. The result of this effort is a new family of commercial FCC catalysts being marketed by Grace under the name AdVanta [14]. These new catalysts have demonstrated properties similar to those of the earlier laboratory-prepared samples. For example, in the initial commercial trial, an ExxonMobil FCCU was operating with an FCC catalyst that was equilibrating at a micro-activity of about 67% conversion as measured by MAT (micro-activity test) and total surface area as reported by Davison was approximately 180 m^2/g. As change-out of the competitor's catalyst to the new AdVanta catalyst progressed at constant catalyst addition rates, surface area fell from 180 m^2/g to 120 m^2/g as indicated by the open squares in Figure 3. However, in spite of this 33% reduction in surface area, equilibrium catalyst activity did not change, as shown by the solid circles in Figure 3.

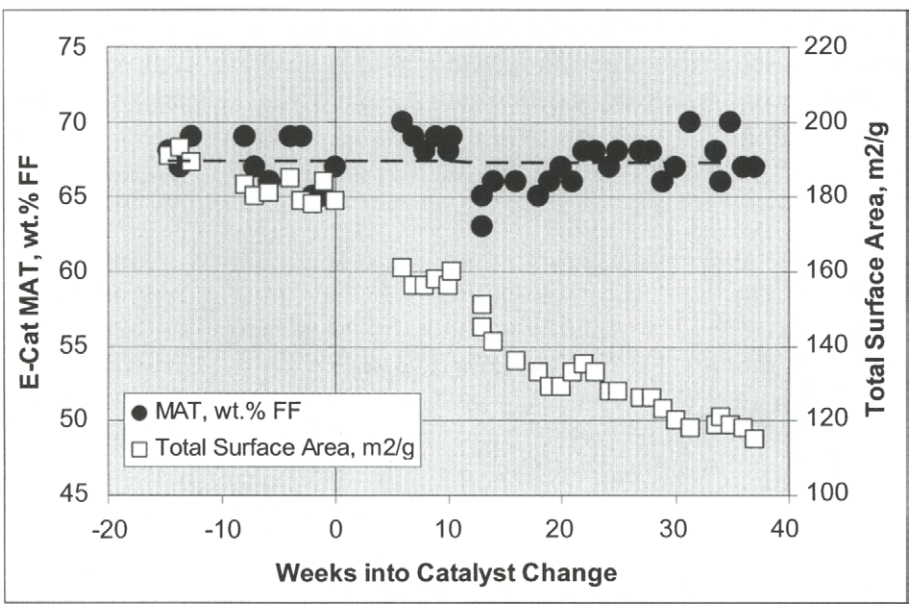

Fig. 3. Initial commercial trial achieves constant activity at 33% lower surface area.

This same performance--that is, high activity per unit of surface area--has been demonstrated in subsequent commercial applications as illustrated in Figure 4. In this figure, equilibrium MAT activity divided by total surface area as reported by Davison is plotted against the ratio of rare earth oxides divided by zeolite surface area or ZSA. This latter ratio correlates with unit cell size but data are presented in this way to demonstrate that the effects observed in AdVanta performance are not simply a function of unit cell size or rare earth loadings.

6. HIGH ACTIVITY ACCOMPANIED BY EXCELLENT COKE SELECTIVITY

In commercial FCC operations, the catalysts become contaminated with metals that are present in the various crude oils. The most common metals include nickel and vanadium. While vanadium can be mobile and may penetrate throughout the catalyst, nickel is found primarily on the catalyst surface. Once on the surface, the nickel may act as a dehydrogenation catalyst. Vanadium also catalyzes dehydrogenation, but is generally considered to have only 20-25% of the dehydrogenation activity of nickel. This metals-catalyzed

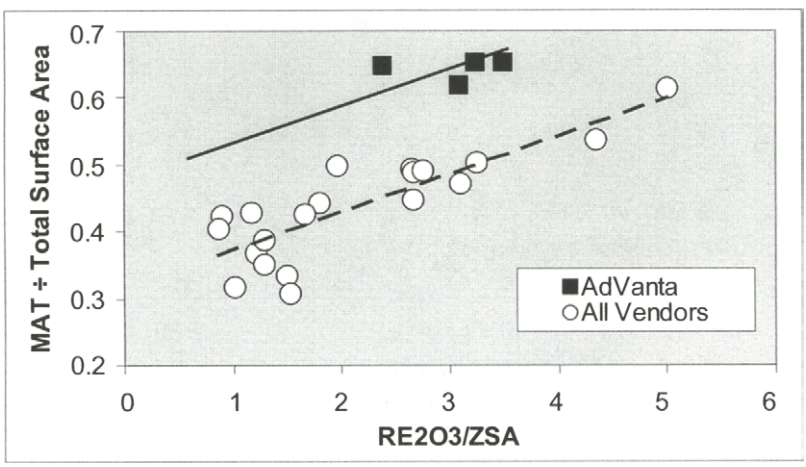

Fig. 4. AdVanta catalysts show high activity per unit of surface area.

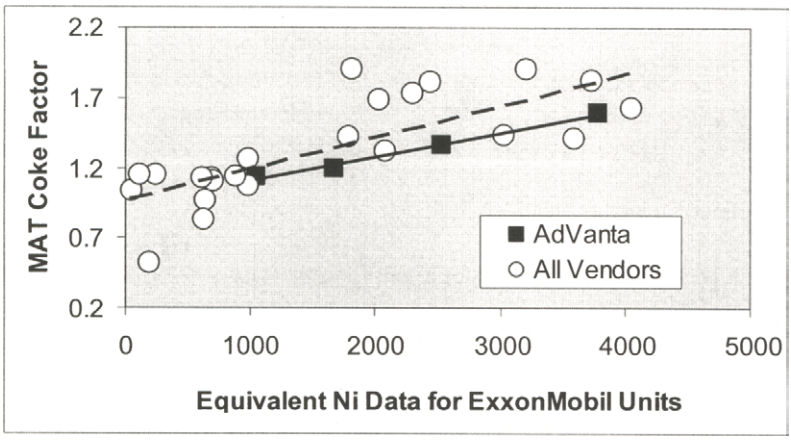

Fig. 5. Vendor e-cat data confirm AdVanta coke selectivity.

dehydrogenation contributes to overall coke make and also results in increased yields of molecular hydrogen.

Without exception, the units using the new AdVanta catalyst observed coke selectivity benefits. These plant observations are consistent with the Davison MAT Coke Factor data presented in Figure 5. At constant metals loadings, the AdVanta catalysts clearly show some of the lowest coke factors from across the ExxonMobil circuit. It is also believed that the lower surface areas obtained with AdVanta catalyst technology may accrue additional coke selectivity advantages as the result of reduced carry-under of adsorbed hydrocarbons to the FCC regenerator.

7. REDUCED HYDROGEN YIELDS A HALLMARK OF ADVANTA CATALYSTS

In addition to coke selectivity improvements observed in the initial commercial trials of AdVanta catalyst, a substantial reduction in hydrogen yield was reported. While yields of hydrogen from commercial operations are not

Table 1

Commercial hydrogen:methane ratios suggest AdVanta mitigates dehydrogenation reactions.

Catalyst:	AdVanta #2	Catalyst X
Commercial Yield Data, H2/CH4	0.26	0.40
Vendor Equilibrium Catalyst Data		
Ni, ppm	564	531
V, ppm	1372	1422
Ni + V/4, ppm	907	887
SA, m2/g	146	215

precise, the magnitude of the change leaves no question that hydrogen production was lower. For example, in Table 1, the ratio of commercially reported hydrogen and methane ratios is shown for two catalysts run simultaneously in identical, side-by-side units processing essentially the same feeds. Equilibrium catalyst inspections are shown in the same table, along with the calculated equivalent nickel (i.e., Ni + V/4; assumes vanadium has 25% of the dehydrogenation activity of Ni). Clearly, the AdVanta shows significant reductions in hydrogen make commensurate with its lower surface area. Other applications of AdVanta showed similar trends in dehydrogenation activity, presumably resulting from a reduction in dehydrogenation activity of contaminant metals as a result of the lower surface area/reduced dispersion of contaminant metals. These low hydrogen yields have become one of the evidences that a catalyst with artificial nonframework alumina is providing desired performance features.

While the overall metals levels are not high for the catalysts in Table 1, AdVanta catalysts have been used in units running at relatively high metals levels on equilibrium catalyst. As illustrated in Figure 6, AdVanta has maintained its activity advantage across a broad range of contaminant metal levels.

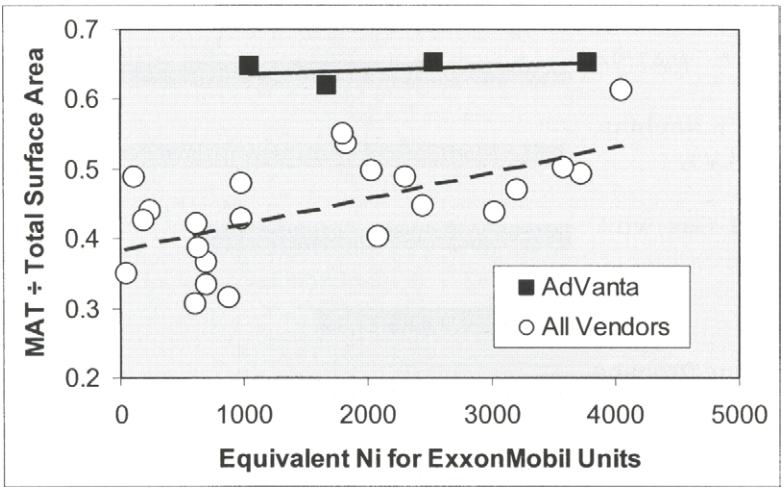

Fig. 6. Activity retention as function of contaminant metals comparable to other commercial catalysts.

8. ADVANTA CATALYSTS HAVE POSITIVE IMPACT ON LIQUID YIELDS

In addition to activity and coke/gas selectivity advantages, commercial trials of AdVanta catalysts containing artificial nonframework alumina have confirmed increased naphtha yields. Directionally, these increases in naphtha are consistent with higher rare earth on zeolite as indicated by the higher unit cell size. However, unlike conventional catalysts that would forfeit light olefins as unit cell size is increased, AdVanta is able to maintain olefin/saturate ratios of light hydrocarbon streams at constant levels. In the commercial example shown in Figure 7, unit cell size on AdVanta was actually 0.04 Å higher than the base catalyst to which it was compared--a large difference for unit cell sizes--and yet C_3 and C_4 unsats/saturates ratios are the same.

As mentioned at the beginning of this paper, refiners generally would prefer to eliminate--or at least minimize--the yield of high boiling bottoms streams. Generally, to enhance bottoms cracking performance of FCC catalysts,

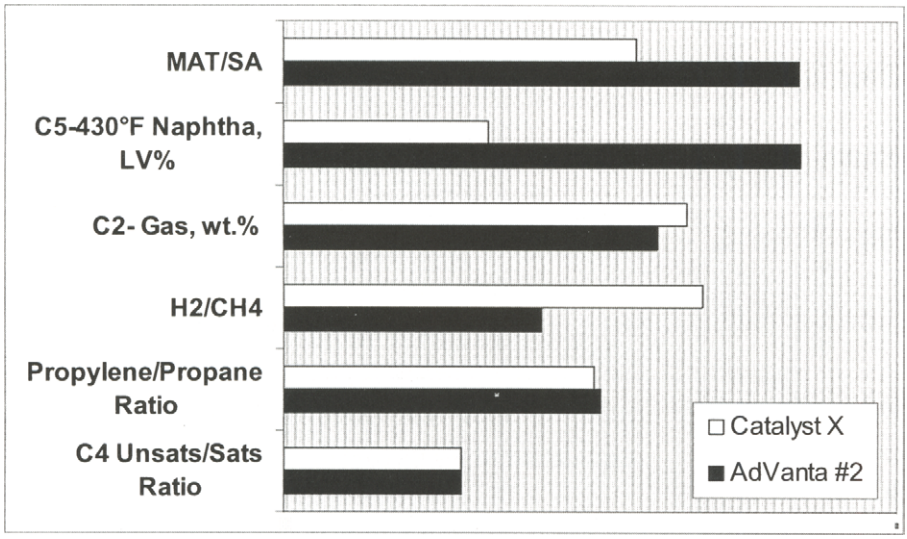

Fig. 7. Commercial results show high naphtha yields and competitive LPG olefinicities.

commercial suppliers incorporate high surface area aluminas or silica-aluminas into the non-zeolite or matrix portion of the catalyst. Thus, bottoms cracking is generally considered to be more a function of the matrix or a function of the relative amounts of matrix and zeolite. Nevertheless, although AdVanta is primarily driven by a modified zeolite, this catalyst has demonstrated competitive bottoms cracking in the various commercial trials. For example, in a third commercial application, plots of bottoms yield at constant coke show comparable or lower yields of bottoms for the AdVanta catalyst. This difference persists even after normalizing for potential feed quality differences as indicated by Figure 8. Bottoms yields are strongly correlated with the amount of multi-ring aromatic cores present in the feed; AdVanta's performance does not appear to be due to a change in feed quality.

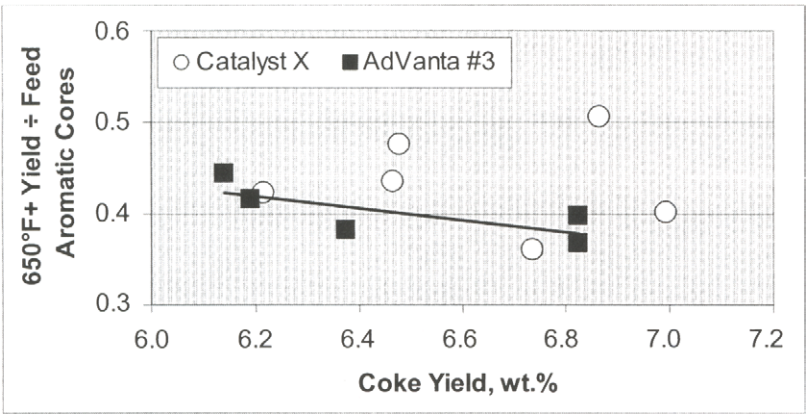

Fig. 8. Bottoms yields normalized to aromatic cores in feed confirm competitive bottoms vs. coke relationship.

9. ONGOING DEVELOPMENT EFFORT IDENTIFIES MODIFIED TREATMENT FOR FURTHER ENHANCEMENTS

Over the last couple of years, AdVanta catalysts have been applied at numerous ExxonMobil sites. As commercial experience with the AdVanta catalyst family has accumulated, an ongoing research program has continued to search for enhancements to this technology. Table 2 reports laboratory results on modified AdVanta catalysts; column 1 shows data on an early commercial preparation while column 2 presents average results on two separate laboratory preparations at constant zeolite loading. Results are presented at constant conversion and activity.

Each of the catalysts shown in Table 2 was deactivated via Davison's CPS steaming [15] at 2000 ppm vanadium and 1000 ppm nickel. As can be seen, the modified catalysts showed improved naphtha yields, lower bottoms yield and improved coke selectivity. Olefinicities were constant for the catalysts, although the modified catalysts did make slightly less LPG. At this writing, efforts are underway to make commercial catalysts using the modified treatment that resulted in the selectivity improvements shown in Table 2.

Table 2

Modified treatment offers further performance improvements

	Column 1	Column 2
Catalyst Description:	Base Commercial Preparation	Average of Lab Preparations w/ Modified Treatment
Surface Area, m2/g	111	108
Unit Cell Size, Å	24.25	24.26
Ni / V , ppm	1076 / 2166	1142 / 2194
ACE Yields, wt.%		
H2	0.19	0.15
Dry Gas	1.34	1.37
LPG	13.55	12.98
Naphtha	46.94	47.79
LCCO	18.93	19.38
Bottoms	15.39	14.95
Coke	2.76	2.49
Propylene/Total C3's	0.87	0.88
Butene/Total C4's	0.63	0.63

10. CONCLUSION

While unit cell size theory appears to adequately capture the effects of varying levels of framework alumina in zeolites used in conventional catalytic cracking catalysts, the role of nonframework alumina continues to attract much attention. Coupling of bifunctional catalysis concepts with unit cell size theory offers possible insights into the relative roles of framework and nonframework alumina in catalytic cracking. Armed with a laboratory demonstration of the concept, researchers at ExxonMobil and Davison Catalysts have had some success in commercializing a new family of catalysts.

Commercial FCC yields have confirmed what may be the highest activity-to-surface area relationship of any commercial FCC catalyst technology. Its low surface areas limit dispersion of contaminant metals thereby mitigating rates of dehydrogenation. At the same time, improved coke

and gas selectivity offer the potential to ease common constraints on many FCC units. At a time when attractive products include both light olefins and gasoline, the new AdVanta technology offers the possibility to shift naphtha selectivity and light olefinicity away from the traditional unit cell size models.

The AdVanta family of catalysts has been used successfully at numerous ExxonMobil locations across the globe. The technology is now being made available to other refiners through the sales organization of Davison Catalysts.

REFERENCES

[1] K. P. Callahan and K. K. Ushiba, (Project Leaders), Advances in Fluid Catalytic Cracking, Part 1, Catalytica, Mountain View, California (1987) pp. 7-8.

[2] A. D. Reichle, "Fifty Years of Cat Cracking at Exxon," Akzo Catalyst Symposium, Scheveningen, The Netherlands (1988).

[3] Davison Chemical 1992 Calendar commemorating the 50th anniversary of the first Fluid Catalytic Cracking Unit.

[4] L. A. Pine, P. J. Maher, and W. A. Wachter, Journal of Catalysis, 85 (1984) 466.

[5] D. W. Breck and E. M. Flanigen, "Molecular Sieves" (R.M. Barrer, Ed.), Society of the Chemical Industry, London (1968) p. 47.

[6] J. A. Rabo et al, NPRA paper no. AM-86-30 (1986).

[7] J. S. Magee, "Fluid Catalytic Cracking: A Short Course" (2000).

[8] A. S. Krishna, "FCC Catalyst Technology Tutorial Session", AIChE Annual Meeting, Los Angeles, California (1991).

[9] G. B. McVicker, G. M. Kramer, and J. J. Ziemiak, Journal of Catalysis, 83 (1983) 286.

[10] M. L. Occelli, M. Kalwei, A. Wölker, H. Eckert, A. Auroux, and S. A. C. Gould, Journal of Catalysis, 196 (2000) 134.

[11] R. A. Beyerlein, C. Choi-Feng, J. B. Hall, B. J. Huggins and G. J. Ray, Topics in Catalysis, 4 (1997) 27.

[12] W. L. Schuette and A. E. Schweizer, Studies in Surface Science and Catalysis, Fluid Catalytic Cracking V: Materials and Technological Innovations, No. 134 (2001) 263.

[13] W. L. Schuette and A. E. Schweizer, United States Patent No. 6,482,313 B1 (2002).

[14] R. W. Fowler and L. McDowell, NPRA Annual Meeting, San Antonio, Texas, paper no. AM-03-27 (2003).

[15] Grace Davison, "Guide to Fluid Catalytic Cracking, Part Three," (1999) pp. 214-226.

Studies in Surface Science and Catalysis, volume 149
M. Occelli (Editor)

Mechanism of Fluid Cracking Catalysts Deactivation by Fe

G. Yaluris[a], W.-C. Cheng[b], M. Peters[b], L. T. McDowell[c], and L. Hunt[b]

Davison Catalysts; [a]5603 Chemical Road, Baltimore, MD 21226; [b]7500 Grace Drive, Columbia, MD 21044; [c]3838 N. Sam Houston Pkwy., Houston, TX 77032.

It has been recently recognized that Fe can be an important factor causing FCC catalyst deactivation, most often in the form of lost activity and bottoms cracking. Using a combination of different techniques such as EPMA, SEM/EDS, Optical Microscopy, XPS and Sink/Float separation to study in-unit deactivated FCC catalysts, we have been able to determine that Fe deposits only on the exterior surface of catalyst particles forming Fe-rich rings. In these areas, Fe, Ca, and Na oxides mix with silica from the underlying catalyst giving the catalyst a characteristic texture with surface nodules and a "glassy" appearance. After Fe deposits, it is generally immobile. However, interparticle Fe transport is possible via a mechanism involving the movement of fine Fe-rich particulates from one catalyst particle to another. In combination with thermodynamic analysis, we have determined that low melting temperature phases containing Fe, Na, and Ca oxides as well as silica form on the surface of catalysts made with silica-based binding systems. These phases cause pore closing and accelerated sintering. The destruction of the surface pore structure in the areas covered by the Fe rings leaves the particle interior largely unaffected. However, the blockage of the surface pores that carry the heavy hydrocarbon molecules inside the catalyst particles for cracking, causes activity and bottoms cracking loss. Alumina does not mix with Fe to form such low melting temperature phases, and when it does the melting temperature remains very high. FCC catalysts made with alumina binding systems have most of the pores carrying the heavy hydrocarbon feed molecules in the alumina structure. Thus, although in these catalysts Fe-rich nodules can form, the surface pore structure is resistant to deactivation by Fe, and the catalysts maintain activity and bottoms cracking even at high levels of Fe contamination.

1. INTRODUCTION

The detrimental effects of contaminant metals, like Ni, V and even Na, on the physicochemical and catalytic properties of Fluid Catalytic Cracking (FCC) catalysts have been well known and studied extensively. Over the years metals tolerant catalysts and other technologies have been developed to help refiners operate at high levels of metals contamination. Fe has also been known to adversely affect the performance of FCC catalysts, but until recently Fe related problems in FCC units were largely unreported. Although the effects of Fe on catalyst conversion and yields during microactivity testing have been studied [1], little work has been done to understand the in-unit effects of Fe on FCC catalysts. Today because of increased processing of high Fe feeds, and the need by many units to process heavy local feeds, the effects of Fe on the unit operation cannot be ignored.

Increasing Fe on the FCC equilibrium catalyst (ECAT) can have serious adverse effects, including loss of activity and bottoms cracking, as well as increased SO_x emissions, and coke on regenerated catalyst (CRC) in partial burn units. ECAT Apparent Bulk Density (ABD) has also been reported to decrease [2]. However, a careful examination of properties of equilibrium catalysts from various FCC units showed that other than ABD very few of the ECAT properties change. For example, catalyst surface area, and microactivity change little as Fe on the catalyst increases. Most often changes in these catalyst properties are due to other contaminant metals, like V and Na, well known for decreasing both catalyst surface area and activity. While, catalyst pore volume in many cases does not change, in other cases a small decrease in pore volume, usually less than 10%, has been observed.

It appears that there are two types of Fe present in an FCC unit. One type consists primarily of particles of inorganic Fe from soil contamination, pipes, storage tanks and other hardware. This type is usually called "tramp" Fe, and to the extent it remains in the unit in the form of large FCC catalyst size particles, it is generally benign in FCCU operation. The other type is organic Fe coming from feed and/or hardware corrosion by naphthenic acids and other corrosive feed components. In addition, dissolved or finely dispersed organic or inorganic Fe may be contained in the feed (e.g. chelating agents used in oil extraction). This feed or colloidal Fe is usually considered more destructive.

In this paper we present the results of our work investigating how Fe deposits on the FCC catalyst and transports from particle to particle. We subsequently discuss the effects Fe has on the FCC catalyst surface and textural properties, the thermodynamics of the phases Fe can form on the catalyst after it is deposited, and the role the underlying catalyst chemical composition plays. Finally, we propose a mechanism on how Fe deactivates FCC catalysts that

explains the available experimental data and provides important insights on how Fe resistant catalysts can be formulated.

2. EXPERIMENTAL

The deposition and distribution of Fe on the FCC catalyst during in-unit deactivation is key to understanding the effects of Fe. Thus, we studied the deposition of Fe on equilibrium catalysts from various FCC units having different levels of contaminant Fe. We obtained qualitative pictures of the distribution of Fe in the catalyst particles by using a Cameca SX50 Electron Probe Microanalyzer (EPMA). Catalyst particles were placed in a resin, ground until the internal matrix was exposed, polished to a 0.25 μm smooth surface, and then scanned by EPMA to obtain color coded pictures of the distribution of specific elements across the particle cross section. This technique can identify the distribution of an element across a section of a particle with a resolution of 1 μm. Areas with high concentration of the element probed are shown as white or red, while low concentration areas are purple or blue. In these pictures the local concentrations are relative. Thus, because the total concentration of an element from sample to sample changes, the same color does not represent the same absolute concentration in each picture.

We obtained quantitative information on the distribution of Fe on catalyst particles using X-ray Photoelectron Spectroscopy (XPS). The catalyst samples were analyzed by a Siemens D5000 Diffractometer with an 18 kW rotating anode X-ray generator regularly operated at 50 kV and 240 mA. This technique can quantitatively analyze the surface composition of catalysts typically to a depth of 50 Å. When the surface composition of catalysts is compared to the bulk composition, a surface enrichment ratio can be calculated. This surface enrichment ratio is a quantitative measure of the concentration of an element on the catalyst particle exterior surface.

Typically we separate equilibrium catalysts to age fractions using a density-based separation technique known as sink/float separation described elsewhere [3]. The basic assumption behind this technique, is that as the catalyst ages, the skeletal density increases. As long as the ECAT does not contain catalysts of different fresh skeletal densities, i.e., it is not a catalyst blend, we can reliably assume that the heaviest fractions are the most aged, while the lightest are the youngest. Using this technique we were able to separate ECAT samples to as many as 8 density fractions representing different stages in the catalyst aging process.

We studied the surface texture changes of catalyst samples after calcination at 867 K for 2 h to remove residual coke by using both Scanning Electron Microscopy (instrument S4500 Hitachi FESEM), and Optical

Microscopy (optical microscopes by Nikon and Zeiss). Using EDS we also measured the local concentration of various elements on the surface of the particles.

We measured the chemical composition of samples by Inductively Coupled Plasma Emission Spectrometry (ICP). We also measured the surface area of the samples using nitrogen BET. By employing the "t" plot method, we were able to determine the zeolite and matrix contributions to the total surface area.

To study the effects of Fe contamination on FCC catalysts in the laboratory, we utilized our measurements of the chemical composition of the external area of the particles and prepared catalysts that have in the bulk of the particles the same composition that Fe contaminated ECAT particles have on the external surface. We made these model catalysts using standard FCC catalyst preparation techniques, and utilizing either silica (Si-sol) or alumina (Al-sol) - based binding systems. In addition, to the normal components of an FCC catalyst (zeolite, matrix, binder and clay), we added 1 wt% Na from $NaNO_3$, 0.9 wt.% Ca from $Ca(NO_3)_2$, and 0, 5 and 20 wt% Fe from Fe gluconate. All chemicals were obtained as research grade chemicals from VWR or Aldrich. After spray drying the raw materials slurry, the resulting catalysts were calcined at 866 K. We simulated in-unit catalyst deactivation of the model catalysts by using the Cyclic Propylene Steaming (CPS) process described elsewhere [4]. We then studied these catalysts after both types of treatment.

We also conducted laboratory simulations of the Fe deposition on FCC catalysts using our FCC pilot plant, the Davison Circulating Riser (DCR) [5]. In these experiments a hydrocarbon feed was spiked with appropriate organic precursors containing Fe, Ca, Na, Ni and/or V, and the feed was cracked on the catalyst forming coke. The coke was then burned with air in the DCR regenerator depositing the metal contaminants on the catalyst in a similar fashion as in the unit. Additional deactivation by steaming or CPS followed if necessary to further simulate the in-unit aging effects of these metal contaminants.

3. RESULTS

3.1. Deposition of Fe on ECAT

We show a representative example of the distribution of Fe on ECAT in Figure 1. Although the work of others was inconclusive [6], the EPMA data unequivocally show that Fe always deposits on the external surface of ECAT particles, creating rings of high Fe concentration around the particles. We also investigated if Fe can penetrate further inside the FCC particle as Fe levels on the ECAT increase. Analysis of the data like the example shown in Figure 1,

suggests that increasing the Fe content of the ECAT increases the concentration of Fe on the particle surface, but not the depth of Fe penetration inside the particle. It appears that Fe does not penetrate inside the ECAT particles much deeper than 1-5 μm. These results show that Fe deposits on the first site of the particle it encounters and continues to do so for the duration of Fe deposition. The raw materials used, the catalyst manufacturing process, the binding system, or other differences among catalysts made by the same or different manufacturers do not appear to have any influence on how Fe deposits on catalyst particles.

Ca is another contaminant that has the same deposition profile as Fe. It also forms rings 1-5 μm deep on the external particle surface (Figure 1), and it does not penetrate further when the levels of Ca deposited on the ECAT increase. The presence of Ca in high concentration on the external surface of catalyst particles, often at the same high Fe concentration areas of the particle, suggests that Ca may be involved in the mechanism by which Fe poisons the FCC catalyst.

The deposition of V and Na, shown in Figure 2, is distinctly different from that of Fe. Within the accuracy of the technique, and in agreement with the work of others [6], both metals deposit throughout the catalyst particle. Ni has a somewhat different deposition profile. The EPMA data in Figure 2 show that Ni can concentrate on the external surface of ECAT particles. However, Ni distribution depends on the unit, the amount of Ni deposited, the average residence time of the catalyst in the unit and the catalyst technology employed [7]. Ni can eventually penetrate throughout the particle, resulting in a deposition profile similar to that of Na or V.

The appearance of Fe-rich rings on the exterior surface of ECATs could be the result of deposition of particles of tramp Fe. However, as we show in Figure 3, lab-deposition of metal contaminants in the DCR confirms that organic Fe is also deposited on the exterior surface of the catalyst particles, and the deposition profiles of the other contaminant metals matches that observed for ECATs very well.

3.2. Fe Concentration on ECAT Particles Surface

Since Fe deposits on the external surface of the ECAT particle, it is critical to measure the surface concentration of Fe as well as its oxidation state. We have compiled in Table 1 the surface enrichment ratios from measuring the surface and bulk compositions by XPS and ICP respectively of numerous ECAT samples. In general, the surface enrichment ratios show that there seems to be little difference between the surface and bulk concentration for Na and Si oxides. This result is not unexpected considering the well known mobility of both of

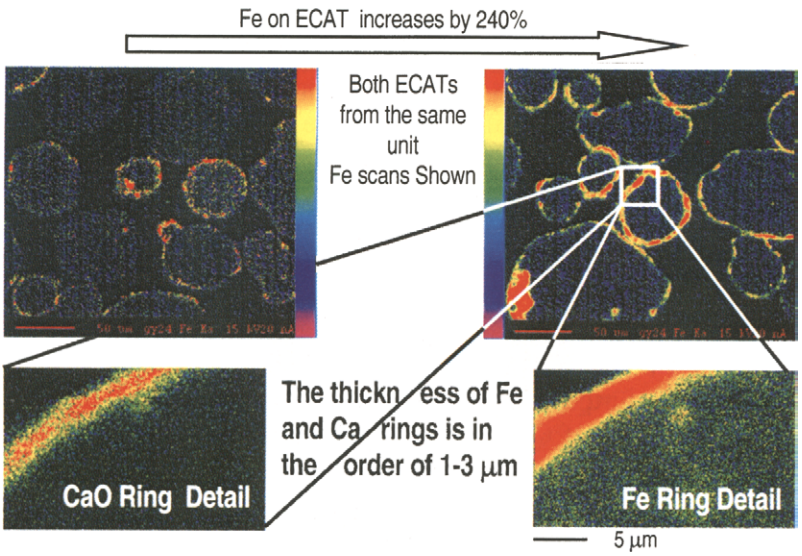

Figure 1. EPMA pictures showing the distribution of Fe and Ca on ECAT particles as Fe levels on the ECAT increase.

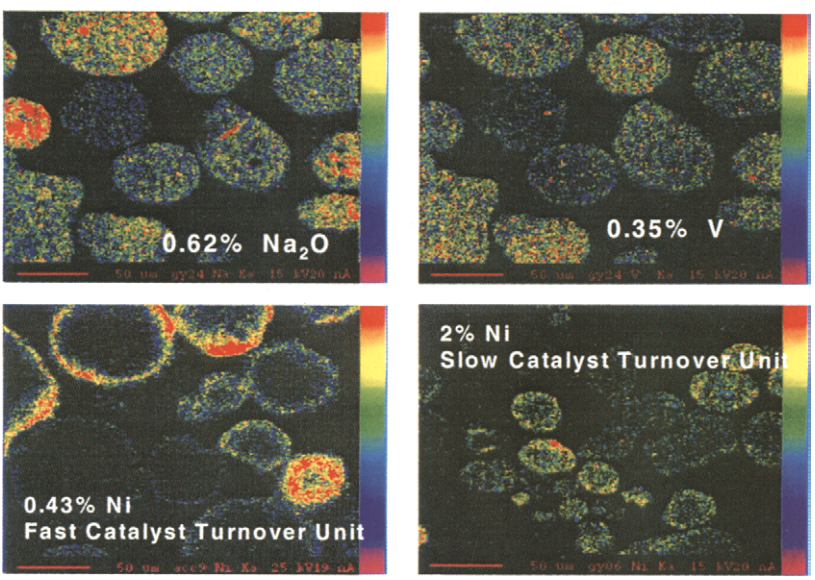

Figure 2. Deposition of Na and V on ECAT particles, as well as Ni deposition on ECAT from two units representing two extreme cases of Ni concentrating on the outward particle areas or distributing throughout the particles.

Table 1
Surface enrichment ratios for elements present in ECAT. The ratios are calculated by dividing the concentration of the element on the surface by its concentration in the bulk.

	Surface Weight (%)	Surface Enrichment Ratio
Na	up to 1%	1 - 2
Al	Varies	0.4
Si	Varies	0.8 - 1.2
Ca	up to 1.2%	2 - 30*
Fe	up to 26%	10 - 18

* Ratios of species in small amounts can change significantly from ECAT to ECAT depending on the amount of them present on the fresh catalyst

these elements under FCC conditions. On the other hand, Al is not very mobile and in general alumina is covered by the depositing oxides (primarily Fe), resulting in a surface enrichment ratio well below 1.

As expected based on the EPMA results, Fe is greatly enriched on the surface by as much as 10-18 times. Since Si and Na are not covered by the depositing Fe, we conclude that they are well mixed with Fe. Ca is also present in the Fe-rich rings formed around the particles, as it deposits in a fashion similar to that of Fe. Aluminum does not appear to mix with Fe and the other elements. Thus, solid phases that contain silica, iron, calcium and sodium oxides may form easily on the surface of ECAT particles with Fe contamination. However, it seems it is difficult for similar phases containing alumina and Fe oxides to form.

The XPS data show that the Fe on the ECAT is in the form of Fe^{3+}. However, this is not necessarily the state of Fe in the riser or the regenerator. ECAT is typically discharged hot from the unit and it is exposed to the atmosphere which most likely will oxidize any reduced iron to the Fe^{3+} state. Our experiments show, that Fe can easily be reduced in the unit. In our partial burn cyclic propylene steaming lab deactivation protocol [4], analysis of the catalyst by X-ray Diffraction, shows that Fe^{3+} is easily reduced to magnetite (Fe_3O_4). Further reduction to Fe^{2+} in the FCC unit is likely.

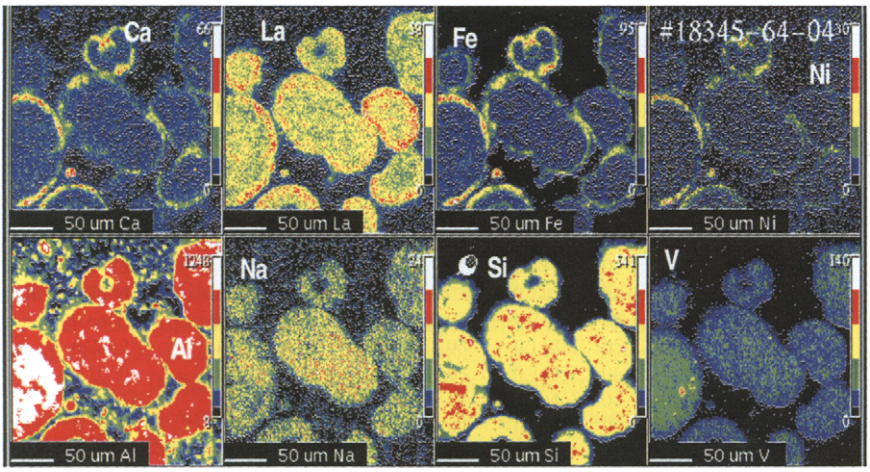

Figure 3. Fe distribution on a lab-deactivated FCC catalyst using the DCR to deposit the contaminant metals.

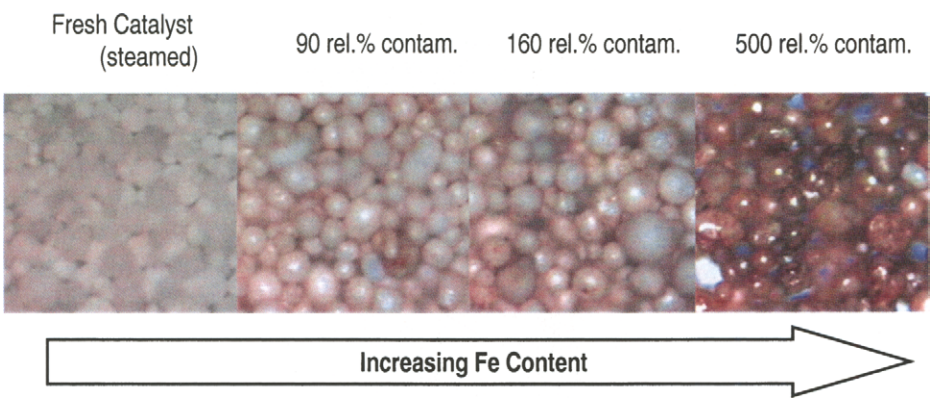

Figure 4. Optical microscopy pictures of lab deactivated catalyst (100% steam, 4 h at 1089 K) with no added Fe, and three ECAT samples of the same catalyst from the same unit taken at different times as Fe levels changed compared to the bulk Fe contained in the fresh catalyst. All pictures taken under the same conditions.

3.3. Morphology and Surface Texture of Fe-Poisoned ECATs

We studied the morphology and surface texture of Fe poisoned ECATs using optical microscopy and Scanning Electron Microscopy (SEM). Optical microscopy shows that the texture of Fe contaminated ECAT changes in an important way. In Figure 4, we show one example of the optical microscopy pictures of ECATs from the same unit taken at different times as the ECAT Fe levels changed. The data show that a lab deactivated sample with no added Fe of the same catalyst as the one used in the unit has a dull texture that does not reflect light very well. As the catalyst ages in the unit with Fe, the ECAT appears to acquire a "glassy" cover which under optical microscopy gives the ECAT particles a sharper definition and glossy appearance. Increasing levels of Fe on the ECAT particles further enhances the observed glassy layer and, as expected, changes the particles color to red/brown similar to the known color of iron oxide.

The SEM data in Figure 5 clearly show that Fe has a distinct effect on the ECAT morphology and texture. Nodules and valleys form on the surface of ECAT particles poisoned with Fe. Nodules appear to be present on the surface of ECAT particles from different units and different catalyst technologies. However, we have also found examples of catalysts with significant levels of Fe contamination on ECAT, but with little evidence of nodule formation.

The results of the SEM analysis of various ECATs have shown many examples of catalyst particles that appear to "stick" together or have irregular shapes. However, we have been able to find similar examples of catalyst particles "stuck" together or with irregular shapes in fresh FCC catalyst samples. Given the limitations of SEM, the evidence is not sufficient at this time to unequivocally conclude that Fe poisoning results in FCC catalyst particles sticking together or having irregular shapes. Thus, claims made [8] based on SEM data that Fe contamination can cause FCC catalyst particles to agglomerate, must be considered as unproven at this time.

3.4. Interparticle Fe Distribution

We examined the distribution of Fe with catalyst age by taking ECAT samples and separating them in eight age fractions using the S/F density separation method. In the case of ECAT containing low to moderate amounts of deposited Fe, we see the profile expected based on the EPMA and XPS data (Figure 6). Fe and Ni are the least mobile species, showing very sharp, non-uniform distributions with catalyst age. On the other hand, V and Na are more uniformly distributed. Still, there is less V on the youngest catalyst particles. The V mobility from the oldest to the youngest particles depends on the V passivation properties of the catalyst and unit design and operation. However, the youngest particles have more Na. This is because the youngest ECAT

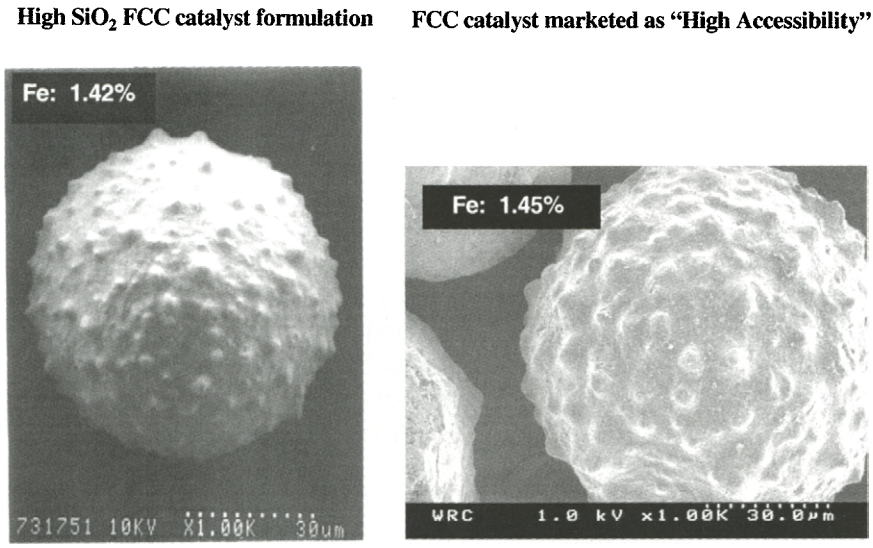

Figure 5. SEM pictures of ECAT particles from two different high Fe units.

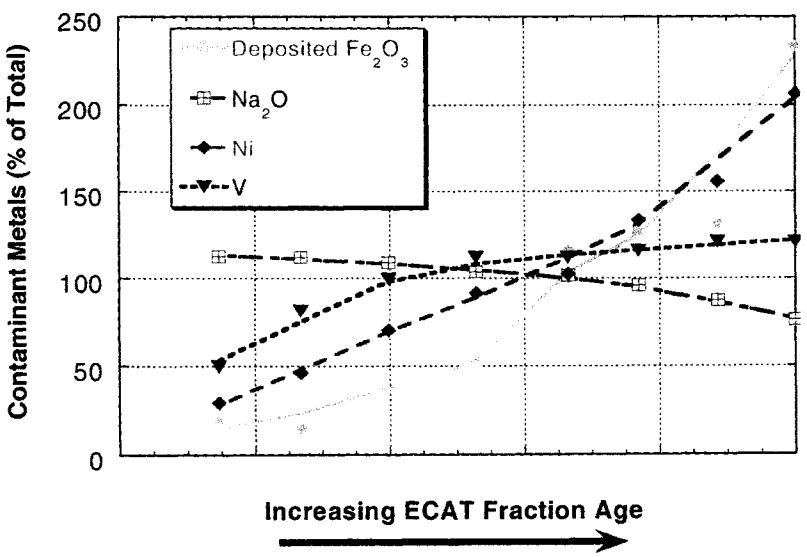

Figure 6. Distribution of Fe, Na, Ni and V on ECAT fractions from a unit with low to moderate amounts of Fe separated by a Sink/Float method. Fe on ECAT 0.74 wt.% Fe_2O_3.

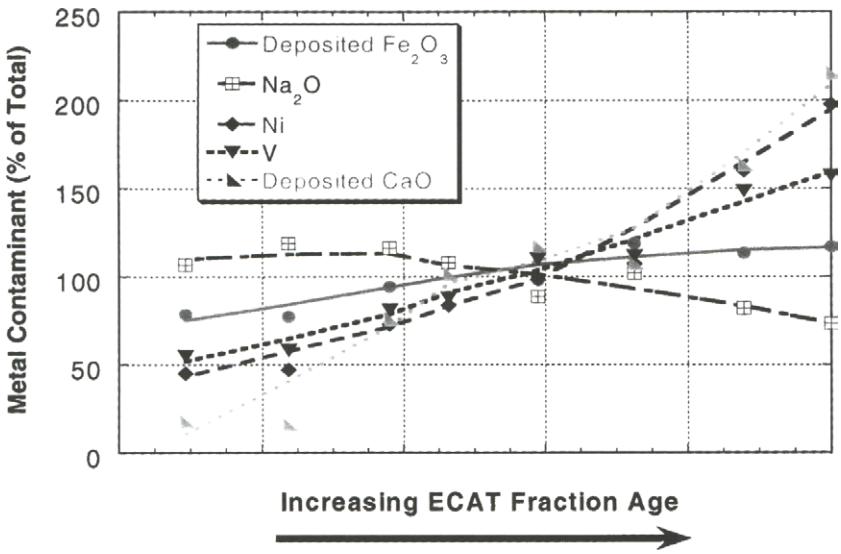

Figure 7. Distribution of Fe, Ca, Na, Ni and V on ECAT fractions from a unit with high amounts of deposited Fe separated by a Sink/Float method. Fe and Ca on ECAT 1.91 wt.% Fe_2O_3 and 0.15 wt.% CaO.

particles contain the highest amounts of zeolite with the stronger acid sites attracting Na.

When we conduct the same analysis of an ECAT from one of the few units with very high levels of Fe deposited on the catalyst, the Fe distribution picture discussed above is reversed (Figure 7). Na and V remain more uniformly distributed than Ni, with V concentrating on the oldest catalyst particles, and Na concentrating on the youngest. Ni and Ca have non-uniform distributions, with the oldest particles having the highest Ni and Ca concentrations and the youngest the lowest. However, Fe appears to be relatively uniformly distributed among the particles of different ages. In fact, in this ECAT, Fe distribution appears to be more uniform than that of V.

3.5. Laboratory Evidence of the Effects of Fe on FCC Catalysts

The data in Figure 8 show the surface area retention of model catalysts made with various levels of Fe and silica or alumina-based binding systems. Without some deactivation treatment there are no differences between Al-sol and Si-sol catalysts. The surface area retention of the catalysts is reduced almost proportionally to the amount of Fe added, probably because iron oxide is a low

surface area oxide contributing weight to the samples, but not as much surface area as the other constituents of the catalyst (e.g., zeolite, matrix, and binder). When the catalysts are treated using the partial burn CPS deactivation protocol, both the Al-sol and the Si-sol catalysts without any added Fe have the same surface area stability. However, as the Fe on the catalysts increases, the surface area of the Al-sol catalysts is much more stable than that of the Si-sol catalysts. In fact, after the deactivation treatment, the Al-sol catalyst with 20% Fe has almost double the surface area retention of the Si-sol catalyst with the same amount of Fe.

Using optical microscopy, we studied the color and texture of these catalysts. The CPS deactivated Al-sol catalysts maintain the same texture regardless of the amount of Fe on the catalyst (Figure 9). Only the color changes from white to a light ferric oxide red/brown and finally to a darker red/brown. However, for the Si-sol catalysts as the Fe level increases, the particles change texture, and a shiny-glassy texture can be identified covering the catalyst particles. As we show in Figure 10, with deactivation, the crystal structure of the components of the Si-sol catalysts gradually becomes amorphous as the Fe content increases to 20%, leaving only some magnetite peaks from the excess iron oxide showing. In contrast, the Al sol catalyst with 20% Fe maintains much more of its original crystallinity than the Si-sol catalyst with the same amount of Fe.

4. DISCUSSION

4.1. Fe Transport in the FCC Unit

The EPMA data show that Fe cannot transport from particle to particle via a gas phase species or by surface diffusion. If one of these mechanisms was operative, then Fe would also be able to transport inside the catalytic particles. Yet there is significant evidence that interparticle Fe transport occurs, at least in some high Fe FCC units. In addition to the data in Figure 7, a relatively uniform distribution of Fe on ECAT has been reported before [9]. The authors speculated that as Fe deposits, and the exterior surface of the catalyst particles is deactivated, catalytic cracking ceases on these particles stopping further Fe deposition on the most aged particles of the inventory. Cracking continues on the younger particles on which Fe now deposits resulting in a relatively uniform particle to particle Fe distribution. However, this mechanism does not explain the data presented here. In our high-Fe case of Figure 7, Ca and Ni have

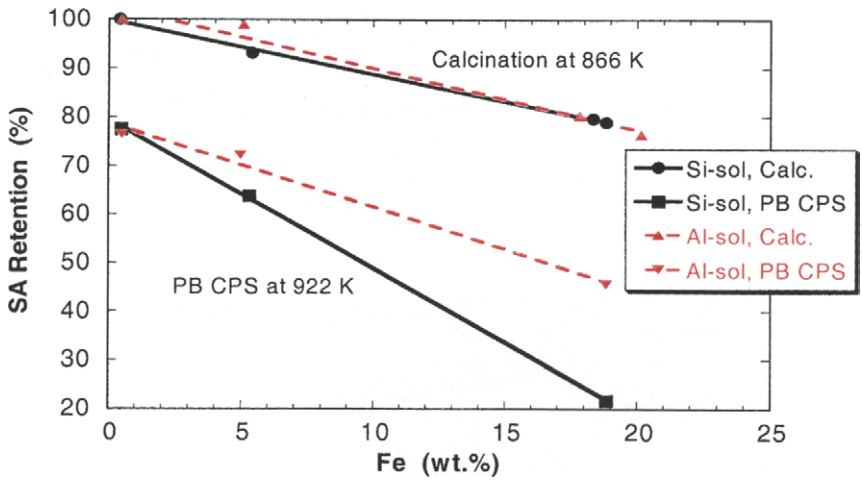

Figure 8. Laboratory evidence of the effects of Fe on FCC catalysts. Surface area retention after the indicated treatment for both Si-sol and Al-sol catalysts at various Fe levels. Surface area retention is expressed as percent of the surface area of the calcined catalysts with no Fe.

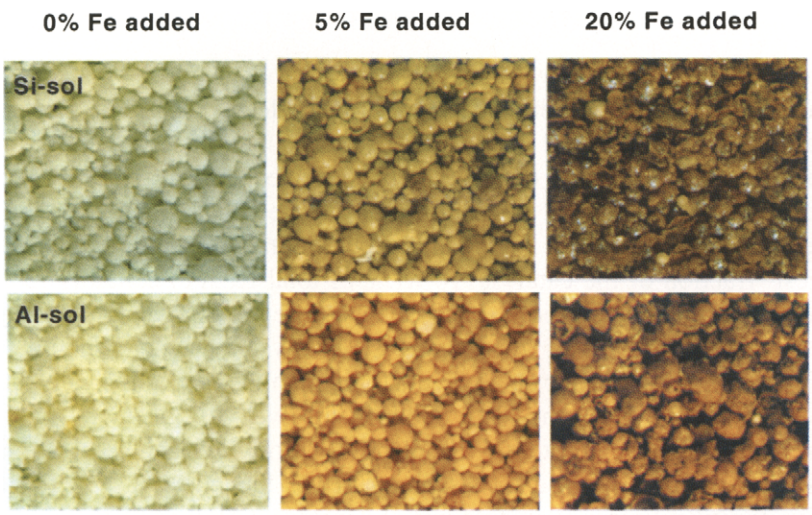

Figure 9. Optical microscopy images of lab-made Si-sol and Al-sol catalysts with 0, 5 and 20% Fe, after partial burn CPS deactivation at 922 K, showing the differences in texture and color between the two classes of catalysts when poisoned by Fe. All images taken under the same conditions.

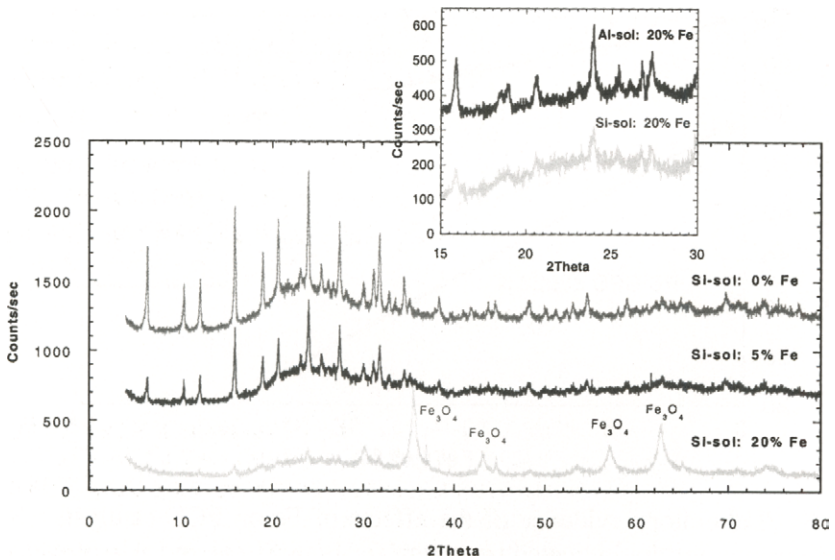

Figure 10. XRD analysis of lab-made Si-sol and Al-sol catalysts with 0, 5 and 20% Fe, after partial burn CPS deactivation at 922 K, showing the effect of Fe on crystallinity.

non-uniform distributions with catalyst age. This suggests that Ca and Ni continue to accumulate on the oldest ECAT particles even though Fe deposition according to the proposed mechanism [9] has stopped. It is difficult to understand how the oldest catalyst particles have been deactivated to such a degree that cracking of feed molecules carrying Fe has stopped, but cracking of the feed molecules carrying Ni, Ca and even V continues. In addition, even the youngest fraction of the catalyst (10 wt.% of total ECAT) contains 75% of the Fe in the oldest ECAT fraction. These levels of Fe are high and according to the proposed explanation [9], the youngest catalyst particles should not be significantly more active for catalytic cracking than the rest of the catalyst.

We believe that the data lend themselves to a much more likely interpretation that is consistent with all observations. Organic or inorganic Fe that is very finely dispersed or dissolved in the feed deposits on the catalyst particles forming Fe rings on the exterior surface. However, there is another mechanism of Fe deposition. Many feeds contain particulate Fe contamination. We show an example of such a feed in Table 2 before and after it was filtered to remove the particulate contamination. With the exception of Ni and V, the majority of the Fe, Na, Ca and other metals are in the filtered particulate

Table 2
Metal contaminants in an FCC feed before and after removal of particulate contamination by filtration. Analysis of the particulate contamination is also included.

Feed Metals Content

	As Received Feed	Filtered Feed
Ni, ppm	5.1	4.8
V, ppm	6.4	6.7
Fe, ppm	32.4	2.2
Na, ppm	4.5	0.8
Al, ppm	3.9	0
Ca, ppm	8.1	2.5
Mg, ppm	0.9	0.2
Zn, ppm	2.3	1.2
P, ppm	1	0
Ba, ppm	2.7	0.2

Feed Filtercake Analysis

Solids in feed: 0.11%

CHEMICAL ANALYSES:

SiO_2	: WT.%	16.0
Al_2O_3	: Wt.%	6.4
Na_2O	: Wt.%	3.3
SO_4	: Wt.%	21.0
Fe_2O_3	: Wt.%	38.2
MgO	: Wt.%	1.3
P_2O_5	: Wt.%	1.3
CaO	: Wt.%	7.2
Cu	: ppm	2400
Pb	: ppm	2850
ZnO	: WT.%	1.3

Particle Size Distribution

d(10)	: µm	11
d(50)	: µm	30
d(90)	: µm	58

contamination. Many of the particles in the feed are fine colloidal Fe, or they may attrite after entering the unit forming a fine, Fe-rich dust that sticks to the FCC catalyst particles. Once such dust is present in the unit, it can easily move from particle to particle until it is permanently attached to the catalyst surface or is entrained out of the unit with the catalyst fines. The result is the easy migration of Fe from the older to the younger particles. As some of the Fe-rich dust particles attach to ECAT particles, nodules rich in Fe form. The effect of these nodules is largely localized to the area on which the Fe-rich particles are

attached, leaving most of the catalytic particle surface unaffected. Potentially deleterious effects of this form of Fe deposition will increase the more numerous and the smaller the Fe-rich particles become on the catalyst surface. It is worth noting that the formation of nodules via this mechanism is not specific to any catalyst technology, manufacturing process, or catalyst chemical composition.

To verify this mechanism of Fe transport in the FCC unit regenerator we examined the fines composition of 16 units with various amounts of Fe on ECAT. The presence of Fe-rich fines in the unit facilitating interparticle Fe transport would result in unit fines enriched in Fe. We show the results in Table 3. For high-Fe units, in virtually all cases, the Fe composition of the fines is 2-3.5 times that of the Fe content of the ECAT itself. There is only one case where the fines Fe concentration is close to that of the ECAT. On the other hand, for

Table 3
Enrichment of FCC regenerator fines in Fe compared to Fe concentration on ECAT. Fe is reported as wt.% Fe.

Unit	ECAT Fe (wt.%)	Fines Fe (wt.%)	Enrichment Ratio
High Fe units			
A	1.27	4.49	3.5
B	0.93	2.38	2.6
C	0.93	2.99	3.2
D	0.88	1.91	2.2
D	0.57	0.71	1.2
E	1.15	2.86	2.5
F	1.1	3.69	3.4
G	0.94	1.87	2.0
H	0.97	1.14	1.2
Low and moderate Fe units			
I	0.51	0.51	1.0
I	0.62	1.23	2.0
J	0.46	0.81	1.8
K	0.56	0.9	1.6
L	0.47	0.5	1.1
M	0.49	0.68	1.4
N	0.48	0.49	1.0
O	0.4	0.52	1.3
P	0.68	0.76	1.1

moderate- to low-Fe units, the ratio of Fe on fines versus that on ECAT never exceeds 2, and in most cases is close to 1. These observations confirm the presence of fine Fe-rich particles in FCC units and suggest that high-Fe units are much more likely to have this form of particulate Fe present than lower-Fe units.

4.2. FCC Catalyst Deactivation by Fe

Our results show that during Fe deposition metal contaminants form what appears to be new phases with the underlying catalyst composition. Thus, to understand the cause of FCC catalyst deactivation due to Fe deposition, it is important to examine the thermodynamics of the phases present on the catalyst particle surface. Of the two major components of FCC catalysts, alumina has the highest melting point, higher than 2320 K after α-alumina is formed. Silica (quartz) melts at lower temperatures, 1986 K. However, when Na, Ca and Fe oxides are present, the melting points of both silica and alumina decrease substantially. In Table 4 we show a compilation of the temperatures at which the first liquid appears (initial melting temperatures) for phases that silica or alumina can form with Na, Ca and Fe oxides present on the catalyst surface. For ranges that contain the Na_2O concentrations we have measured on the surface of FCC ECATs both Na_2O and CaO dramatically reduce the initial melting temperature of silica. However, Na is a much more effective fluxing agent for silica than Ca. The effect of FeO on the initial melting point of phases with silica is not as severe as that of Na_2O, but it is more severe than that of magnetite or Fe_2O_3. The combination of Na with Fe is particularly destructive. Combining Na_2O with FeO and silica at concentrations similar to the ones we measured on the surface of ECATs can lower the initial melting point to less than 773 K. This temperature is lower than the operation temperature of virtually every FCC riser.

Contrary to silica, the melting temperature of alumina is not affected as severely (Table 4). While the mere presence of Na_2O in SiO_2 can lead to the formation of small amounts of liquid at 1050 K, it takes 9.2% Na_2O to decrease the melting temperature of alumina to 1680 K. Like Na, Fe is also less effective in decreasing the melting temperature of alumina than of silica. Even a combination of alumina and unrealistically high amounts of Na oxide with silica and Fe oxide does not bring the melting point of the phases richer in alumina (>15% Al_2O_3) below 1270 K. Thus, for alumina-rich areas of the ECAT surface, and for the levels of Fe, Na, and Ca oxides we can expect to find there, the initial melting temperatures of such alumina-rich phases are expected to be hundreds of degrees higher than similar silica-rich phases.

Every FCC catalyst microsphere is constituted of smaller particles of zeolite, matrix, clay, and the binder that holds everything together. As a result, the exterior surface of the particle is not homogeneous. Rather it has areas of

Table 4
Initial melting temperatures for phase systems containing SiO_2, Al_2O_3, FeO/Fe_2O_3, Na_2O and/or CaO at ranges of concentrations which include those that can be found on the surface of FCC ECATs. Data adapted from refs. 10-17.

System	SiO_2 (%)	Al_2O_3 (%)	FeO/Fe_2O_3 (%)	Na_2O (%)	CaO (%)	First Liquid Temperature (K)
SiO_2	100					1986
Al_2O_3		100				2323
SiO_2-Na_2O	Balance			0*-25		1053
Al_2O_3-Na_2O		Balance		0*-5.5		2273
				5.5-9.2		1853
				>9.2		1683
SiO_2-CaO	Balance				0*-36	1709
Al_2O_3-CaO		Balance			0*-8.4	2123
SiO_2-FeO	Balance		0*-62			1453
SiO_2-FeO• Fe_2O_3	Balance		0*-85			1728
Al_2O_3-FeO		Balance	0*-35			2023
SiO_2-FeO-Na_2O	Balance		0*-57*	25-0*,†		<773
Na_2O-Al_2O3-SiO_2-Fe_2O_3	71.3	4	6.2	18.4		1044
	58.5	9	17.3	15.1		1216
	59.3	16.4	9	15.3		1271
	47.9	24.1	9.7	18.4		1521

* 0% is not included in the composition range with the indicated first liquid temperature.

† The combination of high FeO and high Na_2O concentrations leads to phases that have slightly higher melting temperatures (~ 940 K).

zeolite, clay and matrix (typically added alumina), mostly coated with the binder used. Since clay has a low surface area and few pores, and the zeolite has mainly micropores and some mesopores, many of the large pores responsible for allowing large hydrocarbon molecules inside the particle for cracking come from the binder, the matrix, and the voids between the particles that constitute the catalyst microspheres. Spot analysis of the binder areas by TEM/EDS has

confirmed that Si-sol binder areas of the particle are essentially silica containing only traces of alumina. Similarly, Al-sol binder and alumina matrix areas are essentially alumina containing only traces of silica. As the catalyst ages, Fe, Ca, Na and other contaminant metals deposit on it. At this point a number of changes occur depending on the underlying catalyst make up.

4.2.a. Catalysts with Silica-Based Binders

Fe, Ca, and Na oxides mix with the binder silica (or silica from other silica-rich areas) and form phases that have initial melting temperatures as low as the operation temperatures of the riser or the regenerator. The oxidation state of the Fe on the catalyst surface plays a role in this change. As the catalyst circulates in the unit, Fe spends most of the time in a reduced state (Fe^{2+} or magnetite) further decreasing the melting point of Fe containing phases. The formation of these low melting temperature phases facilitates the fluxing of silica in the binder, thus filling and closing the surface pores and giving the surface the "glassy" texture we have observed. This process is often referred to as vitrification. Even if outright melting does not occur, accelerated sintering, due to the decrease of the melting temperature will have a similar effect. The result is again the destruction of the surface pores. As the Fe accumulates on the surface of Si-sol catalysts, these low melting temperature phases cover an ever larger area of the particle external surface.

The collapse of the surface pore structure where the Fe deposits causes the surface to rescind as the melting and sintering decreases the volume of the affected material. In areas where Fe does not mix well with the underlying components, or if it does, the resulting phases have high melting points (alumina-rich areas), the integrity of the structure is retained. The combination of areas where the particle structure collapses with the areas where it is maintained gives rise to the formation of the nodules and valleys we observed on the surface of ECAT particles. Because of the way they are formed, nodules are rich in Fe and Ca which cover the underlying structure, while in the valleys Fe is diluted by mixing with silica and other compounds.

This is an alternative mechanism for forming nodules on the surface of Fe poisoned FCC catalysts in addition to that involving fine Fe-rich dust. In both mechanisms the nodules are Fe-rich. We have been able to confirm this conclusion by measuring the concentration of Fe, Ca, Si, and Al in nodules and valleys of an Fe poisoned ECAT using SEM/EDS (Figure 11). The two mechanisms of nodule formation explain why some times nodule formation is associated with the catalyst being deactivated by Fe, and why in other cases nodule formation is not accompanied by catalyst deactivation. When the formation of nodules is the result of vitrification caused by the formation of low melting temperature phases, their presence is an indication of catalyst

deactivation by Fe. However, when the formation of nodules is the result of fine Fe-rich particles attaching themselves to the catalyst, the catalyst deactivation associated with these nodules is relatively small. As these Fe particles get smaller and more numerous and they start reacting with the silica-rich surface, they may be better able to affect catalyst deactivation by forming low melting temperature phases. Regardless of how nodules are formed, nodule formation is probably the reason ECAT ABD decreases with increasing Fe. The presence of nodules on the surface prevents them from packing as densely as without the nodules.

Since in most cases Fe does not penetrate deeper than 1-5 μm, the formation of low melting temperature phases only affects a small portion of the particle volume and surface area (typically less than 10%). However, in the FCC unit it is critical that during the time the feed molecules spend in the riser, they diffuse inside the particle and the products diffuse out. Closing of pores by the processes set in motion by Fe deposition on the catalytic particle restricts the diffusion of feed molecules into catalyst particles, thus decreasing activity. Large feed molecules are the ones most affected by pore closing. Thus, bottoms cracking is the catalyst property more severely affected by Fe poisoning.

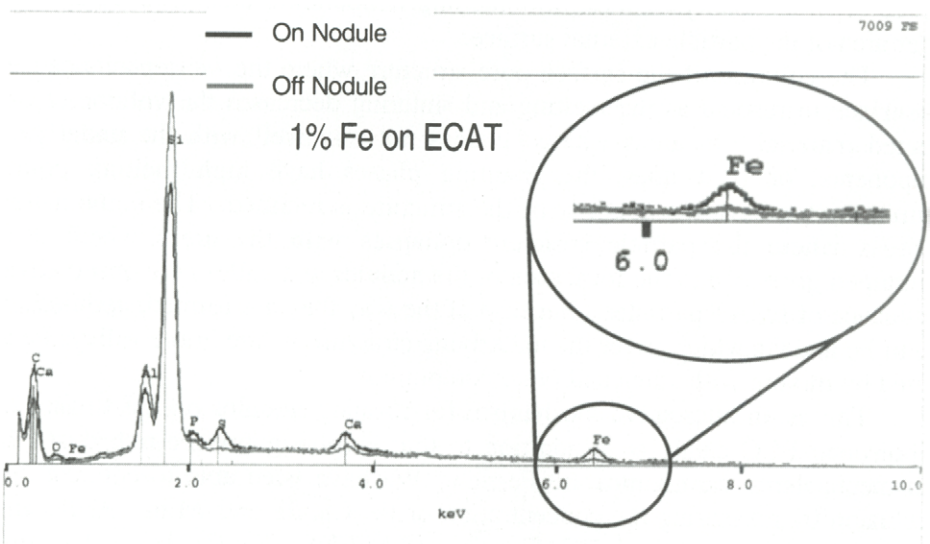

Figure 11. Relative Fe concentration on nodules and valleys formed on an ECAT poisoned by Fe as measured by SEM/EDS.

4.2.b. Catalysts with Alumina-Based Binders

The formation of high Fe low melting temperature phases may also occur at high silica areas of the particle surface of catalysts employing the Al-sol binding system. Nodule formation and some pore closing may occur on these catalysts as well, particularly in units where fine Fe-rich particles are present. However, in Al-sol catalysts the alumina binder and the active matrix component are dispersed throughout the particle, and contribute surface area and cracking activity. The alumina binder and active matrix are also where much of the bottoms cracking occur. These components provide many of the pores needed to transport feed molecules inside the catalytic particle, and these components are essentially pure alumina.

Alumina does not mix with the deposited Fe to form low melting temperature phases. Even if alumina could mix with the depositing Fe, thermodynamics in Table 4 show that alumina phases containing Fe, Na and/or Ca oxides require high temperatures to melt. These temperatures are much higher than the riser and regenerator temperatures. Thus, it is not likely accelerated sintering can occur. As a result of the resistance of alumina to Fe poisoning, the surface pores in binder and active matrix areas remain essentially open allowing the feed molecules to transport inside the catalytic particle for cracking. Hence, these catalysts are resistant to Fe-poisoning offering good activity maintenance and good bottoms cracking even in the face of high Fe contamination.

Recently others have confirmed the role low melting temperature phases play during catalyst deactivation by Fe [18]. However, there seems to be some dispute as to what these phases are and the ability of alumina to retard their formation. These workers suggested that Si does not participate in the vitrification process and FeO does not form during the FCC process. However, the XPS data in Table 1 clearly show that silica is intermixed with Fe, Ca, and Na oxides. It is difficult to reconcile these data with the creation of low melting temperature phases covering the catalytic particle surface which do not include silica. The same data also show that alumina does not participate in the formation of such phases.

As we discussed, due to the difficulties of collecting ECAT samples without exposing them to air while hot, it is not possible to know with confidence the oxidation state or form of Fe in an FCC unit. It is also not necessary that all Fe is available in reduced form to react with silica. As the low melting temperature phases of Fe with silica, Na and Ca begin to form consuming the reduced Fe present, more Fe_2O_3 can be reduced as the catalyst circulates, and the vitrification process can continue. In addition, while FeO may be the most destructive form of Fe, magnetite or even Fe_2O_3 can also lower the melting point of silica in the presence of Na and Ca. The decrease may be

enough to cause accelerated sintering and pore closing, particularly when local hot spots formed on the catalyst during regeneration are taken into account.

4.3. In-Unit Deactivation of Al-sol versus High Silica Catalyst

Evidence of the resistance to Fe deactivation of FCC catalysts made with an Al-sol binding system can be found in the documented cases of excellent performance of these catalysts in FCC units with high Fe levels on ECAT [19-21]. We analyzed two equilibrium catalysts, both with high Fe levels, one made with an Al-sol binding system and the other with a high silica binding system (Table 5). While the two catalysts are not from the same unit, they are from units using similar high-Fe feeds and with similar catalyst inventory age. SEM analysis of the two ECATs in Figure 12 demonstrate that while as many as half of the Al-sol particles show little or no nodules formation, the high silica catalyst shows signs of severe nodule formation and Fe deactivation. Optical microscopy pictures in Figure 13 confirm the SEM data. While the Al-sol catalyst particles show some dark-brown specs due to locally high concentration of Fe_2O_3, they show no signs of the formation of a glassy phase. Clearly, the Fe on the Al-sol catalyst surface has not reacted to form any low melting temperature phases. On the other hand, the high-silica catalyst particles are shiny and indicate the formation of low melting temperature phases. In fact, because Fe has reacted with the silica on the surface forming new phases, even after the oxidation treatment to remove any coke (2 h at 867 K), the catalyst maintains its glassy appearance and the surface Fe is not oxidized to the dark-brown Fe_2O_3 oxide as is the case with the Al-sol ECAT.

5. CONCLUSIONS

Although Fe has only recently attracted attention as a poison of FCC catalysts, it can cause significant loss of activity and bottoms cracking. The ability of Fe to poison the FCC catalyst is largely due to the fact that the deposited Fe concentrates on the exterior surface of the catalyst particles forming Fe-rich rings. In these rings, Fe oxide mixes with silica, CaO, Na_2O and perhaps other contaminants forming new low melting temperature phases. As the catalyst ages, the melting and/or accelerated sintering caused by these phases (vitrification process) closes the surface pores, forms nodules and valleys on the surface, gives the catalyst a glassy appearance, and restricts the transport of large hydrocarbon feed molecules inside the particle for cracking. Thus, the catalyst loses activity and bottoms cracking even though most of the catalyst particle remains unaffected. The presence of Fe-rich fine particles in a unit can

Table 5
Properties of high-Fe Al-sol and high-silica ECAT.

		ECAT A Al-sol	ECAT B High Silica
CHEMICAL ANALYSES:			
SiO_2	wt.%	51.5	58.1
Al_2O_3	wt.%	**42.6**	**36.9**
RE_2O_3	wt.%	2.39	1.86
Na_2O	wt.%	**0.50**	**0.21**
Fe_2O_3	wt.%	**1.41**	**1.75**
CaO	wt.%	0.16	0.11
Ni	ppm	**2090**	**1745**
V	ppm	**4550**	**3370**
PHYSICAL ANALYSES:			
SA	m^2/g	157	174
UCS-ASR	A	24.28	24.26

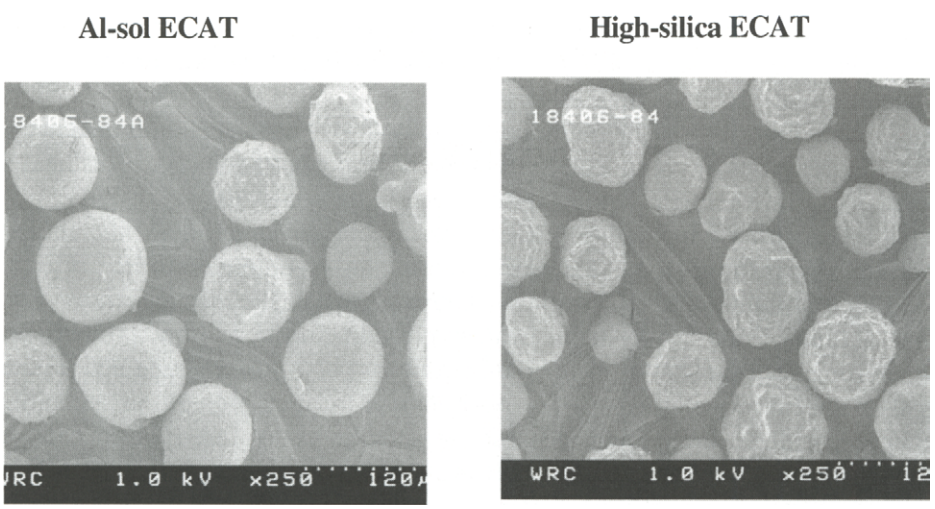

Figure 12. SEM pictures of Al-sol and high-silica ECATs illustrating the resistance of Al-sol catalysts to Fe deactivation.

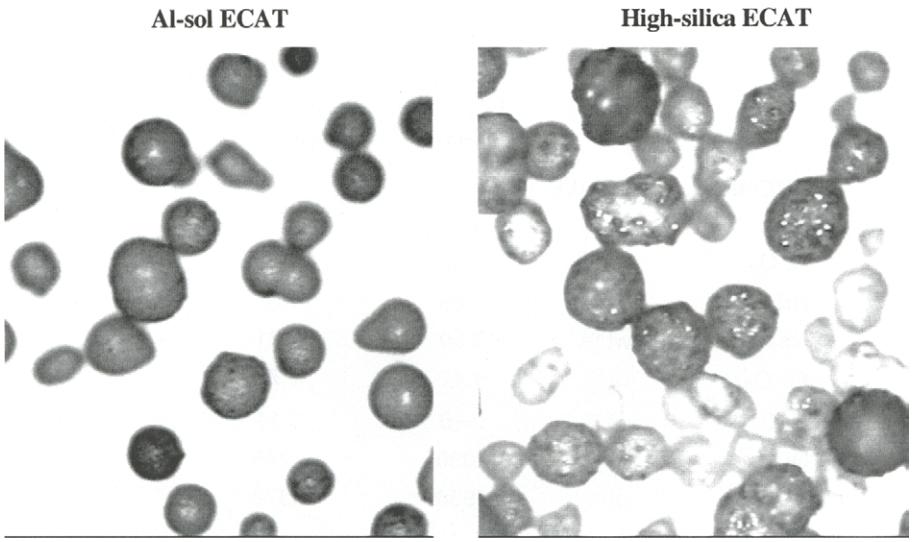

Figure 13. Optical microscopy pictures of Al-sol and high-silica ECATs illustrating the resistance of Al-sol catalysts to Fe deactivation.

facilitate interparticle Fe transport and give rise to nodules formation on ECAT particles without causing significant catalyst deactivation. Nodules formed in this fashion are catalyst independent and by themselves are not a reliable indicator of catalyst poisoning by Fe.

The deposition of Fe on the FCC catalyst does not depend on the catalyst used, its properties or composition. However, the deactivation process is heavily affected by the chemical composition of the underlying catalyst. While silica forms low melting temperature phases with Fe, Na and other elements, alumina does not. Thus, high silica catalysts are particularly vulnerable to Fe poisoning while high alumina catalysts are not. Alumina catalysts, especially those made with alumina binding systems which provide most of the porosity for transporting feed molecules inside the particle and bottoms cracking activity, are highly resistant to the effects of Fe. Nodules can form on high alumina catalysts either in localized high silica areas of the surface, or by fine Fe-rich particles attaching themselves to the catalyst. However, these effects are localized, do not have a major impact on the catalyst performance, and do not affect the ability of the Al-sol binder and matrix to facilitate transport of large feed molecules and maintain activity and bottoms cracking.

REFERENCES

[1] M. L. Occelli, D. Psaras, and S. L. Suib, in Proceedings International Symposium Zeolite Catalysis, Siofok, Hungary, 1985, p. 423.

[2] G. Yaluris, W.-C. Cheng, L.T. Boock, M. Peters, and L.J. Hunt, NPRA, AM-01-59, New Orleans 2001; Hydrocarbon Asia, May/June 2001, 32.

[3] L. T. Boock, J. Deady, T.-F. Lim, and G. Yaluris, in Proceedings, 7th International Symposium on Catalyst Deactivation, C. H. Bartholomew and G. A. Fuentes Eds., Cancún, Mexico, October 1997, Studies in Surface Science and Catalysis 111, Elsevier, Amsterdam, 1997, pp 367-374.

[4] L. T. Boock, T. F. Petti, and J. A. Rudesill, in Deactivation and Testing of Hydrocarbon Processing Catalysts, P. O'Connor, T. Takatsuka, and G. Woolery Eds., ACS Symposium Series 634, Washington, DC, 1996, pp 171-183.

[5] G.W. Young, in Fluid Catalytic Cracking: Science and Technology, J. S. Magee and M. M. Mitchell, Jr. Eds., Studies in Surface Science and Catalysis 76, Elsevier, 1993, pp 257-292.

[6] D. A. Jacobs, G. C. Smith, R. D. Vis, and A. F. H. Wielers, J. Catal., 176 (1998), 387.

[7] M. L. Occelli, in Fluid Catalytic Cracking II: Concepts in Catalyst Design, M. L. Occelli Ed., ACS Symposium Series 452, Washington, DC, 1991, pp 343-362.

[8] E. Rautiainen and P. van Krugten, Catalyst Courier, 40 (2000).

[9] S. J. Yanik, Petroleum Technology Quarterly, Summer 2001, p. 15.

[10] F. C. Kracek, J. Phys. Chem., 34 (1930), 158.

[11] B. Phillips and A. Muan, J. Am. Ceram. Soc., 39[4] (1915), 5.

[12] M. Rolin and P. H. Thanh, Rev. Hautes Temp. Refractaires, 2[2] (1965), 178.

[13] N. L. Bowen and J. F. Schairer, Am. J. Sci., 5th Ser., 24 (1932), 200.

[14] B. Phillips and A. Muan, J. Am. Ceram. Soc., 12[9] (1959), 415.

[15] I. A. Novokhatskii, B. F. Belov, A. V. Gorokh, and A. A. Savinskaya, Russ. J. Phys. Chem., 39[11] (1965), 1498.

[16] P. T. Carter and M. Ibrahim, J. Soc. Glass Technol., 36 (1952), 156.

[17] D. K. Bailey and J. F. Schairer, J. Petrol., **7**, Pt. 1 (1966), 125&126.

[18] W. S. Wieland and D. Chung, Hydrocarbon Engineering, 7(3) (2002), 55.

[19] B. Niess, FCC • Additives • Hydroprocessing • Refining Technology Grace Davison Conference, Singapore, August 16-18, 2000.

[20] K. Meder, J. Nee, and G. Yaluris, Hydrocarbon Engineering, 7(3) (2002), 37.

[21] G. Yaluris, Refining Technology Grace Davison Conference, Singapore, September 18-20, 2002.

Studies in Surface Science and Catalysis, volume 149
M. Occelli (Editor)

Simulating Iron-Induced FCC Accessibility Losses in Lab-Scale Deactivation

D.R. Rainer[a], E. Rautiainen[b], B. Nelissen[b], P. Imhof[b], and C. Vadovic[a]

[a] Akzo Nobel Catalysts LLC, 13000 Bay Park Road, Pasadena, TX 77507
[b] Akzo Nobel Catalysts b.v., P.O. Box 37650, Nieuwendammerkade 1-3 BE, Amsterdam, The Netherlands

Selecting the appropriate catalyst deactivation method is critical in predicting commercial FCC catalyst performance by lab-scale performance testing. One of the most accurate ways of mimicking a commercial equilibrium catalyst is through cyclic deactivation (CD), in which a catalyst is exposed to cracking and regeneration cycles, using a feed with enhanced metals content. In spite of the success of this technique in matching commercial metals deposition profiles and "potencies," there are still shortcomings in simulating the deleterious effects of contaminant iron on catalyst accessibility, as measured by the Akzo Accessibility Index (AAI.) A modified CD method is presented that utilizes a lower steam partial pressure in regeneration that produces realistic catalyst accessibility losses with added iron. Two catalysts have been deactivated by a variety of methods, demonstrating the effect on AAI of different steaming conditions and metals levels. Performance testing results of these catalysts are compared with those of equilibrium catalysts.

1. INTRODUCTION

In order to effectively mimic an equilibrium catalyst in a lab-scale deactivation, the impact of various contaminant metals must be well characterized and understood. The effect of contaminant iron on catalyst morphology, accessibility, and performance has recently emerged as one of the most important aspects of FCC catalyst deactivation. Depending on unit conditions, feeds, and the type of catalyst employed, iron contamination can result in severe catalyst performance degradation, particularly with regard to bottoms cracking [1-5].

The term accessibility when applied to an FCC catalyst refers to the facility of the catalyst for allowing the larger feed molecules to diffuse into the particle interior and reach the active cracking sites within. The most important and direct measurement for quantifying catalyst accessibility is found in the Akzo Accessibility Index (AAI) [1-3, 6-9].

In resid applications, elevated contaminant iron levels typically result in significant decreases in catalyst accessibility, which in turn results in loss of bottoms cracking performance. While this accessibility loss phenomenon has been observed for all the major technologies currently on the market (from all suppliers) [9-11], the choice of catalyst is very important to the success of these high-iron resid operations.

Ideally, high accessibility catalysts should be chosen for resid applications where bottoms cracking performance is critical, particularly in cases where iron levels are high. An alternative approach is to select a catalyst that demonstrates high AAI retention in the face of elevated iron levels under FCCU conditions [1, 3, 4, 7, 12].

Currently, the most widely accepted FCC lab-scale deactivation methods do not adequately predict the response of catalyst AAI's to contaminant iron. Using these methods (steaming, Mitchell impregnation followed by steaming, and conventional crack-on methods), catalyst AAI's are usually observed to increase, even when high levels of iron are added [6-9]. Thus, these standard methods do not at all simulate the typical AAI response to iron observed in the FCCU (as described above.)

This paper describes an integrated effort to characterize the mechanisms of commercial FCC catalyst iron-induced sintering and the effects on performance in a detailed way, and to simulate these effects in lab-scale deactivation. A new Cyclic Deactivation (CD) method is described that employs a lower steam partial pressure during the regeneration step that is more commensurate with actual FCCU operation relative to the conventional methods described above. The successes of this laboratory method in simulating commercial catalyst AAI responses to iron in the FCCU are detailed.

2. EXPERIMENTAL

Two catalysts ("A" and "B") with different accessibility levels were subjected to a variety of deactivation methods. The fresh catalyst properties appear in Table 1.

The basic CD method and apparatus have been described in detail previously [13-16]. A two-hundred gram loading of catalyst is subjected to alternating cracking and regeneration cycles with a vacuum gas oil (VGO) feed doped with organic-metal. Steam is introduced during the regeneration phase. The partial pressure of the steam can be varied. The CD-ALFA method (Cyclic Deactivation with Accessibility Loss by Fe Addition) described here employs a steam partial pressure significantly lower than the range of 40-50% employed in conventional CD, and closer to commercial FCCU regenerator conditions (typically < 10%). The method is designed to give a more realistic catalyst accessibility response to contaminant iron. The most important operational parameters are reported in Table 2, along with analogous parameters for two conventional CD methods.

Table 1. Fresh catalyst properties

	Catalyst A	Catalyst B
Total surface area [m^2/g]	272	243
Meso-surface area [m^2/g]	72	129
Micropore volume [cc/g]	0.093	0.053
RE [wt. %]	1.43	2.51
Unit cell size [Å]	24.59	24.64
Alumina [wt. %]	33.0	53.6
Silica [wt. %]	63.2	41.2
Macropore volume [cc/g]	0.34	0.46
Bulk density [cc/g]	0.84	0.75
Akzo Accessibility Index	2.9	16.0

The feed was doped with combinations of iron-naphthenate, vanadium-naphthenate, nickel-naphthenate and sodium-methoxide in a methanol solution. These were added gravimetrically to the VGO feed to achieve the targeted metals levels on the deactivated catalysts.

Catalyst deactivations with steam only were conducted on 100g loadings using 100% steam to fluidize the catalyst at indicated temperatures and duration.

The lab-scale performance results were acquired using the Fluid Simulation Test (FST), described in detail elsewhere [15, 16]. The general equilibrium catalyst (e-cat) testing results were obtained using a VGO feed at a single cat-to-oil ratio (CTO), while the lab-deactivated catalysts ("A" and "B") were tested at multiple CTO's with a resid feed. The properties for each feed are given in Table 3.

Table 2. Deactivation parameters

	Conventional CD	54 cycle conv. CD	CD-ALFA
Reaction temp. [°C]	770	500	540
Regeneration temp. [°C]	800	788	740
Steam partial pressure [mole %]	47	50	1-20
Feed injection time [s]	75	60	80
Stripping time [s]	800	600	120
Regeneration time [s]	1600	2580	1600

Table 3. Feed properties

	VGO	Resid
API gravity	20.4	18.8
CCR [wt. %]	0.17	3.07
10% point [°C]	425	405
90% point [°C]	505	584
Total sulfur [wt. %]	3.2	2.7
Total nitrogen [ppm]	1009	1351
Aniline point [°C]	81.9	81.8

3. RESULTS AND DISCUSSION

3.1. Effects of Iron Contamination

The deterioration in catalyst bottoms cracking performance associated with iron contamination is invariably accompanied by a specific type of catalyst particle morphology change in which the surface assumes a bumpy or "nodulated" appearance. This type of morphology change is observed for all types of catalyst technologies (Al-sol, Al-gel, and Si-Sol) [1-3, 5, 9-11, 17]. Typical examples are shown in Fig. 1.

Fig. 2 shows high resolution images of the same types of nodules on an e-cat with high contaminant iron. High-resolution Energy Dispersive Spectroscopy (EDS) results have indicated that these nodules are rich in iron, and often calcium, depending on the total contaminant calcium levels [18].

As iron levels increase, catalyst sintering phenomena result in the imposition of diffusional barriers to migration of heavy molecules to the active sites in the interior of the catalyst. At some critically low AAI level, diffusional constraints prevail, and severe performance degradation is encountered. This relationship between unit performance and iron contamination (with attendant AAI decrease) is well-documented and has been observed for all FCC catalyst technologies [1, 3, 5]. The important parameter for loss of unit performance is the AAI decrease, rather than the nodulation of the particle surface. Commercial examples have been observed where AAI drops and unit performance suffers as iron increases, and yet little or no catalyst nodulation is observed.

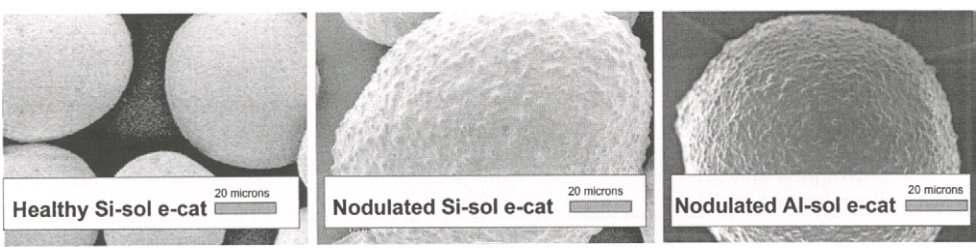

Figure 1. SEM comparing "nodulated" Al-sol and Si-sol e-cats against a normal e-cat.

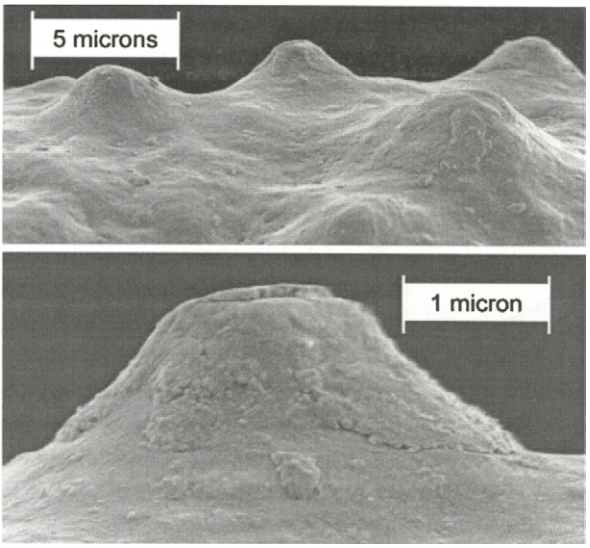

Figure 2. High Resolution SEM high magnification images showing fine structure of iron-contaminated catalyst surface.

3.2 Influence of AAI on FCCU Performance

The influence of catalyst AAI on FCCU performance has been demonstrated for conversion, bottoms cracking, gasoline yield, and other important performance indicators [1, 6, 7, 8]. In fact, analysis of data from multiple commercial FCCU's shows that, given a specific feed and set of operational parameters, there is a critical AAI threshold for each FCCU, beneath which diffusional constraints will begin to negatively impact unit performance.

This is illustrated in Fig. 3. With increasing exposure time in an FCC unit in a resid operation, catalyst AAI's typically decline from the original fresh value. When a particular AAI level is reached (i.e. the "critical AAI threshold"), deterioration in catalyst performance, particularly with regard to bottoms conversion, is observed. Performance continues to degrade with further decreases in AAI.

There are two distinct approaches for increasing the probability that the e-cat AAI will remain above this critical threshold specific to the operation:

1) Use a "high accessibility" catalyst exhibiting a high fresh AAI value.
2) Use a catalyst with a high accessibility retention ("sinter resistant")

In either case, a lab-scale deactivation that simulates the AAI response in e-cat is required to accurately predict how a given catalyst will perform in applications where iron and accessibility issues are important. The CD-ALFA method addresses this need.

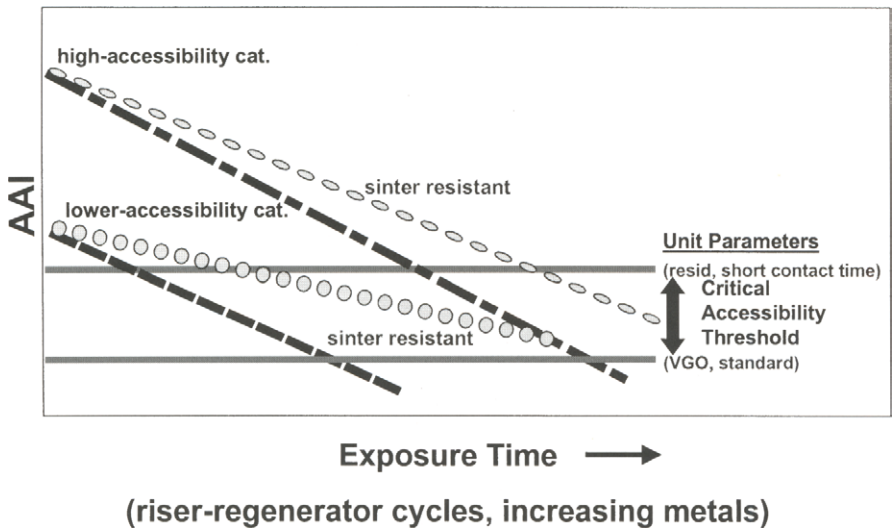

Figure 3. Schematic representation of AAI response to deactivation in the FCCU depicting the "critical AAI threshold".

3.3. Simulating Iron-induced Accessibility Losses

Two catalysts were subjected to 3 basic types of deactivation: steaming alone, conventional CD, and CD-ALFA *type* conditions (lower steam partial pressure relative to conventional CD, both *with* and *without* the inclusion of Fe.) For the CD methods, various combinations of metals were employed.

The primary differences that result from the milder steam employed in CD-ALFA relative to conventional CD include the following:

1) decreased rates of surface area loss, requiring longer deactivation times to match typical e-cat surface areas
2) realistic AAI deactivation responses when combined with iron and vanadium addition

The resulting AAI's after various types of lab deactivations for the two catalysts appear in Table 4, and are displayed graphically in Fig. 4. The responses of the two catalysts are qualitatively the same in that both exhibit AAI increases after steaming at 100% steam partial pressure, consistent with previous observations [6, 7]. Also, for both catalysts, the only treatments that result in significant AAI decreases (> 40%) are those using the CD-ALFA conditions with iron added.

Table 4. Deactivated catalysts properties

Cat. A deac. type	CD cycles	SA [m^2/g]	MSA [m^2/g]	MiPV [cc/g]	AAI	Added Na_2O [wt.%]	Added Fe [wt.%]	Added V [wt.%]	Added Ni [wt.%]
Fresh catalyst	-	272	72	0.093	2.9	-	-	-	-
Steaming 795°C, 5 hrs	-	177	44	0.063	5.1	-	-	-	-
Steaming 788°C, 20 hrs	-	155	36	0.056	6.0	-	-	-	-
CD-ALFA (no metals)*	200	206	55	0.070	4.7	-	-	-	-
CD-ALFA (Fe, V, Na)	200	136	31	0.049	0.0	0.73	0.97	7403	-
CD-ALFA (Fe, V)	200	144	34	0.051	0.2	-	1.13	8654	-
CD-ALFA (Fe, V, Ni, Na)	200	179	42	0.064	0.9	0.33	0.69	4541	972
CD-ALFA (Fe)	200	200	52	0.069	0.3	-	0.96	-	-
CD-ALFA (V only)*	200	179	42	0.064	4.6	-	-	6117	-
Conv. CD (Fe, V)	90	108	22	0.040	2.4	-	0.99	7794	-
Conv. CD (Fe, V, Na)	90	82	18	0.030	2.7	0.38	0.94	6881	-
Conv. CD (V, Ni)	45	150	33	0.054	4.0	-	-	4671	1000

Cat. B deac. type	CD cycles	SA [m^2/g]	MSA [m^2/g]	MiPV [cc/g]	AAI	Added Na_2O [wt.%]	Added Fe [wt.%]	Added V [wt.%]	Added Ni [wt.%]
Fresh catalyst	-	243	129	0.053	16.1	-	-	-	-
Steaming 795°C, 5 hrs	-	160	94	0.030	20.4	-	-	-	-
Steaming 788°C, 20 hrs	-	147	93	0.025	23.1	-	-	-	-
CD-ALFA (Fe)	200	163	97	0.030	15.8	-	0.97	-	-
CD-ALFA (Fe, V, Na)	200	127	79	0.022	5.5	0.73	1.16	6604	-
CD-ALFA (Fe, V)	200	136	84	0.024	9.3	-	1.04	6695	-
CD-ALFA (Fe, V, Ni, Na)	200	149	90	0.027	8.4	0.41	0.60	4543	933
CD-ALFA (Fe)	200	163	97	0.030	15.8	-	0.97	-	-
CD-ALFA (V only)*	200	152	94	0.027	12.8	-	-	6022	-
Conv. CD (Fe, Ni)	90	119	81	0.017	12.9	-	0.57	-	853

* CD-ALFA steaming conditions but with no iron added

The conversions for each deactivated catalyst closely track the total surface area, independent of AAI (Fig. 5.) However, the LCO/bottoms ratio demonstrates a clear correlation with AAI, and is consistent with the e-cat behavior observed in the past.

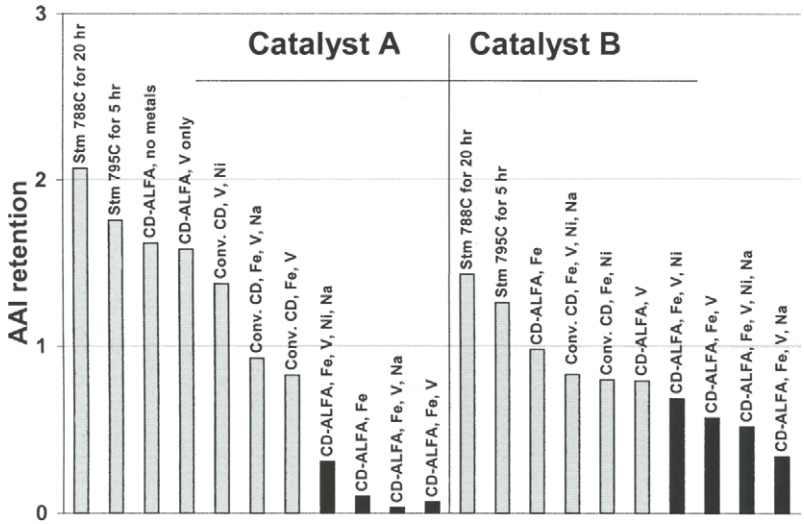

Figure 4. AAI retentions (AAI_{fresh}/AAI_{deac}) for various deactivations of Catalysts A and B.

The impact of AAI on FST performance testing is illustrated in Fig. 6. This data set includes e-cats taken from over 80 refineries and encompasses all types of FCC technologies currently on the market. The full range of typical e-cat surface areas and metals levels are represented. Given the diversity of these e-cats, the relationship between LCO/bottoms ratio and AAI is particularly noteworthy. In fact, statistical analysis for this set confirms that AAI is the most influential measurement for predicting LCO/bottoms ratio in the FST from factors that include meso- and microporous surface area, total pore volume, catalyst density, and individual and collective metal levels.

Fig. 7 shows the relationship between the LCO/bottoms ratio and AAI for the two deactivated catalyst sets (in Fig. 4 and Table 4.) The LCO/bottoms ratio qualitatively responds to these lab-induced AAI decreases in the same manner as observed for equilibrium catalysts (this is discussed in more detail below.) This suggests that the AAI reductions achieved in the lab using the CD-ALFA method are indeed related to the changes that occur in the commercial FCCU.

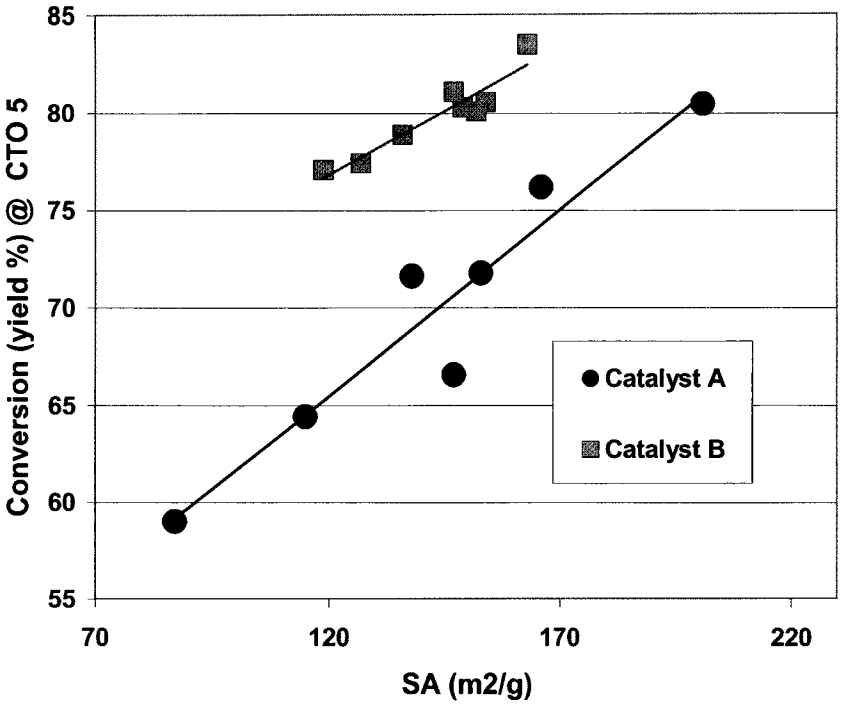

Figure 5. Conversion yield vs. deactivated surface area for Catalysts A and B.

It should be noted that the LCO/bottoms ratio for the deactivated catalyst resulting from Catalyst A treated by CD-ALFA with iron alone (no added vanadium) does not appear to conform to the rest of the data. While this sample exhibits a significantly attenuated AAI (0.3), the lowered accessibility does not seem to be reflected in the performance testing. Also noteworthy, however, is that although the accessibility has dropped dramatically for this sample, the total surface area falls well above the range for typical e-cats, and is certainly much higher than all the other deactivated samples in this set. This, along with the absence of V in this deactivation, suggests that there are additional effects of surface area and metals interactions that have yet to be explained. For this data set, only catalysts deactivated with both Fe and V demonstrate significant AAI attenuation *and* the expected LCO/bottoms effects consistent with the e-cat testing.

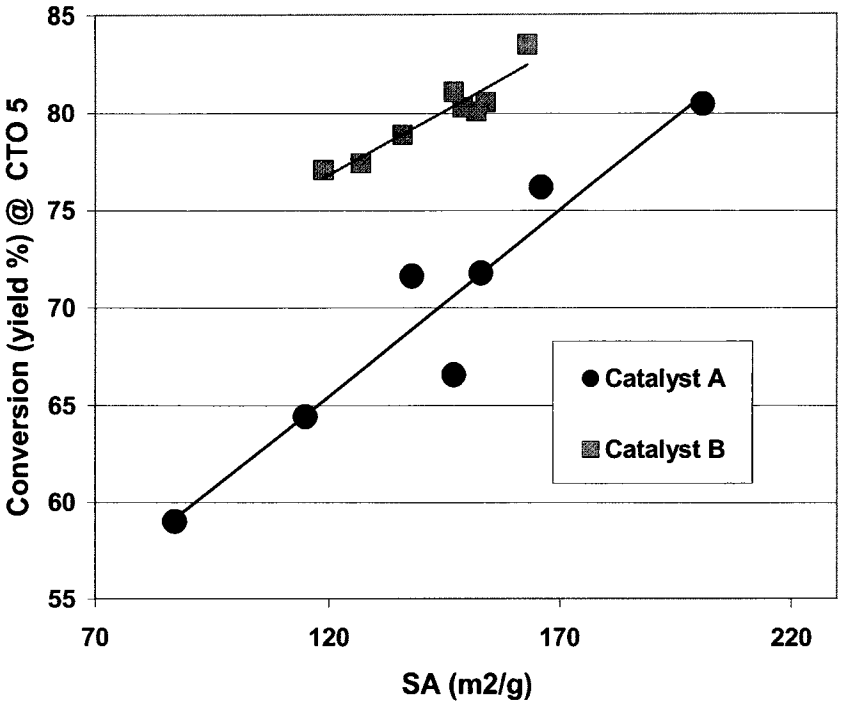

Figure 5. Conversion yield vs. deactivated surface area for Catalysts A and B.

It should be noted that the LCO/bottoms ratio for the deactivated catalyst resulting from Catalyst A treated by CD-ALFA with iron alone (no added vanadium) does not appear to conform to the rest of the data. While this sample exhibits a significantly attenuated AAI (0.3), the lowered accessibility does not seem to be reflected in the performance testing. Also noteworthy, however, is that although the accessibility has dropped dramatically for this sample, the total surface area falls well above the range for typical e-cats, and is certainly much higher than all the other deactivated samples in this set. This, along with the absence of V in this deactivation, suggests that there are additional effects of surface area and metals interactions that have yet to be explained. For this data set, only catalysts deactivated with both Fe and V demonstrate significant AAI attenuation *and* the expected LCO/bottoms effects consistent with the e-cat testing.

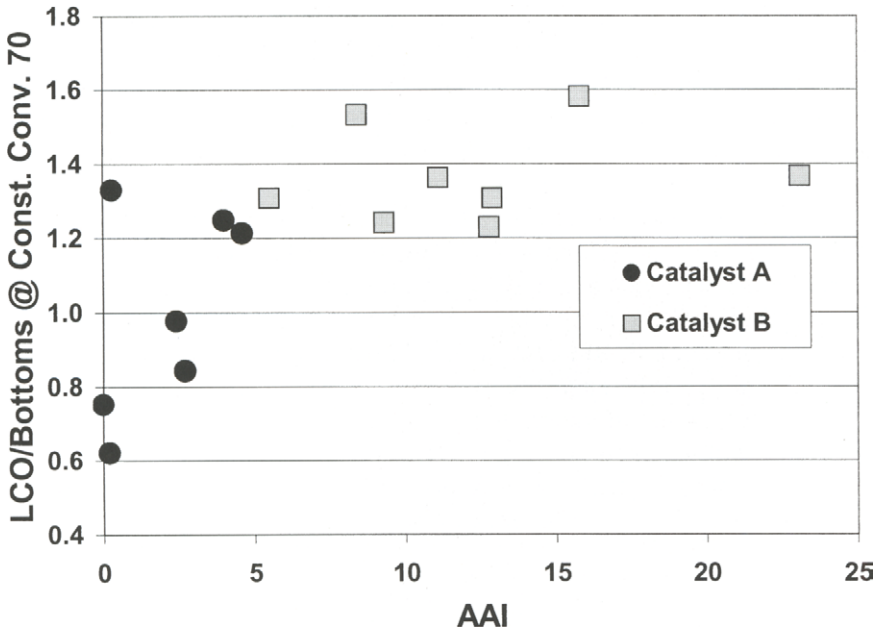

Figure 7. LCO/bottoms vs. AAI at 70% conv. for deactivated catalysts sets A and B.

The FST features long catalyst-feed contact times relative to those of typical FCCU operations and this tends to damp out accessibility related performance effects. Nevertheless, the impact of AAI on LCO/bottoms yields in the FST is clear, both for the e-cats and the lab-deactivated samples studied here. If these two deactivated catalysts could be compared in an actual FCCU, the shorter contact time would lead to more dramatic performance differences. In fact, these differences would be expected to extend to the overall conversion and absolute bottoms yields, as has consistently been observed for comparable AAI differences in commercial data in a variety of applications [1-8].

4. CONCLUSIONS

FCC's undergo specific types of chemical and physical changes as a result of iron contamination, leading to decreased accessibility and deterioration in catalyst performance, particularly with regard to bottoms cracking. This decrease in accessibility is not simulated by most routine lab-scale deactivation methods, including Mitchell impregnation (along with derivative methods, such as Cyclic Propylene Steaming) and conventional CD.

The CD-ALFA method, which employs steaming conditions more commensurate with actual FCCU regenerators, allows significant AAI decreases to be induced as a function of added iron and vanadium, simulating the behavior observed in commercial FCCU's. Furthermore, these accessibility drops achieved in the lab impact the catalyst performance testing results in a manner consistent with that observed for commercial e-cats.

That the absolute deactivated AAI level has a significant impact on FCCU performance has been amply demonstrated. This is reflected in the lab-scale testing reported here by the dependence of the LCO/bottoms ratio on AAI at the lower end of the accessibility scale. Because high accessibility catalysts (those with fresh AAI > 5) can undergo significant accessibility losses as a result of iron contamination, and yet still retain relatively high AAI's, they are more likely to allow the FCCU to operate in the regime above the critical accessibility threshold and are thus eminently suitable for high-iron, resid applications. Furthermore, the catalysts with the very highest fresh AAI's (>12) have demonstrated the best sustained performance in the face of elevated iron levels.

REFERENCES

[1] M. C. J. Hodgson, C. K. Looi, S. J. Yanik, Proc. Akzo Nobel Catalyst Symposium, Noordwijk, The Netherlands, June 1998.
[2] E. Rautiainen and P. van Krugten, Catalyst Courier 40 (2000).
[3] P. Imhof, E. Rautiainen, and K.Y. Yung, Catalyst Courier, 48, (2002).
[4] P. A. Lane and S. J. Yanik, Catalyst Courier 41 (2000).
[5] S. Foskett and E. Rautiainen, Hydrocarbon Processing (2001) 71.
[6] A. K. Hakuli, P. Imhof, and C. W. Kuehler, Proc. Akzo Nobel Catalyst Symposium, Noordwijk, The Netherlands, June 2001.
[7] R. Fletcher, A. Hakuli, and P. Imhof, Oil and Gas Journal, (2002) 54.
[8] K.Y. Yung, R.J. Jonker, and B. Meijerink, ACS National Meeting August 2002 Boston, MA.
[9] D. R. Rainer, E. Rautiainen, and P. Imhof, Applied Catalysis, submitted for publication.
[10] E. Rautiainen and B. Nelissen, Hydrocarbon Engineering, submitted for publication.
[11] W.S. Wieland and D. Chung, Hydrocarbon Engineering, March 2002.
[12] P. O'Connor and A.P. Humphries, "Accessibility of functional sites in FCC" ACS preprints vol. 38, no. 3, p. 598, 1993.
[13] L.A.Gerritsen, H.N.J.Wijngaards, J.Verwoert and P.O'Connor, "Cyclic deactivation: A novel technique to simulate the deactivation of FCC catalysts in commercial units", Catalysis Today, 11 (1991) p 61-72
[14] P. O'Connor and A.C. Pouwels, "Realistic commercial catalyst testing in the Laboratory." Proceedings of 8th International Symposium on Large Chemical Plants, Royal Flemish Society of Engineers, Antwerp, October 1992.
[15] R. Pimenta, A. R. Quinones, and P. Imhof, Proc. Akzo Nobel Catalyst Symposium, Noordwijk, The Netherlands, June 1998.
[16] D. Rainer, E. Brevoord, J. Gonzalez, and P. Imhof, Appl. Catal. A, submitted for publication.
[17] G. Yaluris, W.-C. Cheng, M. Peters, and L. Hunt, Proc. NPRA Annual Meeting, New Orleans, LA, 18-20 March 2001.
[18] D. R. Rainer, C. Vadovic, E. Rautiainen, and B. Nelissen, in preparation.

Studies in Surface Science and Catalysis, volume 149
M. Occelli (Editor)

Reduction of NO_x emissions from FCCU regenerators with additives

D. M. Stockwell and C. P. Kelkar

Engelhard Corporation, Iselin, NJ, USA

Environmental emissions, particularly NO_x emissions, have been a growing concern for refiners in recent years. NO_x emissions from the regenerator are primarily derived from nitrogen in the coke. This work describes the development of active oxides as catalysts for reduction of NO_x. Chemisorption of NO was used as a screening tool to measure and rank performance of metal oxides. The fresh capacity, and more importantly the hydrothermal stability of the chemisorption capacity, of the oxides were considered. Performance of these active oxides formulations were also evaluated during regeneration of spent FCC catalyst in a fluid bed. The resulting materials reduced FCCU NO_x in full burn regeneration by as much as 30-70%.

1. INTRODUCTION

Since 1970, the Environmental Protection Agency (EPA) has tracked emissions of the six principal air pollutants termed criteria pollutants – carbon monoxide (CO), nitrogen oxides (NO_x), sulfur oxides (SO_x), volatile organic compounds (VOC), particulate matter (PM) and lead. Emissions of all of these pollutants have decreased significantly, except NO_x that has increased approximately 10% over this period [1]. NO_x has been identified as the primary cause for formation of ground level ozone (smog) formed when NO_x reacts with VOC's in the presence of heat and sunlight. In 1997, as part of the revision to the Clean Air Act, the EPA issued a stricter ozone standard of 0.08 ppm averaged over an 8-hour period, compared with the older standard of 0.12 ppm averaged over a 1-hour period. According to the EPA, motor vehicles account for 49% of the NO_x emissions [2], utilities contribute about 27%, and industrial and commercial factories account for about 19% of the emissions.

While petroleum refining represents only 5% of the total emissions, these emissions are often concentrated in small areas. Many refineries are located in

so called "non-attainment areas" and can significantly contribute to local concentration of NO_x and the concomitant ozone. The 1997 revision of the Clean Air Act includes a new source review (NSR) requirement, applicable when refineries make modifications that increase emissions. NSR standards require facilities to apply best available control technology (BACT) or lowest achievable emissions reductions (LAER) when grandfathered units are expanded in a way that increases emissions. As of this writing nine refining companies, covering over 30% of the U.S. refining capacity, have voluntarily signed consent decrees with the EPA. The consent decrees will result in criteria pollutant emission reduction of nearly 150,000 tons per year, including NO_x emissions reduction of nearly 20,000 tons per year. The EPA also is negotiating settlement agreements with several other companies comprising an additional 30% of the domestic refining capacity.

In fluid catalytic cracking (FCC), an inventory of microspherical catalyst is circulated between a riser-reactor and regenerator. Hydrocarbon feed contacts the clean regenerated catalyst in the riser reactor at 1000-1200°F. High boiling hydrocarbon feeds crack to produce lower boiling components such as light cycle oil, gasoline, C_3-C_4 hydrocarbons etc. Cracking reactions also deposits coke on the catalyst. The cracked products are separated from the spent catalyst by steam stripping. The catalyst is then transferred to the regenerator where the coke is exothermically burned to regenerate the cracking catalyst. Gaseous products of regeneration are CO, CO_2, H_2O, SO_X, NO_x, HCN, and NH_3.

This paper will deal with additives that will reduce NO_x emissions from a full burn regenerator.

1.1 Chemistry of NO_x formation

NO_x in the regenerator could hypothetically be formed by either of two mechanisms- thermal NO_x produced from the reaction of molecular nitrogen with oxygen or fuel NO_x produced from the oxidation of nitrogen containing coke species. Simple thermodynamic calculations have shown that thermal NO_x is not a significant contributor to total NO_x [3, 4]. To verify this, Dishman et al. [5] regenerated catalyst coked with isobutylene and compared this to catalyst coked with nitrogen-containing gas oil. At comparable regeneration conditions, NO was not detected with the isobutylene coked catalyst but was detected with gas oil coked catalyst. This experiment demonstrated that NO is not produced by thermal fixation of nitrogen. Zhao et al. [6] observed that in a circulating pilot plant, nitrogen-free feed did not produce NO_x emissions even in the presence of platinum promoter. This showed that even the local temperatures around the platinum promoter are not high enough to favor catalytic NO_x fixation from N_2.

The chemistry of how coke-bound nitrogen is converted to NO_x in an FCC is very complex and not well understood. However, analogies can be

drawn to several other processes that involve combustion of similar carbonaceous precursors. NO_x formation during combustion of coal has been well-investigated [7]. The nitrogen containing products were seen to be dependent on the type of coal and combustion conditions. For most coals, HCN was the primary gas phase N-containing species during pyrolysis. NH_3 appeared at the same time as H_2, suggesting that NH_3 is a secondary product of HCN reduction. It is thought that cleavage of heterocyclic forms of nitrogen compounds might be the source of HCN. Lower rank coals with more amino groups did produce some NH_3 as a primary product. Oxygen at low partial pressures actually increased HCN and decreased NH_3 as it scavenges the H_2 otherwise available for reduction. At higher oxygen partial pressures both HCN and NH_3 are oxidized to NO [7].

Regeneration of spent hydroprocessing catalyst also involves oxidation of nitrogen containing precursors from the catalyst surface [8, 9] and similar products were observed. Interestingly, total yields of NO, HCN and NH_3 accounted for only about one-third of the total nitrogen in coke. This indicated that major portion of the nitrogen in coke is converted either directly or indirectly to molecular nitrogen.

Recent environmental concerns have spawned an increasing interest in understanding NO_x chemistry in FCCU's. There are two basic families of regeneration processes, full and partial burn. In partial combustion mode, exactly as the term implies, coke is partially burned off the catalyst. This is achieved by using less than the stochiometric level of air. Typical exit gas composition in partial burn combustion is: 0.4 % O_2, 15% CO_2, 12% H_2O, 200 ppm SO_2, 500 ppm NH_3, 100 ppm HCN, 4% CO and balance nitrogen [10]. For both environmental and economic reasons, this CO rich flue gas is sent to a CO boiler. In the boiler the reduced nitrogen species can be oxidized to NO.

In the full combustion mode, coke is more completely burned off the catalyst. This is achieved by using greater than stochiometric amount of air and also by using platinum-based promoters to oxidize carbon monoxide to carbon dioxide. Typical exit gas composition in full burn combustion is: 1.0 wt% O_2, 16% CO_2, 100 ppm CO, 12% H_2O, 400 ppm NO, 15 ppm N_2O [11]. It should be noted that the above gas compositions are meant to convey ranges and will vary from unit to unit. The presence of precious metals and an oxidizing environment increases the oxidation of the reduced nitrogen species to NO and N_2O. At regenerator temperatures thermodynamics favors NO over NO_2. Therefore although the term NO_x is commonly used in referring to emissions, the primary constituent is NO.

Recently Dishman et al. [5] and Zhao et al. [6] have carried out regeneration studies to study the evolution of gas phase nitrogen species during spent FCC catalyst regeneration. Temperature programmed oxidation (TPO) of spent catalyst in both studies show that carbon oxides evolve first and NO_x

evolution is observed only after most of the coke has been oxidized. Dishman et al. [5] analyzed the spent catalyst for C and N during the regeneration process. Results of these experiments showed that nitrogen is removed throughout the regeneration. Therefore, it was believed that molecular nitrogen is more likely a secondary product from the reduction of NO either with CO or coke [5].

In addition to the pathways involving nitrogen species there are several other competing reactions. Each of these competing reactions can affect the nitrogen pathway by either occupying a catalytic site or by affecting the concentration of another reactant. The most critical one is the CO promotion pathway. The presence of a platinum additive promotes oxidation of CO to CO_2. A decrease in the CO concentration in the regenerator reduces the rate of the NO + CO reaction, causing the NO_x emission from the regenerator to increase. NO_x emissions could also increase because platinum is catalytically active for oxidation of NH_3/HCN to NO_x. Whichever mechanism applies the increase in NO_x emissions when using a platinum-based CO combustion promoter has been observed in many commercial units.

1.2 Strategies for reducing NO_x

Several approaches are available to deal with NO_x. These are (a) feed hydrotreating to remove NO_x precursors, (b) FCC process hardware for reducing NO_x formation, (c) catalytic approaches compatible with the FCC reactor which will either suppress NO_x formation or catalyze its reduction, and (d) "end of the tailpipe" type solutions like SCR/SNCR.

Feed hydrotreating is the most expensive approach. It also limits the refiner's flexibility in terms of being able to use different feedstocks and is probably not viable strictly from a NO_x perspective. Process approaches focus on modifying the regenerator to facilitate better contact between NO and CO or coke. An example is Kellogg's Orthoflow regenerator that is claimed to produce 60-80% lower NO_x than other designs [12]. These types of options are not immediately implementable by a refiner for an existing unit and may require drivers in addition to NO_x reduction. Selective catalytic reduction (SCR) is a proven approach to reduce NO_x with NH_3. It has well-established history in reducing NO_x in gas turbines and coal fired power plants but needs to be properly evaluated for FCCU's.

Catalytic approaches that can be employed inside an FCC are a very cost efficient and rapid way to reduce NO_x. These materials are commonly referred to as additives in FCC literature, due to small amounts required to be blended in the circulating FCC inventory, but these additives are catalysts in their own right. A comprehensive review of all the additives for NO_x reduction is not within the scope of this paper, but a review of different additives evaluated prior to 1998 can be found in Chen et al. [3]. A number of different classes of materials, such as perovskite- based, spinel-based, lanthanum or yttrium oxides,

titanates, copper impregnated on ZSM-5, and ceria-based materials [6] have found to reduce NO_x. Ceria based materials utilize the redox ability of ceria to cycle between Ce^{3+} and Ce^{4+} oxidation states. Ceria is reduced in the riser and serves as an agent to reduce NO in the regenerator. The presence of reducing agents in the regenerator will be required to maintain the ceria in the +3 state. Copper oxide is also part of many NO_x reducing additive formulations [13]. Mixtures of NO and propane used to simulate reducing conditions were shown to reduce NO with high activity. As oxygen was introduced into the mixture the NO conversion activity declined. This could be due to the oxidation of hydrocarbon being the preferred route and the desired reductant no longer available for NO_x reduction.

2. EXPERIMENTAL

2.1 Catalysts

We prepared a series of additive formulations. An alumina support with particle and attrition characteristics suitable for use in cracking applications was used. Different active components were deposited on the support by incipient wetness impregnation of nitrate salts. A constant level of copper oxide was included in the formulations. After drying overnight, the catalysts were calcined at 1200° F for 2 h. For additive D where the solution of total nitrate required exceeded the pore volume, the process was repeated with a calcination step in between.

Deactivation of the additives was done by steaming at 1500°F for 4 h in 100% steam. Chemical and physical characterization of the different additives evaluated in this work is shown in Table 1.

2.2 Testing

Catalytic performance of the additive was evaluated by NO chemisorption, NO/CO testing and temperature programmed oxidation of coked cracking catalyst.

Table 1
Chemical and physical characteristics of different catalysts

Catalyst	Composition	Surface Area ($m^2.g^{-1}$)	Pore Volume ($cc.g^{-1}$)
A	9.6 wt% CeO_2	90	0.42
B	5.5 wt% Active oxide	75	0.39
C	10.5 wt% Active oxide	92	0.31
D	20.7 wt% Active oxide	78	0.32

2.2.1 NO chemisorption

NO chemisorptions were carried out in a fixed bed reactor. The reactor was connected to a manifold that permitted us to feed NO containing gas stream to the reactor after appropriate pretreatment. Typically 1.0 g of additive was blended with inerts to make 2 g of total solids in the reactor. The catalyst was pre-reduced in H_2 at 1300°F. Upon cooling down to room temperature (< 80°F) flow was switched to an argon stream containing 235 ppm NO. We used both a chemiluminescence meter and a quadropole mass spectrometer to measure the gaseous effluent during chemisorption. Both fresh and deactivated additives were tested for NO uptakes.

2.2.2 NO/CO testing

Steady state testing of NO/CO chemistry was carried out in a fixed bed reactor at 1300°F for the deactivated additives. After pre-reduction in H_2 at 1300°F and sweeping with Ar, flow was switched to a gas stream consisting of 235 ppm NO and 400 ppm CO at 1300°F. This type of test at slightly "rich" condition has been described earlier [14]. At these conditions spent promoted equilibrium catalyst by itself yielded 0% NO conversion. Compare this to previous work [5] which showed that exposing spent equilibrium cracking catalyst; to a stream consisting of 124 ppm NO/ 10% CO gave ~100% NO conversion.

2.2.3 TPO of coked catalyst

Coking and regeneration experiments were performed in a fixed fluid bed reactor. Coke was deposited with a light gas oil (CCR = 0.39%) containing 938 ppm total nitrogen at 970°F. Regeneration was done in a 19% O_2 containing gas stream while ramping from 970° to 1300°F. Carbon and nitrogen oxides generated during the TPO were measured by infrared and chemiluminescence cells respectively. Similar type of test with some variation has been reported earlier [15].

Each deactivated additive was blended to a 2 wt% level with a promoted commercial equilibrium catalyst (ECAT). The ECAT had a surface area of 171 $m^2.g^{-1}$ with a zeolite surface area of 95 $m^2.g^{-1}$ and contained 262 ppm and 615 ppm Ni and V respectively. 9 g of catalyst/additive blend was used for each experiment. Different amounts of coke were deposited on the catalyst by changing the amount of oil fed to the reactor.

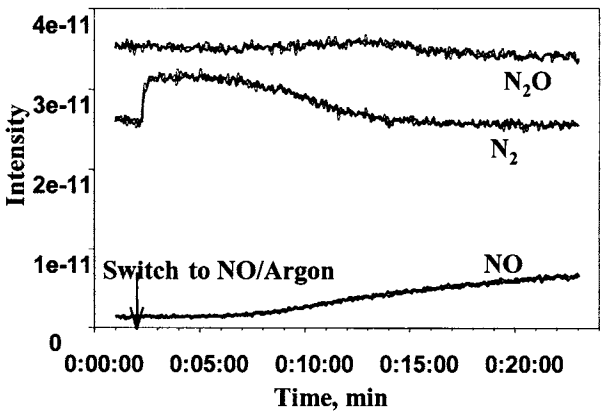

Fig. 1: NO chemisorption over bulk ceria

3. RESULTS & DISCUSSION

3.1 NO titration

We hypothesize that NO reduction takes place via a Langmuir-Hinshelwood type of mechanism involving dissociative adsorption of NO. This adsorption tendency for NO was evaluated in the laboratory for many different materials. Typical results are shown in Figure 1. Introduction of NO gas causes the N_2 signal to immediately and sharply increase. This shows that dissociative adsorption of NO and recombination and desorption of molecular nitrogen are facile, even at room temperature. As the surface of the material is saturated with the left over adsorbed oxygen, breakthrough of NO occurs. The areas over the curve for NO after subtracting for the appropriate physical lag measures the total number of sites available for dissociative adsorption. In the regenerator, CO will scavenge the adsorbed oxygen, producing CO_2. This in turn makes the site available for further reaction, thereby completing the catalytic cycle.

NO uptake capacity of commercially available CeO_2 was measured (Table 2). The cerium oxide was then deactivated by calcining or steaming at 1500°F.

Table 2
NO titration of calcined and steamed cerium oxide

	NO uptake mmol. g-1	NO uptake retention (%)	Surface area retention (%)
As-is	0.233		
Calcined @ 1500°F	0.046	20	11
Steamed @ 1500°F	0.035	15	7

These results are also shown in Table 2. There is an 80% loss of NO uptake capacity upon calcination and further additional 5% loss of capacity upon steaming.

At the harsh conditions of steam and temperature prevailing in the regenerator, catalytic materials deactivate. Additives are no different. Hence additives with higher steamed NO uptake capacities, i.e. more sites, should have improved performance. At room temperature, the sites we are titrating are probably mainly the surface sites with very little sub-surface oxidation. At higher temperatures, NO uptakes would be higher due to sub-surface oxidation. We believe that in a regenerator, oxidation-reduction cycling of a site is rapid and only surface sites take part in NO_x reduction.

NO uptakes were measured on fresh and steamed additive A through D. Results are shown in Table 3. Note that A is a base formulation containing only cerium and copper oxides. Additives B through D are proprietary active oxide formulations with sequentially increasing loadings that also have a constant level of copper oxide. Surface area retentions in these cases are primarily a measure of surface area loss of the support.

Note that additive A has slightly more than ten times the steamed NO uptake of bulk ceria on a per unit of ceria basis. This is expected if only surface sites participate, since supported ceria should have better dispersion. Additionally, copper oxide is also present in additive A, which will contribute some to the uptake. In this work, we have not tried to separate the effects copper oxide and ceria and their dispersions.

Building on the deactivation hypothesis, proprietary active oxide formulations were developed with steam stability features superior to ceria.

Additive B had fresh NO uptake capacity approximately half that of A. This is roughly in line with half the oxide content for B. The important difference is the steamed NO uptakes are almost identical. Therefore we see that these proprietary oxides can provide same number of sites for NO uptake at half the oxide loading. This could translate to a refiner needing to use less additive to achieve a constant NO_x reduction.

Table 3
NO uptake capacities of different steamed additives

Catalyst	NO uptake fresh, mmol.g-1	NO uptake steamed, mmol.g-1	Uptake Retention (%)	Surface area retention (%)
A	0.045	0.010	22	84
B	0.018	0.012	65	85
C	0.038	0.024	62	76
D	0.078	0.046	59	74

Doubling the active oxide loading from 5.5 (B) to 10.5 (C) doubled both the fresh and steamed NO uptakes. Further doubling the active oxide loading from 10.5 to 20.7, further doubled the uptakes. This suggests that the dispersion of active oxide is remaining fairly constant over a wide range of loadings, and that the relative dispersions are not being affected by deactivation. Note that additives A and C have very similar oxide loadings and show very similar fresh uptakes. Once again, the improvement is evident in the steamed uptakes. Additive C has twice the uptake as that of A.

It is expected that providing sites for NO dissociation will lead to NOx reduction. If these sites deactivate rapidly, additive performance will also degrade. By providing active oxides with sites for NO reduction that are less prone to deactivation, the performance of the additive should be improved relative to ceria-based additive at constant loadings.

3.2 NO/CO testing

Steamed additives were also tested for NO conversions under slightly fuel-rich conditions, as described earlier. NO conversions at two different weights of additives in the blend are shown in Table 4. Considering that additive B had a slightly higher NO uptake than A, it is expected that B would display slightly higher NO conversions. Although the NO conversions with both the formulations are very close, additive A displayed somewhat higher NO conversion at both active weights. We believe the differences are small but we are continuing to investigate the reason for it. Systematically increasing the loading of active oxide from additive B through D increased NO conversion as would be expected.

The similarity between results from NO uptake and NO/CO conversion are expected if only surface sites are involved. Both the tests are just different ways of measuring sites for NO dissociation. In one case we are measuring how many sites are available for dissociation of NO. In the second case the oxygen atom left over after the dissociative adsorption of NO is being rapidly scavenged by CO thus regenerating the site.

3.3 TPO studies

Cracking catalyst regeneration studies were used to further test additive

Table 4
% NO conversions at two different weights of additives for the NO/CO test

Catalyst	0.05 g	0.15 g
A	16	62
B	12	56
C	23	72
D	36	85

formulations. The test employs the full sequence of reactions of nitrogen deposition in coke via cracking gas oil, through NO_x generation from coke during coke burning in air. It also employs realistic conditions for oxygen, from its compositional gradients due to the introduction of air near the bottom of a fluid bed, to the formation of oxygen-rich bubbles in the midst of carbon-containing catalyst, and the nearly complete consumption of oxygen during coke combustion. Although not shown here, the profiles of CO, CO_2, NO and O_2 look similar to the earlier work of Dishman et al. [5] and Zhao et al. [6]. Figure 2 shows total integrated NO_x evolved vs. total integrated coke regenerated during a run. This data was generated from a conventional C/O study. As C/O was decreased from 9 to 3, total coke on catalyst increased from about 45 to 60 mg. As more coke is deposited on the catalyst, more NO_x is emitted during the regeneration. Assuming that the carbon to nitrogen ratio of the coke is not changing dramatically with C/O, it makes intuitive sense that more NO_x is emitted from catalyst with more coke.

ECAT makes ~15 to ~20 μmoles of NO_x with increasing coke in the C/O study. The same C/O experiment was repeated but with the ECAT blended with 2% by weight of deactivated additives, A through D. All the additives lowered NO_x emissions compared to the ECAT. Additives A and B, both demonstrated ~ 30-35% NO_x reduction over ECAT. Increasing the weight of active oxide loading from 5.5 wt% to 10.5 wt% further decreased NO_x by an additional 7 % for a total of 41% reduction over ECAT. Subsequent increases in loading of the active oxide to 21 wt% (D) did not further lower NO_x emissions.

Compared to the previous two tests, which relied on NO as a target molecule, this test involves regeneration of FCC coke. This in essence permits the in situ formation of NO_x, as it would be in a commercial unit. It is pleasing to note some similarities between the different tests. Additive A and B have similar number of sites available for NO decomposition. The NO_x reductions obtained in the TPO test were also similar. Doubling the active oxide loading from B to C to D had a proportional response on the number of sites. The NO_x reduction due to additive C in the TPO test was also higher, but returns were clearly diminishing. Additive D, for example did not lead to any further NOx reduction. Apparently the higher number of active sites could not be fully utilized for some reason in the TPO test. On the other hand, in one commercial trial, we did test additives with two different oxide loadings and saw a more proportionate response.

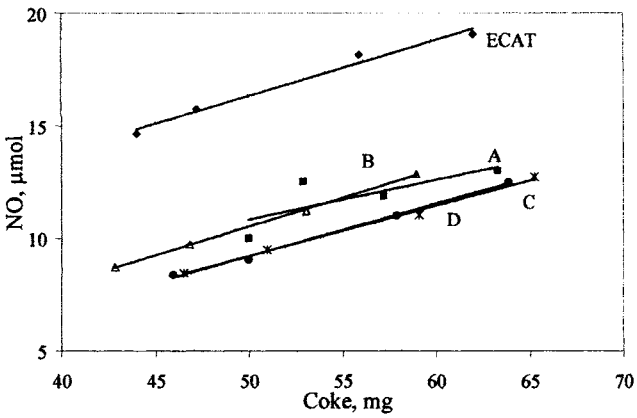

Fig. 2: TPO of coked blends of ECAT's with different catalysts

Analysis of cracking yields done as part of the TPO experiments showed a small increase in H_2 yields (+0.02 wt %) at constant conversion. There was no impact for increasing the loading of active oxides on hydrogen yields and the debit was constant across all the tested formulations.

3.4 Commercial trial

A refinery trial of the new NO_x control additive was performed on a full burn unit that has an average baseline NO_x level of approximately 65 ppm and uses oxygen enrichment. During the trial period the exit oxygen concentration was maintained between 0.4 to 0.6 wt% and the total feed nitrogen was around 550 ppm. The unit continued to use a conventional platinum-based CO combustion promoter during the trial to control afterburn at a relatively constant level. We observed about 48% reduction with a formulation similar to those described in this paper. A statistical process model confirmed these results [16]. The unit observed no noticeable change in coke or dry gas yields during the additive trial.

4. CONCLUSIONS

We have developed new, proprietary additives for NO_x reduction that have improved steam stability compared to previously known ceria materials. The improved steam stability translates to better NO_x reduction in an FCCU. We used chemisorption of NO at room temperature to titrate for NO decomposition sites. Steady state testing with slightly rich NO-CO mixture at regenerator temperatures validated the effectiveness of these sites. TPO of spent cracking catalyst blends was also used to comprehensively simulate regeneration

chemistries in the laboratory. The TPO test confirmed improved performance of additives with enhanced steam stability, and commercial trials have validated these laboratory results.

REFERENCES

[1] National Air Quality – 2000 Status & Trends, U. S. Environmental Protection Agency, September 2001.
[2] NO_x – How Nitrogen Oxides Affect the Way We Live and Breathe, EPA, Office of Air Quality Planning and Standards, September 1998.
[3] W.-C. Cheng, G. Kim, A. W. Peters, X. Zhao, K. Rajagopalan, M. S. Ziebarth and C. J. Pereira, Catal. Rev.-Sci. Eng., 40 (1998), 39.
[4] A. W. Peters, X. Zhao and G. D. Weatherbee, NPRA AM-95-99 (1995).
[5] K. L. Dishman, P. K. Doolin and L. D. Tullock, Ind. Eng. Chem. Res., 37(1998), 4631.
[6] X. Zhao, A. W. Peters and G. W. Weatherbee, Ind. Eng. Chem. Res., 36(1997), 4535
[7] M. A. Wojtowics, J. R. Pels and J. A. Moulijn, Fuels Process. Tech., 34 (1993), 1.
[8] E. Furimsky, A. Siukola and A. Turenne, Ind. Eng. Chem. Res., 35(1996), 4406.
[9] P. Zeuthen, P. Blom and F. E. Massoth, Appl. Catal., 78(1991), 265.
[10] G. L. Johnson, N. C. Samish and D. M. Altrichter, US Patent 4,744,962 (1988).
[11] D. A. Cooper and A. Emanuelsson, Ener. & Fuels, 6(1992), 172.
[12] R. B. Miller, T. E. Johnson, C. R. Santner, A. A. Avidan and J. H. Beech, NPRA AM-96-48 (1996).
[13] A. Corma, A. E. Palomares, F. Rey, F. Marquez, J. Catal., 170 (1997), 140.
[14] A. Bhattacharya, M. J. Foral, W. J. Reagan, US Patent 5,750,020 (1998).
[15] A. A. Chin, US Patent 5,021,146 (1991).
[16] C. P. Kelkar, D. M. Stockwell, S. Winkler, S. Tauster, J. A. Sexton, G. A. Cantley, J. P. Wick, NPRA AM-02-56 (2002).

Studies in Surface Science and Catalysis, volume 149
M. Occelli (Editor)

Oxygen partial pressure effects on vanadium mobility and catalyst deactivation in a simulated FCCU regenerator

G. Krishnaiah, L. V. Langan, J. A. Rudesill, and W-C. Cheng

GRACE Davison, W.R. Grace & Co. – Conn., 7500 Grace Dr., Columbia, MD 21044

The rate of interparticle vanadium transfer in FCC catalysts as a function of the degree of oxidation of the steaming environment has been determined. The rate of interparticle vanadium transfer is low when the atmosphere in the steamer is reducing, but increases dramatically as the mole % excess oxygen becomes greater than zero. High rate of vanadium transfer is accompanied by a greater loss of surface area and catalytic activity. XPS measurements show that the oxidation state of vanadium increases from +3 when the steamer atmosphere is reducing to +5 when the % excess oxygen is greater than zero. Surface vanadium concentration follows a similar trend. In addition, data from a commercial resid FCCU operating in a partial burn were analyzed. The results of the analyses show that defining a partial burn operation with the flue gas CO/CO_2 ratio is not adequate for characterizing the vanadium oxidation state. Carbon on regenerated catalyst is a better marker for the vanadium oxidation state in the regenerator.

1. INTRODUCTION

The Fluidized Catalytic Cracking Unit (FCCU) remains the "heart" of the refinery, even more so with the recent demand for clean fuels. The demand for high-octane gasoline (albeit low sulfur) has remained unchanged with increased emphasis on alkylate feed. Narrow refining margins and increasing crude prices are limiting the refiners processing flexibility. Crude run reductions and increased bottom of the barrel (resid) processing in the FCCU are natural outcomes of these factors.

Resid processing in the cat cracker brings with it additional challenges. The poorer feed quality and increased Conradson Carbon Residue (CCR) results in decreased yield selectivity and increased coke yields. The higher coke yields require heat rejection options such as catalyst coolers or partial burn regenerator operation. Resid feeds bring along increased nickel and vanadium contaminants (as porphyrins) that deposit quantitatively on the catalyst, negatively impacting catalyst activity and yield selectivity. The dehydrogenation activity of nickel and vanadium results in increased coke and dry gas yields. In addition, vanadium deactivates the catalyst by attacking the active sites and destroying the zeolite crystal structure. Furthermore, unlike nickel, vanadium tends to be very mobile, increasing its potential for deactivating the catalyst.

Nickel passivating technologies, such as antimony and specialized matrix materials, have allowed the refiner to process higher nickel containing feeds while minimizing the nickel related dehydrogenation activity. It has long been accepted though not quantified that vanadium is most mobile when it exists in the +5 oxidation state in the regenerator [1, 2]. Therefore it is reasonable to state that an effective catalyst management practice that would minimize catalyst deactivation with vanadium would ensure that the bulk of the vanadium is either maintained in the +4 or lower oxidation state or bound in a form that is not mobile. It also follows that one would expect vanadium mobility to be minimized in a partial burn operation (over a full burn operation).

Significant earlier work by several investigators has established that vanadium is mobile in laboratory catalyst deactivations that include 540 C calcination followed by 760 C steaming [3]. The mobile V species is reported to prefer a basic surface like layered magnesium silicate and to form heat stable vanadates such as beta-$Mg_2V_2O_7$ and $Mg_3V_2O_8$ identified by Laser Raman Spectroscopy (LRS) [4,5]. It is asserted that the mobile V species indicated is $H_2V_2O_7$ formed from steam and vanadia [6]. Ortho vanadates were not seen by either LRS or ^{51}V NMR; thus suggesting that H_3VO_4 may not be the mobile species [7,8]. Since $AlVO_4$ is not thermally stable, it will not likely provide vanadium passivation [9]. The exact nature of the mobile V species awaits actual in-situ detection, and that remains a difficult analytical challenge.

To the best of our knowledge, a systematic study evaluating vanadium mobility on catalysts between the partial and full burn modes has not been conducted. The objective of this work is to measure the rate of vanadium transfer as a function of the level of excess oxygen in the steaming environment. We conducted experiments in a modified Cyclic Propylene Steam (CPS) deactivation unit. The CPS deactivation method was introduced to simulate catalyst deactivation by metals in a commercial FCC unit [10,11].

2. EXPERIMENTAL METHODS

Properties of two commercially manufactured fluid cracking catalysts are shown in Table 1. The catalysts were selected based on the difference in their skeletal density so as to allow for easy sink/float separation. Catalyst D (Donor) was impregnated with 6000 ppm V (from vanadium naphthenate) and calcined at 1100°F. In a typical steaming experiment, a 100 gram sample, consisting of a 3 to 1 blend of vanadium impregnated Catalyst D and Catalyst A (Acceptor), was placed in a quartz reactor and immersed in a sand bath, maintained at 1400°F. The sample was fluidized and steamed for varying lengths of time (1, 2, 4 and 24 hours) in a mixture of steam, nitrogen, air, and 5% propylene in nitrogen. The atmosphere in the steam consists of 60 v% steam and 39 v% nitrogen; the remaining 1% is a mixture of oxygen and propylene. The flowrate of the air and 5% propylene streams was adjusted to give a wide range of propylene/oxygen molar ratios. Complete combustion of one mol of propylene to CO_2 and H_2O consumes 4.5 mols of O_2. We define:

$$\% \text{ Excess } O_2 = (\text{mols of } O_2 - 4.5 \times \text{mols } C_3H_6)/\text{total mols of gas}$$

The % excess O_2 concentration was varied from a deficient –3.7% (highly reducing) to an excess 1.07% (oxidizing). In each case, the total flows in the bed were adjusted to maintain the superficial gas velocity below 0.1 ft/sec.

Table 1.
Fresh catalyst properties

		Catalyst A	Catalyst D	Catalyst D (Post 6000 ppm V)	Blend: 75/25 (D/A)
Chemical Analysis:					
Al2O3	: Wt.%	49.85	33.47	34.13	37.87
RE2O3	: Wt.%	3.07	0.97	0.99	1.48
Na2O	: Wt.%	0.38	0.31	0.33	0.34
Ni	: ppm	27	<30	<19	<20
V	: ppm	48	30	5670	4240
Physical Analysis:					
SA	: M2/GM	314	252	249	268
Zeolite	: M2/GM	266	213	210	231
Matrix	: M2/GM	47	39	39	37

Steam deactivated catalysts were examined by X-ray Photoelectron Spectroscopy (XPS) to determine the surface composition and the oxidation state

of vanadium. The steam deactivated catalyst blend was separated by the variable density sink/float method that utilizes mixtures of tetra chloro and tetra bromo ethane solvents.

Both the sink and float fractions were characterized by ICP to determine the extent of vanadium migration from the donor (float) to acceptor (sink) fractions. Surface area (t-plot), zeolite unit cell size, and microactivity of the catalyst fractions were also determined.

3. RESULTS AND DISCUSSION

3.1. Vanadium Oxidation State and Surface Composition

The samples after the 24 hour steam were characterized by XPS. The binding energy (BE) values of vanadium are shown in Figure 1. As reference, V_2O_3 has a BE of 515.7 to 515.8 eV, and V_2O_5 has a BE of 516.6 to 517.7 eV. The data clearly illustrate that below 0% excess O_2, vanadium is in the +3 oxidation state. As % excess O_2 becomes positive, there is a sudden jump in the vanadium binding energy. Above 1% excess O_2, vanadium is essentially in the +5 oxidation state. Woolery et al., [12] have shown by x-ray absorption spectroscopy that the vanadium on catalyst is in the +4 oxidation state after hydrocarbon cracking and in the +5 oxidation state after regeneration in air. It is likely that our steaming conditions, with below stoichiometric oxygen (20 hours at 1400°F with excess propylene), is more reducing than a single cracking experiment (ca. 1 minute at 1000°F with 100% hydrocarbon).

The surface compositions of the 24-hour steamed samples, depicted as atomic ratios of V/Al and V/Si, are represented in Figure 2. Below stoichiometric O_2, V/Al and V/Si surface atomic ratios are essentially constant at 0.007. However, as the O_2 flow becomes higher than stoichiometric, there is a sudden rise in the surface V/Al and V/Si, indicating that the vanadium has become more mobile and is covering a greater fraction of the surface, i.e., by vapor deposition. This is consistent with the fact that the vapor pressure of vanadium is higher when it is in the +5 oxidation state, i.e., H_3VO_4 [1].

3.2. Sink Float Analyses

A plot of vanadium on both the donor and acceptor catalysts versus time, for the case of 1.07% excess oxygen is shown in Figure 3. The transport of vanadium is initially rapid when the concentration of vanadium on the donor

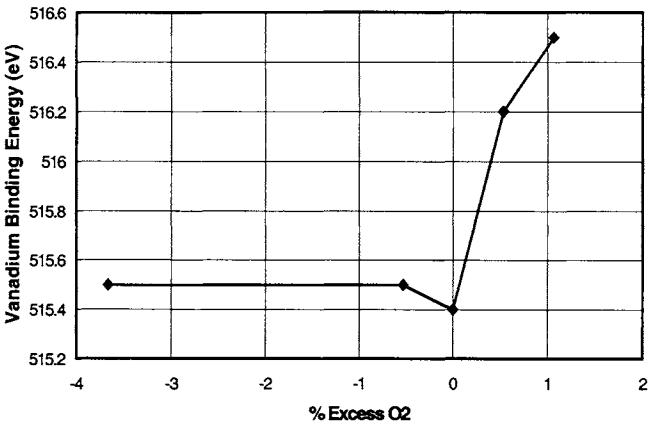

Figure 1. Binding energy of vanadium by XPS measurement

catalyst is high, but decreases and appears to level off after 24 hours. The steady state vanadium concentration is dependent on the relative affinity of the acceptor and donor catalyst for vanadium. In this case, the vanadium on the acceptor exceeded that on the donor after 24 hours.

The concentration of vanadium on the acceptor catalyst as a function of time and % excess oxygen is shown in Figure 4. When the atmosphere is reducing, the transport of vanadium is slow. However, as the relative proportion of oxygen in the bed is increased an increase in vanadium transport is observed. For all steaming durations, a maximum value of vanadium transport is reached when the bed oxygen content is in excess of stoichiometric combustion requirements. The loss in surface area and activity as a consequence of vanadium transport is shown in surface area Figures 5 and 6. The loss in catalyst activity and reduction in total surface area track each other well. During the shorter steam durations (1,2 and 4 hours), the loss in surface area and activity is less pronounced. This is attributed both to less hydrothermal deactivation and to lower amounts of vanadium transferred onto the catalyst. In comparison, the loss in activity and surface area is rather significant for samples steamed for a period of 24 hours. In particular, it is more pronounced when the relative oxygen concentration is in excess of the stoichiometric combustion requirements. The above results, which demonstrate the enhanced vanadium mobility with increasing oxygen concentration in the system, are consistent with an increasing fraction of vanadium in the +5 oxidation state.

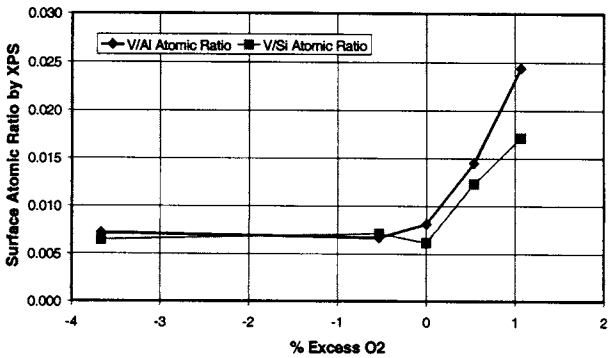

Figure 2. Surface composition determination by XPS

3.3. Commercial Example

There have been reports from the industry of catalyst deactivation in partial burn units, which show a strong correlation with the CO/CO_2 ratio in the flue gas at a constant vanadium and sodium level. This variation in unit catalyst activity has been noted as units drift in and out of partial burn (or varying degrees of partial burn). This paper documents a recent commercial refinery experience of catalyst deactivation with a change in the level of partial burn.

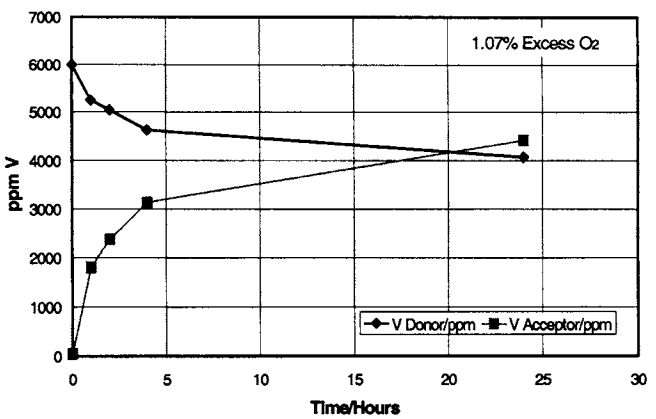

Figure 3. Interparticle vanadium transfer

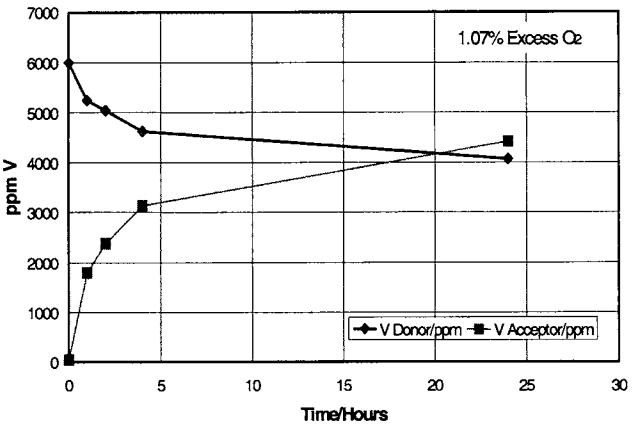

Figure 4. Vanadium on acceptor catalyst

This particular refiner operates the FCC regenerator in a partial burn mode. The FCC unit typically processes an aromatic resid with metals on Ecat ranging from 4000-6000 ppm vanadium and 3000-5000 ppm nickel. The unit is limited to processing resid with a CCR $\leq$ 4 wt% due to an air blower constraint. The refiner was interested in evaluating a more coke selective catalyst, as this would enable processing of incrementally higher CCR feedstocks. Soon after the catalyst (Catalyst "B") trial began, the refiner noticed a dramatic reduction in

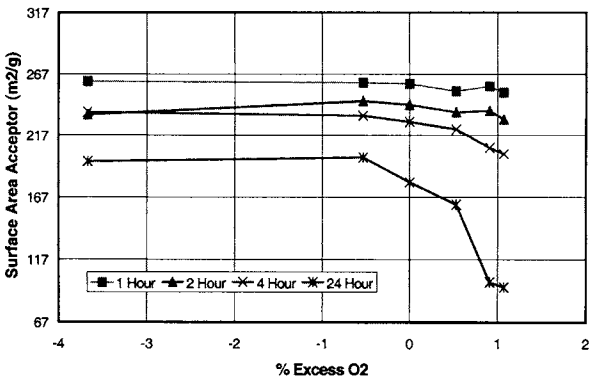

Figure 5. Surface area of acceptor catalyst

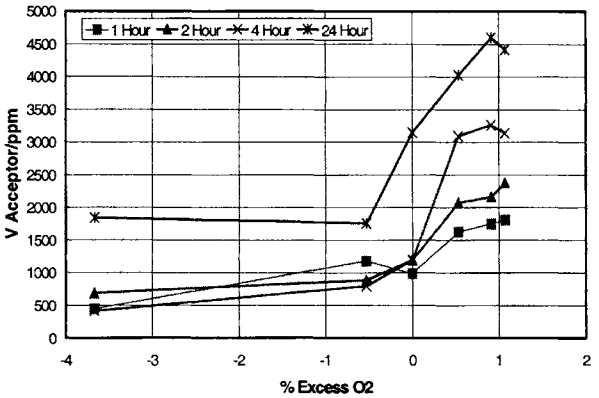

Figure 6. Microactivity of acceptor catalyst

equilibrium catalyst surface area and activity (Figures 7, 8). The catalyst deactivation could not be explained either on the basis of the regenerator temperature or increased metals on Ecat. These values remained within historical levels.

Upon evaluation, it became clear that the feed quality had actually improved! The refiner had switched to processing a more paraffinic crude with a FCC feed K factor ≥ 12.2! At one point, the regenerator temperature dropped dramatically and the refiner briefly used torch oil to increase regenerator temperature and lower catalyst circulation rate. A closer examination of the Ecat

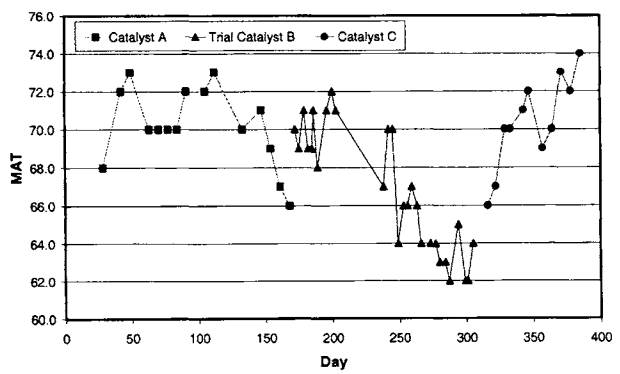

Figure 7. Ecat microactivity

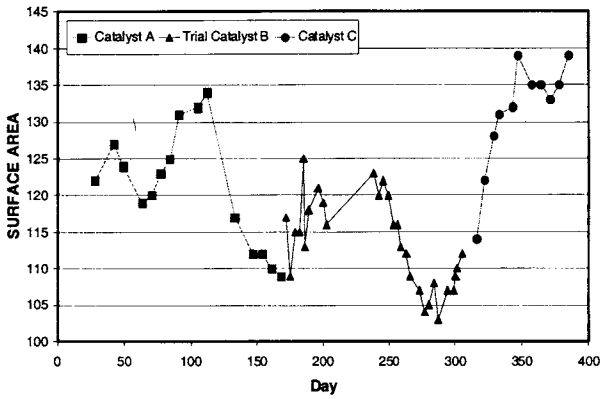

Figure 8. Ecat surface area

showed that the carbon on regenerated catalyst (CRC) had decreased, corresponding with the decrease in catalyst surface area (Figure 9).

For the most part during this period, the feed rate was nearly constant. The unit air rate was also fairly constant over the entire period and followed unit feed

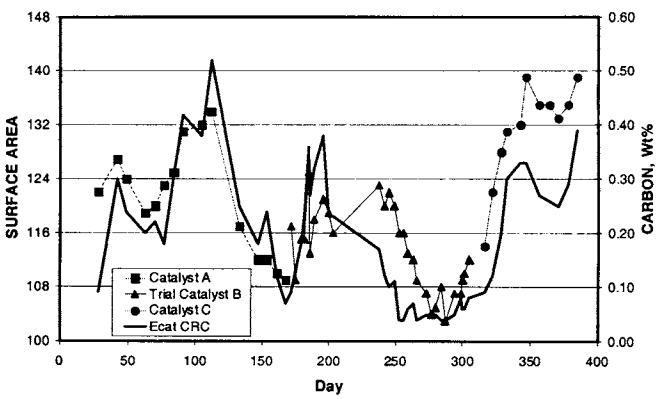

Figure 9. Partial burn RFCC regenerator surface area and carbon

rate. The regenerator flue gas CO/CO_2 ratio trended down (with Ecat CRC) during the same period (Figure 10). Hence the decrease in CRC should be the result of a reduction in delta coke–a consequence of processing a low delta coke feed and using a more coke selective catalyst.

It should be noted that the flue gas CO/CO_2 was within historical norms. However, the CRC on Ecat was at its lowest value in recent unit history. More importantly, this low CRC on Ecat was sustained for a period of more than two months. Taken in conjunction with the decreasing regenerator flue gas CO/CO_2 ratio, the reduction in Ecat CRC indicates an increasingly oxidizing atmosphere in the regenerator catalyst bed. It is clear that the vanadium mobility increased as a result of these changes in regenerator operation, resulting in increased catalyst deactivation.

In fact, the data indicate that surface area retention improved with increased CRC on the catalyst (Figure 11). Note that the differences in surface areas among the catalysts, at the higher CRC on Ecat, are due to the differences in starting fresh catalyst surface area.

3.4. Vanadium Mobility of Commercial Ecats

In order to get a better understanding of vanadium mobility in partial and full burn units, we analyzed Vanadium Mobility Index (VMI) data generated with Ecats collected from several units (both partial and full burn units). A

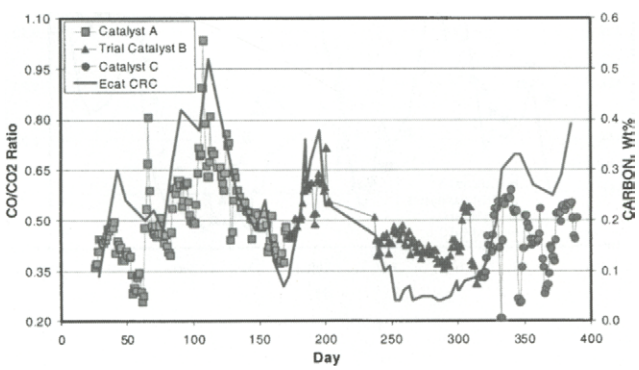

Figure 10. Partial burn RFCC regenerator CO/CO_2 and Ecat carbon

discussion of the VMI, and the experimental procedure for calculating the VMI for Ecat is described elsewhere [13]. Figure 12 shows that in general, the VMI for partial burn units is lower than for full burn units for the same level of vanadium. However, there appears to be no clear trend with vanadium.

As shown in the commercial example, CRC is a good indicator of the degree of partial burn or the degree of oxidation of the regenerator atmosphere. Low CRC on Ecat is an indication that a high proportion of the vanadium on Ecat is in the +5 oxidation state. Indeed Figure 13 shows that the experiments, which indicated that rate of vanadium transfer increases with vanadium concentration and % excess oxygen are also seen in the commercial FCCU.

VMI correlates well with the parameter vanadium divided by CRC. This suggests that for a given level of vanadium on Ecat, the vanadium mobility decreases as CRC on Ecat increases. This is true both for partial and full burn units. In short, we can infer that for a given unit, the "deeper" the unit is in partial burn, the lower is the vanadium mobility on Ecat. This is consistent with the laboratory steam deactivation experiments, which indicated that rate of vanadium transfer increases with vanadium concentration and % excess oxygen.

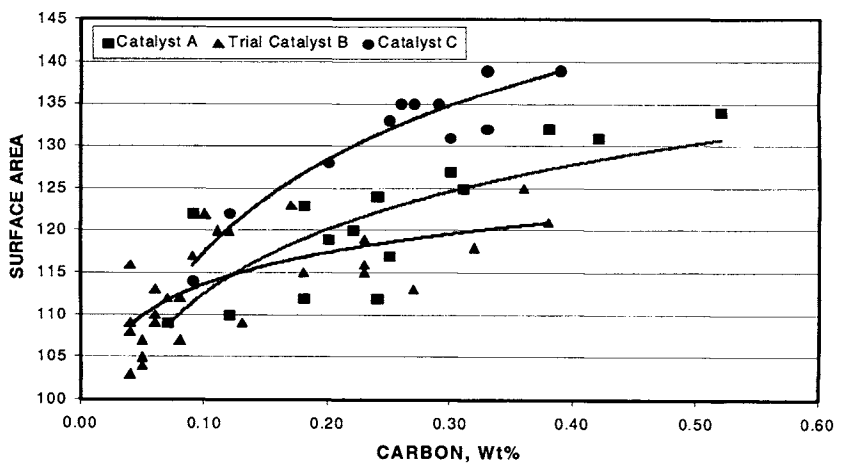

Figure 11. Partial burn RFCC Ecat surface area

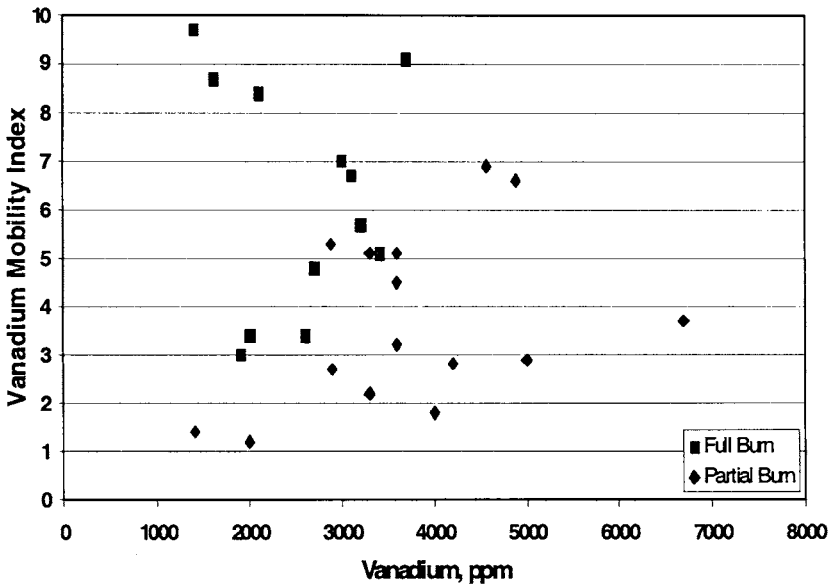

Figure 12. Vanadium mobility versus vanadium on Ecat

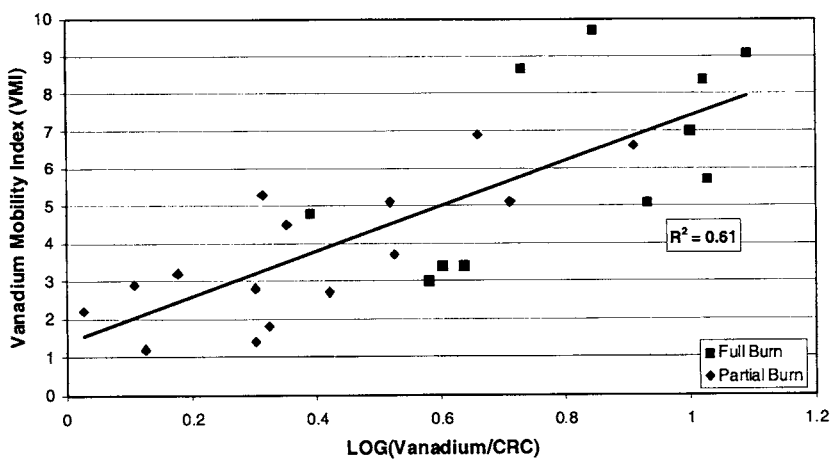

Figure 13. Vanadium mobility versus carbon on Ecat CRC

4. CONCLUSIONS

The rate of interparticle vanadium transfer is low when the atmosphere in the steamer is reducing, but increases dramatically as % excess oxygen becomes greater than zero. High rate of vanadium transfer is accompanied by a greater loss of surface area and catalytic activity. XPS measurements show that the oxidation state of vanadium increases from +3 when the atmosphere is reducing to +5 when the % excess oxygen is greater than zero. Surface vanadium concentration follows a similar trend.

A partial burn regenerator operation is typically defined by the flue gas CO/CO_2 ratio. However, this ratio is inadequate to characterize the oxidation level in the regenerator atmosphere and thereby the oxidation state of the vanadium on catalyst. A better marker for the vanadium oxidation state in a regenerator is the carbon on regenerated catalyst (CRC). Vanadium Mobility Index (VMI) correlates well with the parameter V/CRC. This implies that refiners operating partial burn regenerators so as to achieve a low CRC can in many cases incur unintentional increased vanadium mobility and catalyst deactivation.

REFERENCES:

[1] R.F. Wormsbecher, W.C. Cheng, G. Kim, and R.H Harding in Deactivation and Testing of Hydrocarbon Processing Catalysts; P. O'Connor, T. Takatsuka, and G.L. Woolery, Eds., ACS Symposium 634, 283 (1995).
[2] J.A. Rudesill, A.W. Peters, in Fluid Cracking Catalysts; M.L. Occelli and P. O'Connor, Eds.; American Chemical Society; Marcel Dekker, Inc, Publishers, 1998, pp 71-83
[3] M.L. Occelli, in Fluid Catalytic Cracking: Role in Modern Refining, M.L. Occelli, Ed., ACS Symposium Series, Vol. 375, pp 162-181 (1988)
[4] M.L. Occelli, and J.V. Kennedy, US Patent 4,465,588 (1984)
[5] M.L. Occelli and J.M. Stencel, in Fluid Catalytic Cracking: Role in Modern Refining, M. Occelli, Ed., ACS Symposium Series, Vol. 375, pp 195-214 (1988)
[6] O. Glemser and A.Z. Muller, Anorg. Allg. Chem. 325, 220 (1963)
[7] M.L. Occelli and J.M. Stencel, in Zeolites as Catalysts, Sorbents and Detergent Builders, H Karge and L.J. Weitkamp Eds., Elsevier, 127 (1989)
[8] P.S. Iyer, H. Eckert, and M.L. Occelli, in Fluid Catalytic Cracking II: Concepts in catalyst Design, ACS vol. 452 M.L. Occelli Ed., ACS Washington DC., 242 (1991)
[9] M.L. Occelli and J.M. Stencel, in Zeolites, Facts, Figure, Future, P.A. Jacob and R.A. van Santen Eds., Elsevier, Part B 1311 (1989)
[10] W.C. Cheng, M.V. Juskelis, and W. Suarez, in Appl. Catal. A: General, 103, 87 (1993).
[11] L.T. Boock, T.F. Petti, and J.A. Rudesill, in Deactivation and Testing of Hydrocarbon Processing Catalysts; P. O'Connor, T. Takatsuka, and G.L. Woolery, Eds.; ACS Symposium Series 634, 171 (1995).

[12] G.L. Woolery, A.A. Chin, G.W. Kirker, and A. Huss, Jr., in Fluid Catalytic Cracking, M.L. Occelli, Ed., ACS Symposium Series 375, 215 (1988).
[13] L.T. Boock, J. Deady, T.F. Lim, and G. Yaluris, in Proceedings, 7th International Symposium on Catalyst Deactivation, Cancún, Mexico, October 1997, Studies on Surface Science and Catalysis, 111, 367 (1997).

Studies in Surface Science and Catalysis, volume 149
M. Occelli (Editor)

Comparison of NIR and NMR Spectra Chemometrics for FCC Feed Online Characterization

William R. Gilbert[a], Flavio S. Gusmão de Lima[a] and Aeerenton F. Bueno[b]

[a]PETROBRAS R&D Center (CENPES)
Cidade Universitária, Quadra 7, 21949-900 Rio de Janeiro, Brazil.
[b]PETROBRAS/REVAP
Rodovia Pres. Dutra, km 143, 12220-840, São Jose dos Campos, Brazil.

The FCC unit is one of the most profitable units in a refinery, and small improvements in product slate or throughput substantially increases to the refinery revenue. One of the ways of enhancing FCC unit profitability is using sophisticated control systems, based on process simulators that ensure that the unit is always run at optimum performance. The difficulty of this approach is that it is often hard to measure the properties of the FCC feedstock, one of the most important determining factors in the FCC process, with the necessary speed, for it to be of use in a control system. To overcome this problem, on-line analyzers using Chemometrics and either near-infrared (NIR) or nuclear magnetic resonance (NMR) spectroscopy are offered to refiners by different suppliers, and both techniques are claimed to be effective. In this work, FCC feedstocks from three Brazilian refineries were analyzed during the course of one year, and Chemometric models of feed properties were developed using both NIR and NMR and the accuracy of feed characterization by each of the two techniques for a control system application was then compared, with the help of an FCC process simulator.

1. INTRODUCTION

FCC is the major conversion process in the refinery, upgrading heavy vacuum gasoil (VGO) or atmospheric residue (ATR), which distills from 350°C to temperatures well above 550°C, into light products, predominantly high octane gasoline and LPG (C3 – C4 hydrocarbons). Coke, which rapidly deactivates the

catalyst, is also produced as a by-product of the cracking reactions, and the spent catalyst must be sent to a Regenerator, where the coke is burned, cleaning the catalyst for another cycle and generating most of the energy needed for VGO vaporization and the endothermic reactions in the Riser [1].

Energy integration between the cracking reactions in the Riser and coke combustion in the Regenerator is a key feature of the FCC process, as temperature control of the Riser is accomplished through hot catalyst circulation from the Regenerator. If more fuel is made available by a small increase in coke make per mass unit of catalyst in the Riser, the Regenerator tends to heat up, Riser temperature control responds by reducing circulation, which in turn reduces coke make, pushing the system back to the original equilibrium state.

The task of an FCC process simulator is to predict the properties of the equilibrium state with the information available. FCC reactor models within the simulator estimate product profiles and particularly coke make for a given feed quality, catalyst concentration (catalyst/oil ratio) and temperature. However, catalyst/oil ratio is not an independent variable in the FCC unit, and other modules in the program, which calculate the heat balance must correct the original value. The procedure is repeated iteratively until a consistent description of the system is produced.

In Real Time Optimization (RTO), a process simulator is required at the highest level of the control hierarchy, allowing the operator to determine specific targets, such as maximizing a given product with particular specifications, and automatically generating set-points to all the underlying levels in the control hierarchy. In the absence of a sophisticated control system, the operator must decide on how to run the FCC unit in the most profitable way. The lack of good data, particularly in the case of feed quality, forces the operator to use considerable safety margins that will guarantee product specification and operational continuity. It is by reducing the operational safety margins and allowing for a quick response in the case of changes in market demand for different products or abrupt variations of feed quality that RTO systems make money.

A large number of physical-chemical properties of the feedstock must be given to the process simulator before it can calculate the FCC results and the use of individual on-line analyzers for each of the required feed properties would be out of question. However, on-line analyzers that measure the spectral output of the hydrocarbon mixture which compose the feed and then estimate its physicochemical properties using correlations obtained from Chemometrics [2,3,4], allow a single instrument to measure several different properties simultaneously and greatly simplify the analytical scheme. Even so, the costs involved in the

acquisition and setting up of spectral on-line analyzers, including fast-loop sampling devices and shelters that will protect the apparatus from the hostile refinery environment may exceed U$ 500 thousand. In addition, there are different choices of technology, such as near infrared (NIR) or nuclear magnetic resonance (NMR), which must be evaluated before deciding on the spectral on-line analyzer to be used.

A short explanation of Chemometrics may here be appropriate. Lamber-Beer's law states that light absorption by a chromophore is proportional to its molar concentration, so that the intensity of absorption bands in a spectrum may be used to calculate the concentration of a given compound. The absorption spectra of mixtures of several compounds is more complex, as each compound may absorb light at different wavelengths with intensities that are proportional to their concentration, but it is still feasible, in principle, to decouple the spectrum and calculate the concentrations of the individual components in the mixture. The physicochemical properties of a mixture are also a function of its composition, so it is possible to correlate many of the mixture's qualities to the absorption intensities of selected wavelengths of its spectrum. This second approach is the method of choice in the case of complex hydrocarbon mixtures. Chemometrics provides the mathematical tools for the model development. The predictive capacity of the chemometric correlation for a given property will depend on the sensitivity of the property affecting compound to the chosen spectroscopy method. For instance, sulfur compounds in hydrocarbon mixtures don't have good spectral signatures in the NIR spectrum, so the NIR based chemometric models for sulfur concentration in hydrocarbons will have larger errors. The great advantage of chemometrics is that it enables a lot different characteristics of a sample of unknown composition to be estimated from its spectrum, often with a high degree of precision.

In this work, feedstock samples from four Petrobras FCC units were fully characterized using standard analytical procedures during the course of one year. The NMR and NIR spectra from each sample were also obtained and used to construct Chemometric models for the feed properties used in the Petrobras proprietary FCC simulator. The quality of the NMR and NIR models was then compared both by the values of their standard mean errors and by the differences between the FCC simulator results using either the standard feed characterization, the NIR predictions or the NMR predictions.

2. EXPERIMENTAL

In Table 1 are summarized the feed quality properties used by the FCC process simulator, and the corresponding standard analytical procedures. The typical composition of the feedstocks used was the following: (1) Unit A – 18% coker gasoil, 17% atmospheric bottoms, 65% vacuum gasoil; (2) Unit B – 35% atmospheric bottoms, 65% vacuum gasoil; Unit C – 70% vacuum gasoil, 30% deasphalted oil; Unit D – 100% atmospheric bottoms. All four units processed feedstocks derived from Campos Basin Brazilian heavy crude oils. Table 2 presents the number of measurements from each of the four units used in the spectral correlations. The total number of samples collected was 174.

Table 1
Feed properties used in the FCC process Simulator

Property	Method	Unit	Property	Method	Unit
Aniline point	ASTMD 611	°C	Viscosity	ASTMD445	cstk
Spec. gravity	ASTMD 4052	g/cm^3	Carb resid.	ASTMD524	wt%
Basic. Nitrog	UOP 269	ppm	Distillation	ASTMD1160	°C
Sulfur	ASTMD 1552	wt%	Sim.Distill	HT750 GC	°C

Table 2
Number of samples analyzed from each FCC unit.

Unit	C	D	A+B	Unit	C	D	A+B
Samples	54	53	67	Sulfur	49	47	62
NMR	34	47	66	Viscosity	48	42	51
Aniline pt.	54	49	65	Carb. Res.	36	49	63
Spec.gravity	53	52	66	1160 Distl.	15	30	33
Basic Nitrog	52	51	65	SimDis	29	20	50

The wave number range of the NIR spectra used in the correlations was between $5000cm^{-1}$ and $4000cm^{-1}$. The spectra were produced from a Bomem MB-160 spectrometer, using a calcium fluorite cell of 0.5mm optical pathway at 40°C. The software used in the Chemometrics calculations of the NIR spectra was Infometrics Pirouette, and the technique used was Partial Least Squares Regression (PLSR) with cross validation. Root Mean Square Error of Prediction values (RMSEP) was calculated with an external data set. Figure 1 shows FCC feedstock NIR spectra of two samples from the study data set.

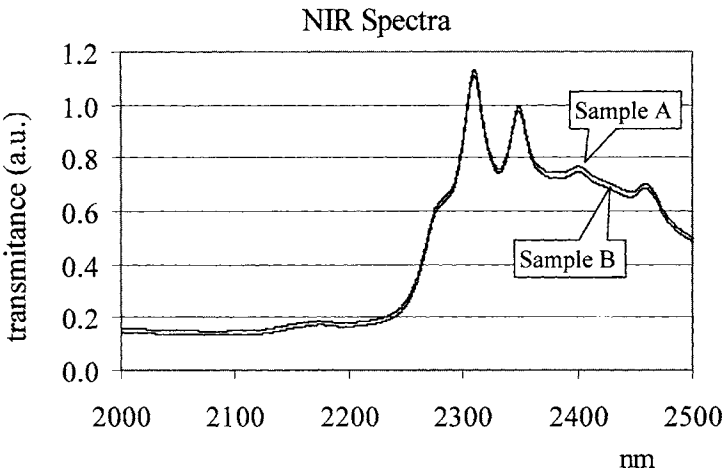

ʒ. 1. NIR spectra of two FCC feed samples (A and B). Differences in the absorption intensity at :ticular wavelengths are correlated to the hydrocarbon physicochemical properties.

^{1}H NMR spectra were obtained from 5% solutions of the hydrocarbon mple in a 1:1 mixture of $CDCl_3$ and Tetrachloroethylene. The spectrometer used as a Varian Inova-300, 7.05T magnetic field (300MHz frequency), 5mm probe be, 45° pulse, 4500Hz spectral window at room temperature. Chemometrics was lculated from the integrated signal, using 0.1ppm slices between 0 and 10ppm. alculations were done with the help of the software Unscrambler from Camo SA. The technique used was also PLSR with full cross validation and an external .ta set was used to calculate the RMSEP. Figure 2 shows a typical gasoil ^{1}H NMR ectrum.

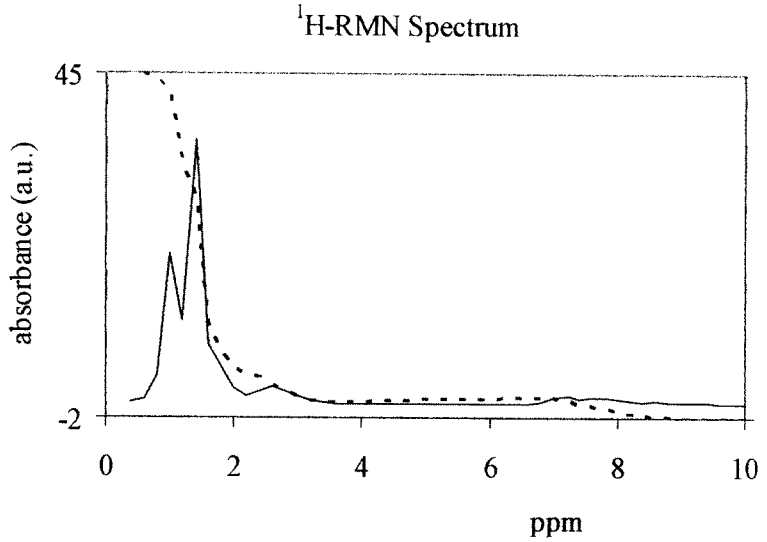

Fig. 2. NMR spectrum of an FCC feed sample. The dashed line corresponds to the integral of the spectra.

3. RESULTS AND DISCUSSION

When developing a Chemometric model from spectral data, a compromise between accuracy (error magnitude) and robustness (capability of predicting the properties of widely different products) must be achieved. In the case of the FCC feedstocks in this study, those from Unit D were much heavier than the others, with Carbon Residue in the 5 to 6 wt% range, compared to less than 2 wt% for Units A, B and C. Principal component analysis of the spectra, either in the case of NIR or NMR, didn't indicate a clear necessity of separating the data from Unit D. For the NIR models the spectra of the four units were lumped together in the model development (results shown in Table 3). In the case of NMR, models were developed for two different procedures: (1) using Unit D spectra with those of the other units (Table 4); and (2) treating Unit D separately from Units A, B and C (Tables 5 and 6). The analysis of the models from the NMR spectra shows a clear advantage of using specific models rather than generalized models. The error (RMSEP) of the specific models is much smaller in the case where Unit D is treated separately, the improvement is even more pronounced in the case of

properties which are very different for vacuum gasoil and atmospheric bottoms, as is the case of the T50 (RMSEP goes from 16.5°C to 6°C) in the Simulated Distillation curve and the Carbon Residue (RMSEP changes from 0.6 to 0.2 wt%).

Table 3
NIR FCC feed property prediction models inclu-ding data from units A, B, C and D.

	RMSEP	Units	R
Specific Gravity	0.0007	g/cm^3	0.988
Carbon Residue	0.24	wt %	0.990
Aniline Point	2.1	°C	0.950
Sim.Dis. IBP	24.1	°C	0.610
Sim.Dis. 10%	17.0	°C	0.883
Sim.Dis. 50%	6.5	°C	0.960
Basic Nitrogen	90	mg/kg	0.954
Sulfur	0.031	wt %	0.928

RMSEP = Root mean square error of prediction. R = Correlation coeficient for the Predicted *vs* Measured plot.

Table 4
NMR models including data from units A, B, C and D.

	RMSEP	Units	R	Error %†
Specific Gravity	0.004	g/cm^3	0.97	0.4
Sim.Dis. IBP	21.2	°C	0.63	7.7
Sim.Dis. 10%	5.8	°C	0.86	1.6
Sim.Dis. 50%	16.5	°C	0.99	3.4
Aniline Point	1.4	°C	0.95	1.6
Basic Nitrogen	54	mg/kg	0.96	3.5
Sulfur	0.05	wt %	0.91	7.5
Carbon Residue	0.6	wt %	0.97	22.0

† Error% is calculated by dividing RMSEP by the estimated property average value.

Table 5
NMR models including units A, B and C (predominantly VGO units).

	RMSEP	Units	R
Specific Gravity	0.0019	g/cm^3	0.978
ASTM D1160 Dist. IBP	9.1	°C	0.997
ASTM D1160 Dist. 10%	6.4	°C	0.987
ASTM D1160 Dist. 50%	8.6	°C	0.994
Aniline Point	2.1	°C	0.969
Basic Nitrogen	85	mg/kg	0.982
Sulfur	0.047	wt %	0.750
Carbon Residue	0.3	wt %	0.936

Table 6
NMR models of unit D feeds (Atmospheric Resid.)

	RMSEP	Units	R
Specific Gravity	0.0015	g/cm^3	0.956
ASTM D1160 Dist. IBP	9.0	°C	0.951
ASTM D1160 Dist. 10%	11.0	°C	0.927
ASTM D1160 Dist. 50%	8.0	°C	0.958
Aniline Point	2.2	°C	0.844
Basic Nitrogen	44	mg/kg	0.903
Sulfur	0.021	wt %	0.888
Carbon Residue	0.2	wt %	0.890

Figure 3 and 4 further illustrates the heterogeneous character of the data, with the points from unit D concentrated on the top right end of both graphs. Nevertheless the quality of the NIR model prediction is still good. The RMSEP for Carbon Residue for the Unit D results (atmospheric residue) is 0.26 wt%, the error for the gasoil units is 0.30 wt% and for the whole set is 0.29 wt%, showing that there is no significant difference in accuracy between the two groups of results.

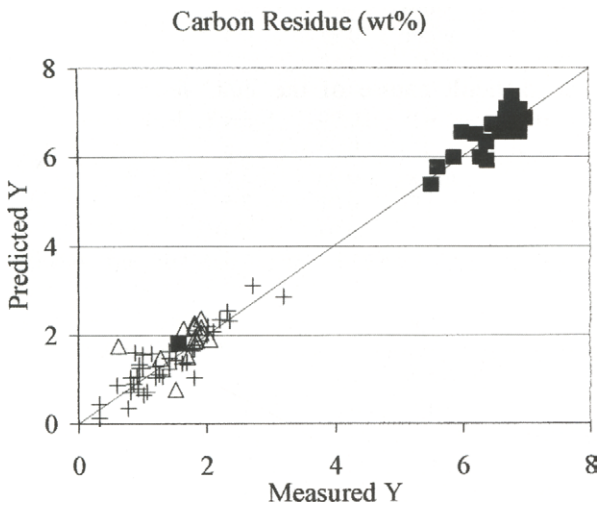

Fig. 3. Predicted versus Measured plots of the NIR models for Carbon Residue. (+) Units A+B, (■) Unit D, (△)Unit C.

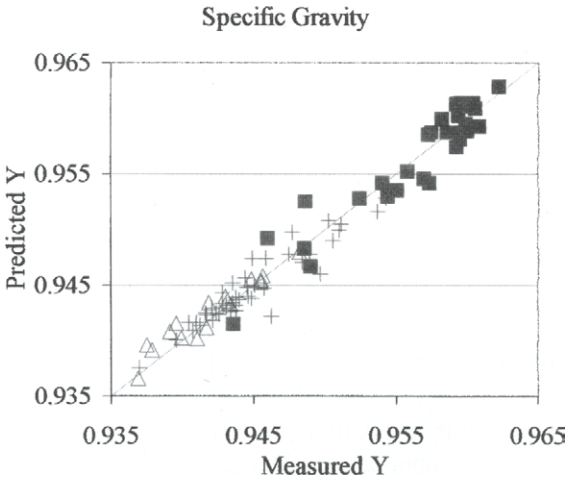

Fig. 4. Predicted versus Measured plots of the NIR models for Spec. Gravity. (+) Units A+B, (■) Unit D, (△)Unit C.

NIR models used in other on-line analyzer applications, such as product blending, are often capable of outdoing the standard analytical method reproducibility. The difficult nature of the FCC feed make the RMSEP values rather high when compared to those for lighter hydrocarbons, but it also must be mentioned that property prediction for process simulation doesn't have to be as accurate as in the case of product specification and that the errors in FCC process modeling are comparatively large and are capable of absorbing the smaller errors from the Chemometric models. Table 7 shows the accuracy of the NIR and NMR models and the Reproducibility of reference analytical methods. NIR and NMR model prediction errors in this study were comparable and were close to the standard method Reproducibilities.

Table 7
Comparison of the NIR and NMR VGO property prediction models with the Reproducibility of Standard characterization methods. NIR data includes units A, B, C and D; NMR data includes units A, B and C only.

	RMSEP NIR	RMSEP NMR	Reprod.	Method
Spec.Gravity	0.0007	0.019	0.0005	ASTM D 4052
Carbon Resid.	0.24	0.3	0.05	ASTM D 524
Aniline point	2.1	2.1	1.0	ASTM D 611
Dist. IBP	24.1	9.1	-	ASTM D 1160
Dist. 10%	17.0	6.4	23	ASTM D 1160
Dist. 50%	6.5	8.6	14	ASTM D 1160
Basic Nitrog.	90	85	65	UOP 269
Sulfur	0.031	0.047	0.066	ASTM D 2622

To allow for a fair evaluation of the NIR and NMR generated feed characterizations in a RTO application, data from Unit C, which included a period when feed quality was drastically varied, was fed to the Petrobras FCC process simulator. Four unit simulation studies were performed: (1) using the feed properties measured by the standard methods, (2) using the average feed properties of the period, (3) using the NIR models and (4) using the NMR models. Table 8 and Figure 4 summarize the results. Feed quality changed during the test period, Aniline Point varied from 78 to 88°C, specific gravity from 0.938 to 0.947 g/cm3, and Carbon Residue from 1.1 to 1.9 wt%.

The second simulation experiment, which used average feed properties, illustrates the case where process simulation is attempted without adequate knowledge of feed properties. The graph in Figure 5 shows how the simulated conversion using average feed properties tends to stay close to the average conversion value, and errors become more pronounced for extreme values of conversion. The error in the economic evaluation of unit C (12000m3/day capacity) was estimated as 400 thousand US$ per year per unit of conversion miscalculated. Although there is a considerable amount of scatter, both NIR and NMR were capable of reproducing the effect of changes in feed quality on the FCC results, and can be used to substitute the standard analytical procedures of feed characterization.

Table 8
Differences for the FCC conversion and coke yield calculated for the four case studies*.

	Δ *FCCU*	Δ*Averag*	Δ*NIR*	Δ *NMR*
Conversion wt%	2.8	2.8	1.6	1.6
Coke wt%	0.15	0.12	0.11	0.11

*Where ΔFCCU is the difference between measured conversion in the FCCU and that predicted using standard feed characterization, ΔAverage, ΔNIR and ΔNMR are the differences between calculated results using the feed standard characterization in the first case and NIR and NMR in the following cases.

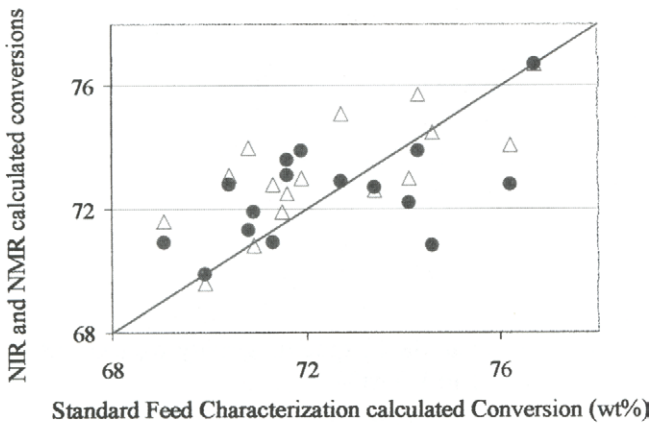

Fig. 5. FCC Process Simulator calculated conversions using Standard Characterization (X axis) and NIR (Δ) or NMR (●) in the Y axis.

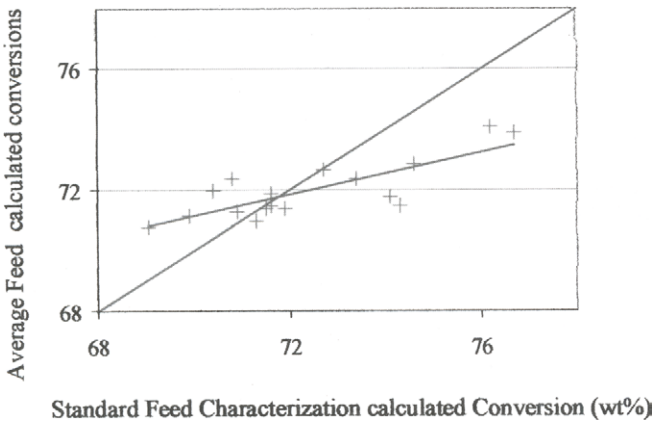

Fig. 6. FCC Process Simulator calculated conversions using Standard Characterization (X axis) and average feed properties (+) in the Y axis

4. CONCLUSIONS

Even small improvements in FCC unit performance brought by Real Time Optimization may bring considerable gains to refiners, and on-line feed characterization is essential to achieve a good simulation of the unit required by RTO. From the study of the feed quality from four FCC units in Petrobras and the development of Chemometric models for the FCC simulator feed quality input variables using both NIR and ^{1}H NMR spectroscopy, it was shown that the two spectroscopic methods for feed characterization produce comparable results and are viable choices for on-line FCC feed analyzers. The use of specific data bases in model development, as is the practise in most NIR on-line analyzer applications, is also recommended for ^{1}H NMR, as the use of generalized models may lead to large errors in key FCC feed properties which could be very different from the model's predictions in units that process out of the ordinary feedstocks.

REFERENCES

[1]. P.B.Venuto, E.T.Habib Jr., Fluid Catalytic Cracking with Zeolite Catalysts, Ed.; M.Dekker, New York, 1979.
[2]. D.Burns, E. Ciurczak (Editors), Handbook of Near-Infrared Analysis, Marcel Dekker, inc, New York, 1992, 329-363.
[3]. A. Espinosa, D. Lambert, M. Valleur, , Hydrocarbon Processing, 86-91, February 1995.
[4] K.R. Beebe, R.J. Pell, M.B. Seasholtz, Chemometrics: A Pratical Guide, Wiley and Sons, New York, 1998.
M.Otto, Chemometrics, Wiley-VCH, Weinheim, 1999.

Studies in Surface Science and Catalysis, volume 149
M. Occelli (Editor)

Cracking behaviour of aromatic- and organic sulfur compounds under realistic FCC conditions in a microriser reactor

Xander Dupain, Michiel Makkee*, and Jacob A. Moulijn

Reactor and Catalysis Engineering,
DelftChemTech,
Faculty of Applied Sciences,
Delft University of Technology,
Julianalaan 136, 2628 BL Delft, The Netherlands
*e-mail address: m.makkee@tnw.tudelft.nl

Cracking of an aromatic-spiked hydrowax, an aromatic gas oil, and of an extra heavy gas oil in a once-through microriser reactor demonstrated that aromatics and aromatic sulfur species do not crack under realistic FCC conditions. The conversion by cracking reactions is limited to the paraffinic fraction of the feed and the alkyl groups associated to the benzene ring in aromatic compounds. Cracking of the benzene ring is expected to be low due to the high resonance stabilising properties of the π-electrons, which hinders the activation by a Brønsted acid and the subsequent weakening of the bond at the β-position. Therefore, for the (poly)aromatic feed species only the side-groups are susceptible to bond breaking.

1. Introduction

Global environmental legislation imposes constraints on the maximum amount of aromatics and sulfur in gasoline and diesel. As crude oils are becoming ever heavier and sourer, refiners continuously have to change their refinery operations in order to meet the tiers. For Europe by 2005 the EURO 4 tier will come into effect, which imposes a maximum aromatics amount of 35 v% and 15 wt% for gasoline and diesel, respectively. For both fuels the maximum sulfur

concentration will be 30 wppm, and will be lowered to sulfur-free specifications (< 10 wppm) in the near future *[1]*.

As the Fluid Catalytic Cracking process is one of the key processes in the production of gasoline and LCO, where the latter is an important diesel blend, it plays an important role in the discussion of aromatics and sulfur reduction. Aromatics and aromatic sulfur compounds are claimed to be refractory to crack under FCC conditions and, consequently, removal of these components might be a real challenge. Although hydrotreatment of the FCC feedstock and product thereof is a very effective way to remove sulfur and aromatics by means of hydrolysis c.q. hydrogenation, the high hydrogen pressure and high temperature make this a very costly process. Besides that, hydrotreatment of gasoline can lead to a significant decrease in the octane number.

In this work the cracking behaviour of aromatics and sulfur compounds has been investigated under realistic FCC conditions in a qualitative way. To approach the industrial conditions to a high degree, a once-through microriser reactor has been used. With this device the residence time, temperature, and catalyst-to-oil ratio (CTO) can be varied to obtain different feed conversions. The evaluation of the results is based on the five-lump model by Francés and Corella *[2]*. Den Hollander *et al.* adapted this model for the fact the coke is only formed during the first 50 ms of catalyst-oil contact *[3]*. The five-lump model is represented in Fig. 1.

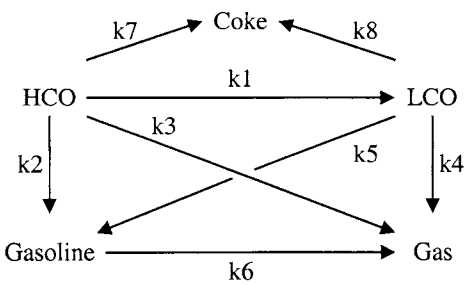

Fig. 1. The five-lump model of catalytic cracking, after *[2]*.

2. Experimental

2.1. Equipment and experimental procedure

A once-through microriser reactor has been used to perform the cracking experiments. A schematic overview of this isothermal plug-flow reactor is given in Fig. 2.

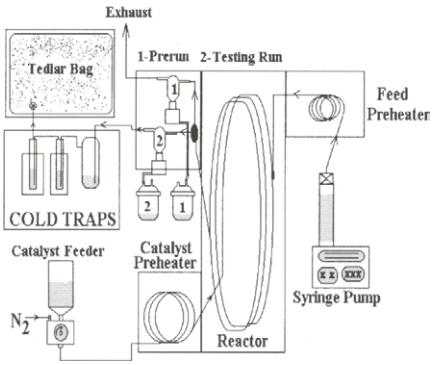

Fig. 2. Schematic overview of the microriser reactor.

The set-up consists of four ovens: a reactor oven, a disengager oven, a catalyst pre-heat oven, and an oil pre-heat oven. In the reactor oven a looped tube with a 4.55 mm internal diameter is placed. This reactor consists of mountable parts, so that the reactor length can easily be varied. The catalyst is fed through a catalyst feeder with nitrogen as carrier gas. As the catalyst flows through the catalyst pre-heating oven the nitrogen expands and the catalyst particles are further accelerated. At the injection point the evaporated feed is sprayed perpendicularly into the catalyst flow. This oil feed is fed through a syringe pump and passes through a feed pre-heating oven prior to injection. In the disengager oven the gaseous product is separated from the catalyst by means of a cyclone, where the catalyst is stored in a hopper. Three cold traps in series capture the gaseous product; one operating at room temperature, and two operating at -60 °C. Finally, the uncondensed product is captured in a gasbag. An experimental consists basically out of three steps: a pre-run, the experimental run, and a stripping procedure. During the pre-run the system is allowed to reach a steady-state operation. Since there are placed two cyclones in the disengager oven the system then can be switched to the experimental run, in which the product is collected for a given time. After the experimental run the system is switched back to the original configuration to purge the reactor. A stripping procedure with nitrogen is performed to collect the products, adsorbed on the catalyst.

The liquid product is weighed and analysed with simulated distillation, according to the ASTM D2887 method. The mass and the composition of the gasbag are calculated by analysis with a gas chromatograph, equipped with a thermal conductivity detector and a flame ionisation detector. The amount of coke is analysed with a LECO C-400 device. Consequently, the mass balance of the experiment can be determined, which should be at least 95 wt%.

Prior to all experiments the catalyst was regenerated in air in a fluidised bed at 600 °C for three hours. A detailed description of the equipment and procedure can be found elsewhere *[4]*.

2.2. Materials

A hydrowax spiked with naphthalene, phenanthrene, and anthracene, was cracked over a commercial cracking catalyst (equilibrated at 815 °C for four hours in pure steam) at 575 °C, a CTO of 4.8 $g_{catalyst} \cdot g_{oil}^{-1}$, and a residence time of 6.7 s. The amount of the aromatic probes was approximately 2.5 wt% each, and was verified by simulated distillation, see Fig. 3. As a result of the similar boiling points of phenanthrene and anthracene, these compounds could not be separated over the applied analysis equipment and are detected as a single peak.

Additionally, an aromatic gas oil has been processed over the same commercial catalyst as described above to evaluate the behaviour of aromatics. The properties of this feed are given in table 1. The experiments were done at a fixed temperature of 525 °C and a fixed catalyst-to-oil ratio (CTO) of 5.5 $g_{catalyst} \cdot g_{oil}^{-1}$. The residence times were varied from 0.05-8.5 s by means of changing the reactor length.

Table 1
Basic properties of the aromatic gas oil.

Property	**Unit**	**Value**
API Gravity at 15.5 °C	[-]	19.17
Conradson Carbon Residue	[wt%]	0.22
Pour Point	[°C]	33.3
Aniline Point	[°C]	75
Basic Nitrogen Content	[ppm]	351
Total Nitrogen Content	[ppm]	1235
Aromatic Content	[wt%]	33.28
UOP K-Factor	[-]	11.47
Initial Boiling Point	[°C]	306
10 % Off	[°C]	376
Final Boiling Point	[°C]	542
HCO	[wt%]	94.6
LCO	[wt%]	3.4
Gasoline	[wt%]	2.0

An industrial extra heavy gas oil (containing 0.34wt% sulfur) was processed over an equilibrium catalyst at 525, 555, and 585 °C to evaluate the cracking behaviour of sulfur compounds. The properties of this feed are

described in table 2. The CTO was varied between 2-8 $g_{catalyst} \cdot g_{oil}^{-1}$; the residence times was varied between 0.3-5 s.

Table 2
Basic properties of the extra heavy gas oil.

Property	**Unit**	**Value**
Density	[kg/l]	0.8558
Viscosity at 100 °C	[m^2/s]	$2.75 \cdot 10^{-6}$
Average Molecular Weight	[g/mol]	299
Sulfur Content	[wt%]	0.34 *
Nitrogen Content	[wt%]	0.028
Carbon Content	[wt%]	86.92
Hydrogen Content	[wt%]	12.72
Initial Boiling Point	[°C]	251
10 % Off	[°C]	309
Final Boiling Point	[°C]	524
HCO	[wt%]	80.2
LCO	[wt%]	18.8
Gasoline	[wt%]	1.0

* *Measured by Sievers Chemiluminescence Detector*

2.3. Calculations and Kinetics

The results of the cracking experiments were qualitatively evaluated based on the five-lump model, shown in Fig. 1. The upper cutpoints are 25 °C for gas, 215 °C for gasoline, and 325 °C for LCO. The conversion of the feed is based on the amount of converted HCO, which is a function of temperature, CTO, and residence time:

$$X(T, CTO, \tau) = \left(\frac{y_{HCO,0} - y_{HCO}}{y_{HCO,0}} \right) \cdot 100\,\%$$

Where X is HCO conversion, T is temperature, CTO is catalyst-to-oil ratio, τ is residence time, $y_{HCO,0}$ is the HCO feed fraction, and y_{HCO} is the HCO fraction in the product. In all experiments the oil partial pressure was kept constant.

As it was difficult to set the CTO to the predetermined exact values for each experiment it should be kept in mind that a variation of the data is present. The solid lines shown in the figures for the cracking of the extra heavy gas oil are to guide the eye, and only represent the general trend.

3. Results

In Fig. 3 the feed and product distribution are shown for the hydrowax spiked with naphthalene, phenanthrene, and anthracene, obtained from the GC analysis.

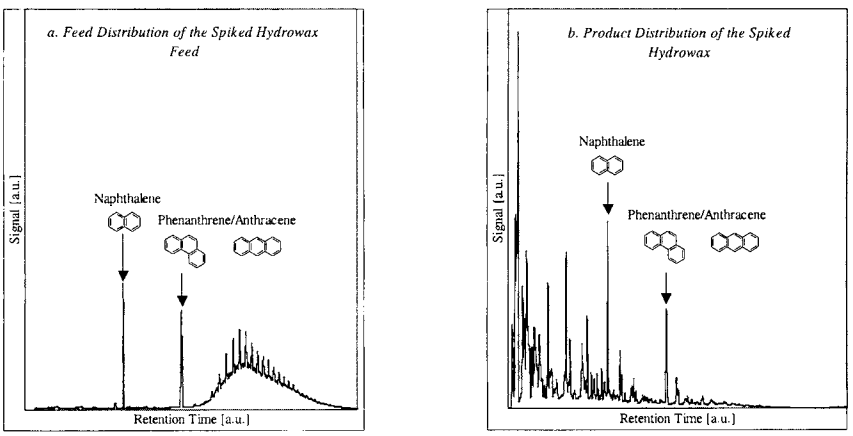

Fig. 3. Feed and product distribution of the spiked hydrowax. (a) Feed, and (b) product at 87 % HCO conversion (575 °C, CTO 4.8 2 $g_{catalyst} \cdot g_{oil}^{-1}$, and 6.7 s).

The phenanthrene and anthracene probes form one single peak as a result of their similar boiling points. The product distribution in Fig. 3b shows a typical spectrum for a cracked hydrowax at 87 % HCO conversion, including the aromatic probes, which are still present. It has been verified that the amount of phenanthrene and anthracene are equal to those present in the feed, and that for naphthalene in fact a significant increase was found.

In Fig. 4 the cracking of the aromatic gas oil is shown against residence times at 525 °C and 5.5 $g_{catalyst} \cdot g_{oil}^{-1}$. The solid lines represent calculated values from the five-lump model, described in detail in *[5]*.

For this work it suffices to describe the observations in a qualitative way. The graphs show that 19 % of the HCO fraction is 'uncrackable' under the applied conditions. This value is lower than the aromatic content of the feed (33.3 %, see table 1), but one should keep in mind that aromatics are transferred to the other product fractions. This should balance to the total amount of aromatics. The selectivity for HCO towards gasoline is 71 %, and no overcracking of gasoline takes place.

Fig. 4b shows that the net LCO fraction displays a maximum; first LCO is formed, but at higher residence time more LCO starts to be consumed.

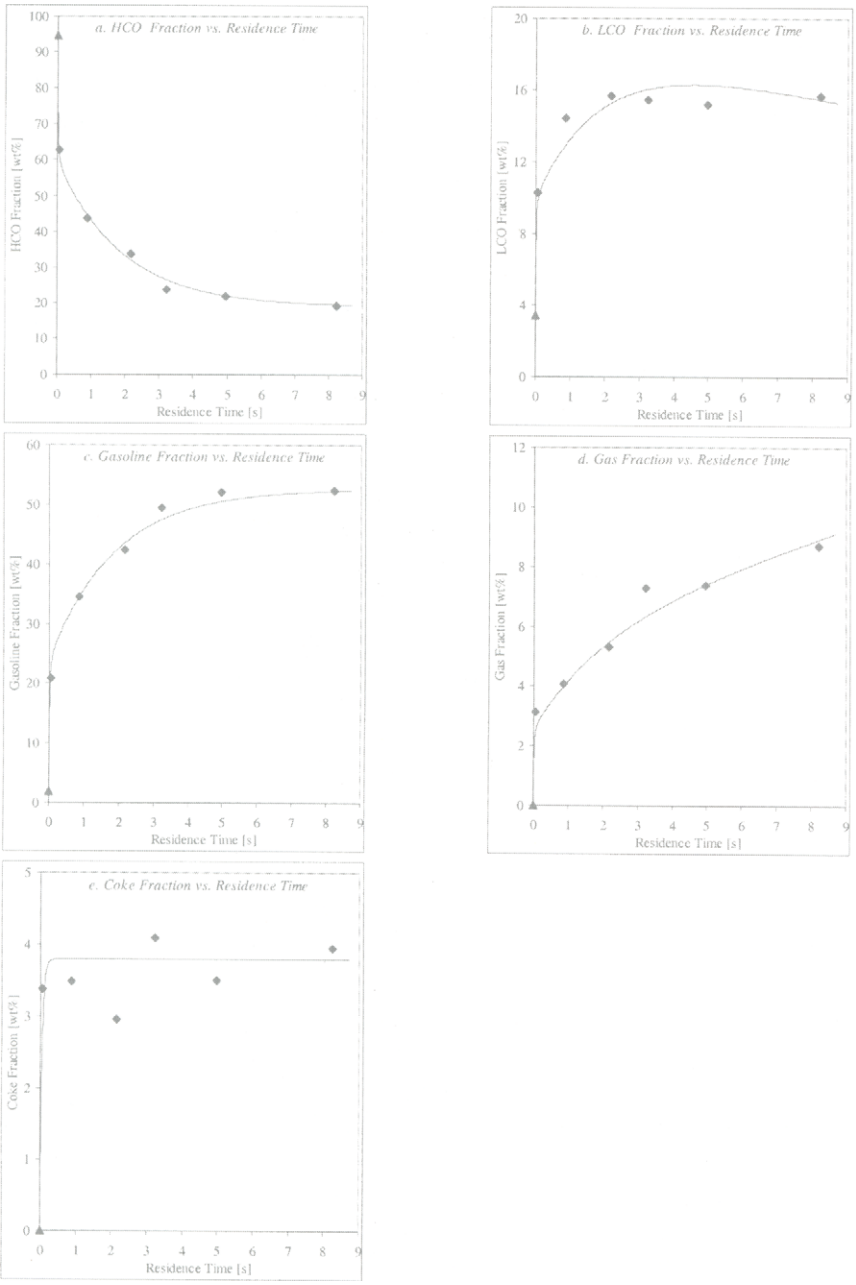

Fig. 4. Product fractions versus residence time for the cracking of an aromatic gas oil at 525 °C and 5.5 $g_{catalyst} \cdot g_{oil}^{-1}$. The solid lines represent the calculated model values, after *[5]*. (a) HCO, (b) LCO, (c) gasoline, (d) gas, and (e) coke. ▲ = fraction in feed.

Gas is formed predominantly during the first two seconds of contact time, and then starts to saturate. In Fig. 4d it can be clearly observed that coke is only formed in the beginning, which is agreement with the work of Den Hollander *et al. [4]*. During the first 50 ms of contact time already 34 % of the HCO fraction is converted.

In Fig. 5 the HCO and gasoline fraction in the cracking of the extra heavy gas oil are shown versus residence times at 525, 555, and 585 °C. The CTO was kept constant at a value of 2 $g_{catalyst} \cdot g_{oil}^{-1}$. The solid lines are included to guide the eye.

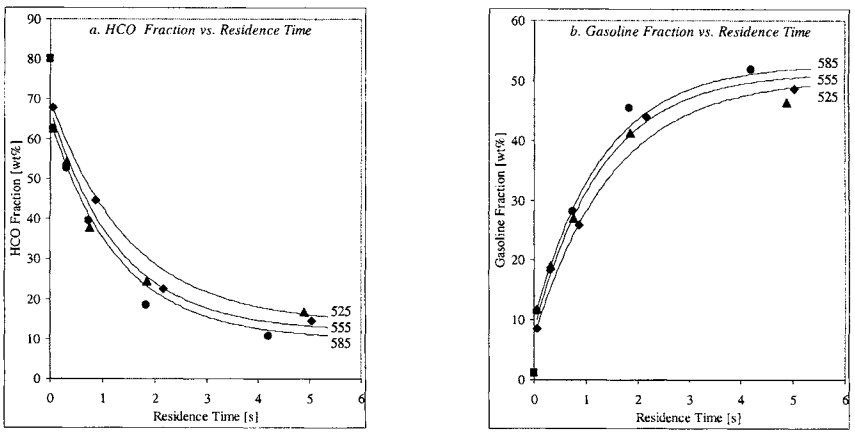

Fig. 5. HCO and gasoline fractions versus residence time for the cracking of an extra heavy gas oil at 525, 555, and 585 °C and CTO 2. The solid lines are included to guide the eye. (a) HCO, and (b) gasoline. ◆= 525 °C, ▲= 555 °C, ● = 585 °C, and ■ = fraction in feed.

The observations are analogous to the results in the cracking of the aromatic gas oil. Approximately 10 to 15 % of the HCO fraction is 'uncrackable'. The graphs show that at higher temperature the cracking activity increases, although the selectivity of HCO towards gasoline after 50 ms is about 78 %, and is independent on temperature. Furthermore, once more no gasoline overcracking takes place. Increment of the CTO at a constant temperature of 585 °C and constant reactor length of 1.2 m led to an increase in HCO conversion from 32.8 % for 1.9 $g_{catalyst} \cdot g_{oil}^{-1}$ to 49.9 % for 4.2 $g_{catalyst} \cdot g_{oil}^{-1}$, to 65.6 % for 7.7 $g_{catalyst} \cdot g_{oil}^{-1}$.

In Fig. 6 the product fractions are plotted versus HCO conversion for different temperatures. The HCO conversion is varied by means of variation of the three process parameters; temperature, residence time, and CTO.

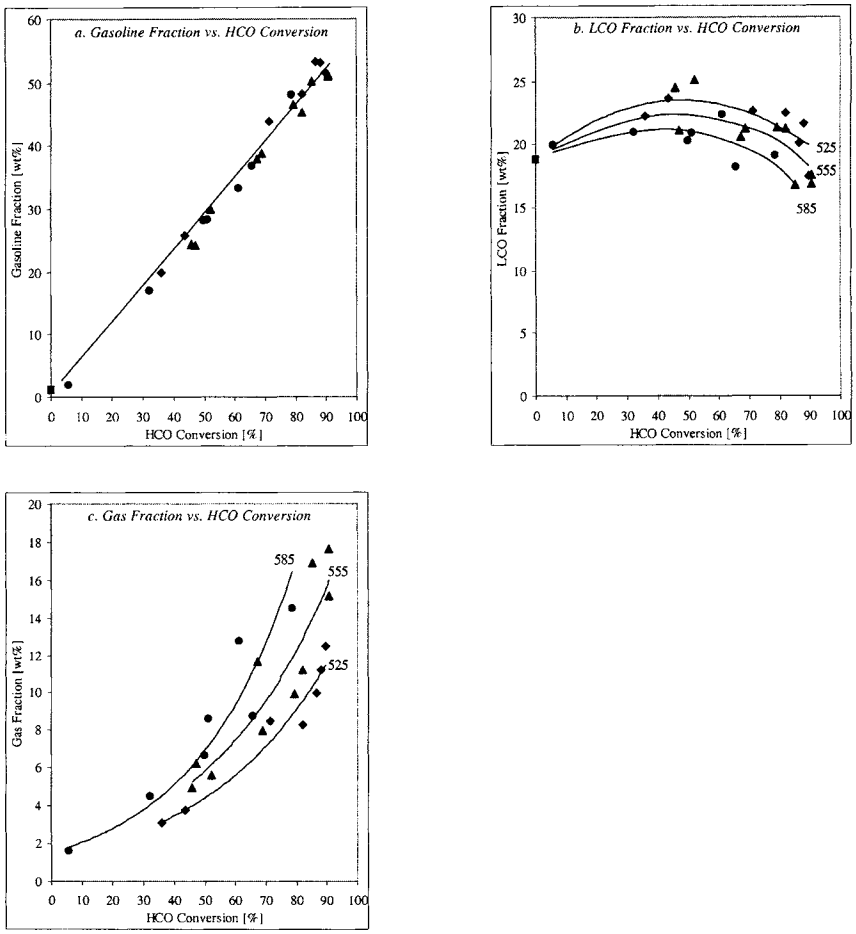

Fig. 6. Gasoline, LCO, and gas versus HCO conversion for the cracking of an extra heavy gas oil. The solid lines are included to guide the eye. (a) Gasoline, (b) LCO, and (c) gas. ◆= 525 °C, ▲= 555 °C, ● = 585 °C, and ■ = fraction in feed.

Since the gasoline selectivity is independent of temperature the gasoline fraction plotted versus the HCO conversion yields a straight line, which is shown in Fig. 6a. Fig. 6b and 6c show that the LCO and gas fraction are in fact dependent on temperature. Increasing the temperature leads to a lower LCO fraction and at the same time a higher temperature yields more gas. As already observed in the cracking of the aromatic gas oil, the LCO fraction also passes here trough a maximum, as is demonstrated in Fig. 6b. At higher HCO conversion level LCO will start to react.

In Fig. 7 the sulfur amount in the liquid product fractions are shown against HCO conversion. The data represents the absolute amount of sulfur in a specific

lump (HCO, LCO, or gasoline) based on the amount of total feed (hydrocarbons plus sulfur). The graph includes the data from 525, 555, and 585 °C. As no temperature dependency for the absolute sulfur yields was found it is plotted in one graph.

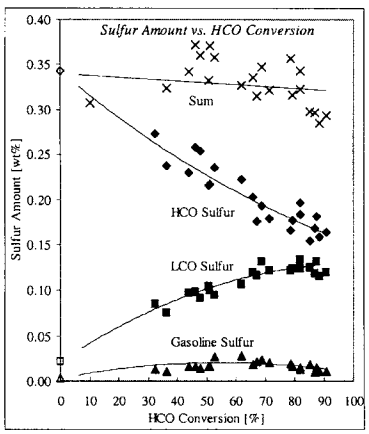

Fig. 7. Amount of sulfur in the liquid product fractions versus HCO conversion for the cracking of an extra heavy gas oil. Combined data of 525, 555, and 585 °C. The solid lines are included to guide the eye. ◆ = HCO sulfur, ■ = LCO sulfur, ▲= Gasoline sulfur, and × = sum of sulfur in the liquid product. Open symbols represent the amount of feed sulfur for a given product fraction.

The amount of sulfur in the HCO fraction decreases with higher HCO conversion, whereas sulfur in LCO fraction strongly increases, and starts to saturate at 60-70 % HCO conversion. The sulfur in the gasoline fraction increases up to 50 % of the HCO conversion, but thereafter starts to decrease again. There is a decrease in the sum of the three liquid products, which can be ascribed to the formation of gaseous sulfur species. The sulfur level in the coke lay below the detection limit and, consequently, plays no role in the sulfur mass balance.

In Fig. 8 the sulfur concentrations in the HCO, LCO, and gasoline fractions are shown. As opposed to Fig. 7 this data represent the amount of sulfur in a given lump (e.g. gasoline) divided by the total amount of hydrocarbons (and sulfur) of that specific lump.

The HCO sulfur concentration remains constant up to 60 % conversion, and then rapidly increases. The LCO sulfur concentration does not only increase, but is temperature dependent as well, as the result of the temperature dependence on the LCO hydrocarbon fraction (see Fig. 6b).

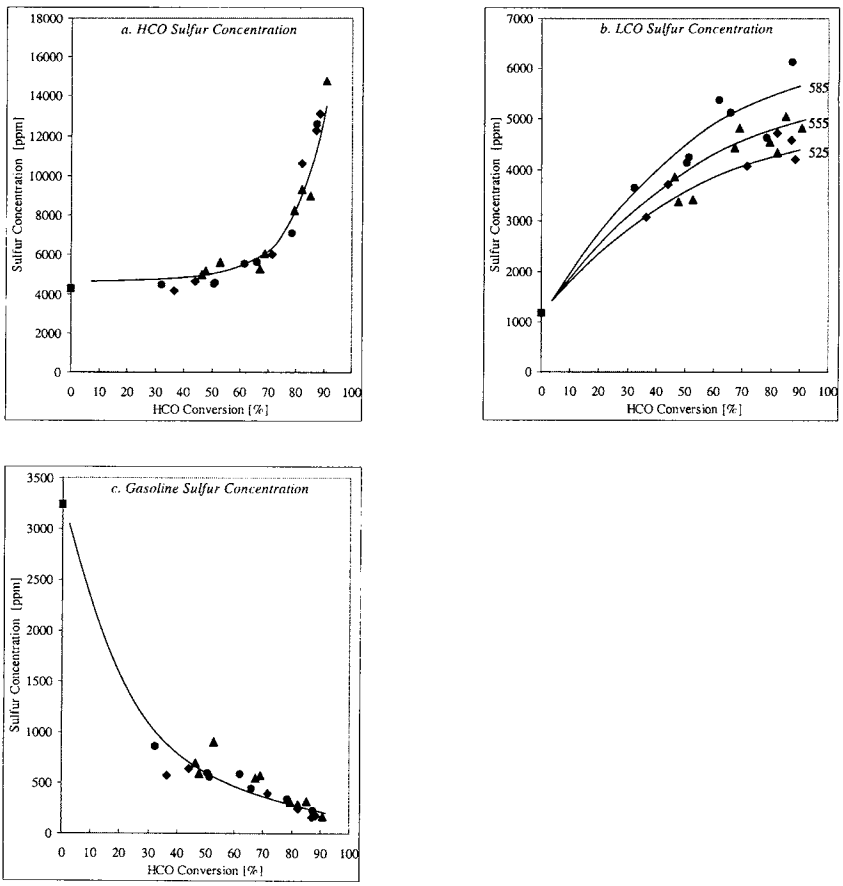

Fig. 8. Sulfur concentration in the liquid product fractions versus HCO conversion for the cracking of an extra heavy gas oil. The solid lines are included to guide the eye. (a) HCO sulfur concentration, (b) LCO sulfur concentration, and (c) gasoline sulfur concentration. ◆= 525 °C, ▲= 555 °C, ● = 585 °C, and ■ = sulfur concentration in feed for a given product fraction.

The gasoline sulfur concentration rapidly decreases up to 35 %, and then decreases further with a smaller slope, but this sulfur concentration is independent of temperature.

In Fig. 9 the sulfur distribution plots are given for the feed and at a HCO conversion of 52 and 82 % at 555 °C and CTO 2. The feed distribution shows that most sulfur lies in the HCO range, and that the high number of different sulfur species lead to a hill, as the analysis method is unable to discriminate between them. The spectra reveal that no new sulfur compounds form after 52 % conversion, i.e. the fingerprint of the product spectra does not change, only the peak heights increase.

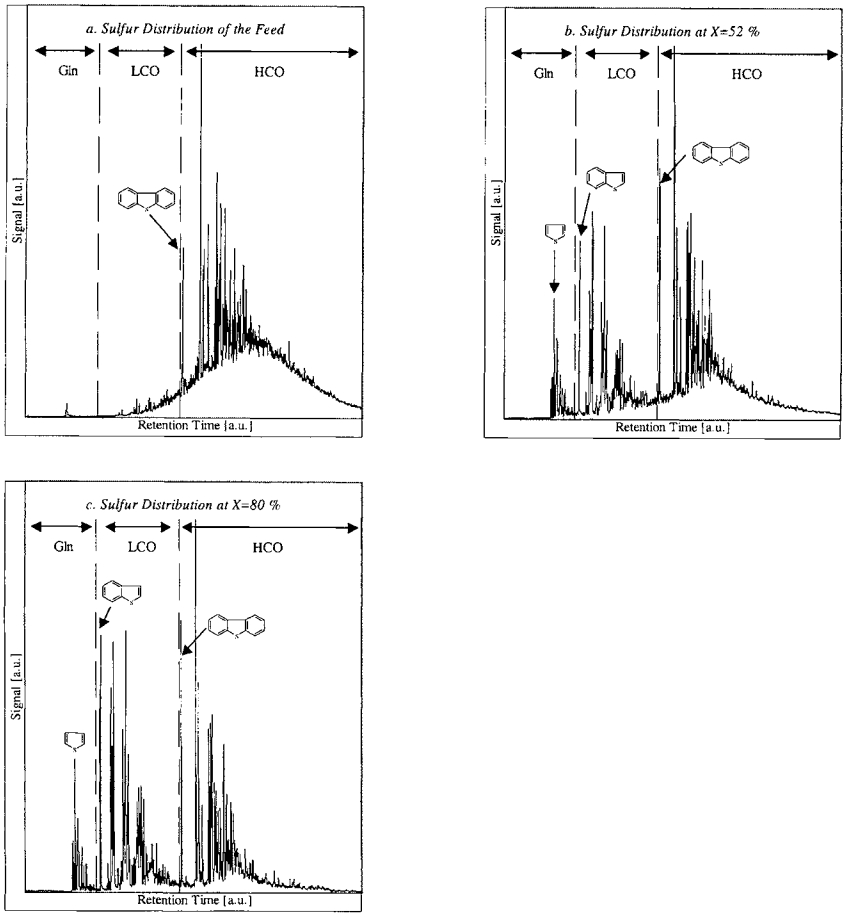

Fig. 9. Sulfur distribution in the feed and products of an extra heavy gas oil. (a) Feed, (b) product at 52 % HCO conversion, and (c) product at 80 % HCO conversion.

It has been verified that changing the process parameters, such as CTO, temperature, and residence time, does not yield different spectra.

4. Discussion

The reactivity of the HCO fraction is highest during the first two seconds of contact time. A higher temperature enhances the cracking activity, though after two seconds HCO is converted only little further, and approaches an asymptotic value. Increment of CTO enhances the cracking rate, but the same asymptotic value is approached under the applied conditions a fraction of the feed will not crack, and remain in the HCO fraction. Both the extra heavy gas oil and the aromatic gas oil display this similar behaviour, where the latter has a higher

'uncrackable' fraction. The refractory character of the 'uncrackable' fraction is directly demonstrated by the spiked hydrowax. Where the aromatic spiked hydrowax displays a normal cracking behaviour, the aromatic probes do not convert, and in fact naphthalene is formed.

During the first two seconds of contact the gasoline fraction rapidly increases, after which it starts to saturate. Overcracking of gasoline does not take place and the gasoline selectivity is independent of temperature. The gasoline formation from HCO is the most dominant reaction and, therefore, the gasoline selectivity can be described as:

$$S_{gasoline} = \frac{k_2}{(k_1 + k_2 + k_3)}$$

Where $k_2 >> k_1 + k_3$.

On the other hand, the LCO and gas fraction in cracking of extra heavy gas oil show a clear temperature dependency. At higher temperature more LCO is converted and more gas is formed. These effects are coupled to one another. Since no substantial coke formation takes place after 50 ms a cracking scheme for the extra heavy gas oil can be derived as shown in Fig. 10a. This reaction scheme is also applicable for the aromatic gas oil, since the cracking chemistry is the same. This has been demonstrated in *[5]*.

Clearly, a given part of the HCO fraction does not crack. The results with the spiked hydrowax demonstrate that this 'uncrackable' fraction consist of aromatics. Activation of aromatics can be expected to be very difficult as a result of the resonance stabilisation by the π-electrons in the benzene ring. Moreover, even if the benzene ring would be activated it does not allow the formation of an attractive product spectrum upon β-scission. Cracking reactions of the multi-substituted polycyclic aromatics of the feed will be limited to dealkylation of the polycyclic cores, which subsequently accumulate in the HCO fraction.

As the majority of sulfur in the feed has an aromatic character, it is interesting to see how these species behave under the applied conditions. The amount of sulfur in the product fractions is only dependent on the conversion, not on the temperature.

Most of the sulfur from the HCO fraction ends up in the LCO fraction. This is in agreement with what is observed in the sulfur spectra. Predominantly LCO range sulfur species are formed by dealkylation of HCO range alkyl-benzothiophenes.

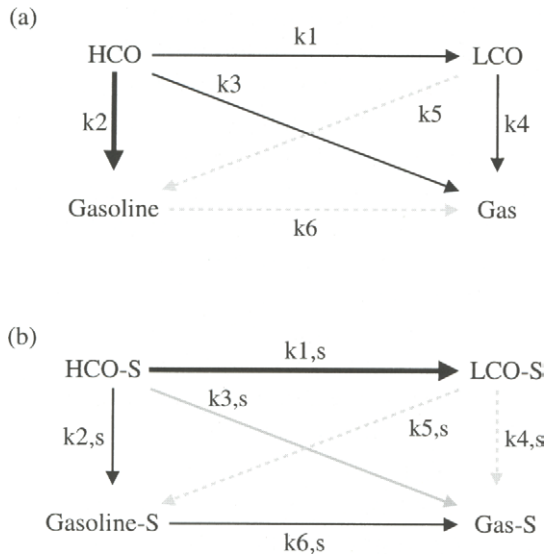

Fig. 10. The cracking model for hydrocarbons and sulfur species for an extra heavy gas oil. (a) hydrocarbons, and (b) sulfur species. (⟶) = primary reaction, (⟶) = secondary reaction, and (⟶) = incidental reaction.

The benzothiophene cores accumulate in the LCO fraction, and due to their aromatic characteristics they are unable to react further. The dealkylation of alkyl-dibenzothiophenes goes accompanied with the formation of dibenzothiophenes, which lie in the HCO range.

For gasoline sulfur some secondary reactions are observed. Liberation of thiophene molecules out of the large polycyclic feed species cause that these species evolve in the gasoline fraction. However, at higher conversion level some sulfur starts to disappear again. As the sum of the sulfur in the HCO, LCO, and gasoline fraction decreases this demonstrates that gaseous sulfur species are formed, i.e. some overcracking of aliphatic gasoline sulfur occurs. The observation that for gasoline sulfur overcracking takes place, whereas for hydrocarbons this is not the case can be explained from the relative amounts of both. Conversion of some gasoline range molecules will hardly be noticed in the large gasoline fraction, whereas for sulfur it will. The cracking scheme for sulfur species is shown in Fig. 10b.

The combination of the hydrocarbon and sulfur cracking schemes explain the observed behaviour for the sulfur concentrations in the product fractions. Up to 50 % conversion the HCO hydrocarbons and sulfur species crack with the same rate, and the concentration of HCO sulfur remains unaffected. After 50 %

conversion the reactive sulfur species have already cracked, whereas the HCO hydrocarbons participate in cracking reactions. The result is that the HCO fraction gets more concentrated with sulfur. The opposite is the case for gasoline sulfur. Although, the gasoline sulfur concentration decreases, it is not a result of cracking of sulfur species. Where for sulfur cracking the dominant route is from HCO to LCO, the most dominant route for hydrocarbons is from HCO to gasoline. The accumulated sulfur species in the gasoline fraction are, therefore, diluted with cracked hydrocarbons from the HCO fraction. The increase of sulfur concentration in the LCO fraction is a result of the accumulation of the benzothiophenes. Where the hydrocarbons in the LCO range are fairly unreactive, the concentration increases. The temperature dependence is a result of the temperature dependence of hydrocarbon cracking reactions from LCO to gas and not of the cracking of sulfur containing molecules in the LCO fraction.

In Fig. 11 a reaction scheme is presented that summarises the cracking behaviour of aromatic- and organic sulfur species as discussed in this section. This figure shows that under the applied conditions the aromatic species do not crack. Only the side-chains of these species will dealkylate from the stable cores. Note that only aliphatic sulfur species crack to hydrocarbons and hydrogen sulfide, and that the thiophene-, benzothiophene- and dibenzothiophene cores accumulate in the gasoline-, LCO- and HCO fraction, respectively.

5. Conclusion

In conclusion, the aromatic backbone will not crack under realistic FCC conditions. Only the paraffinic fraction of the feed and the alkyl groups associated to the benzene ring in aromatic compounds are susceptible to cracking reactions. This is not surprising as the cracking of the benzene ring is low because of the resonance stabilising properties of the π-electrons. This stabilisation hampers the activation by a Brønsted acid and the subsequent weakening of the bond at the β-position. As a consequence only the side-chains of the (poly)aromatic feed will break, leaving the polycyclic cores in the HCO fraction, which account for the 'uncrackable' fraction.

References

[1] ACEA World-Wide fuel charter (2002), http://www.acea.be/

[2] J. Corella and E. Francés, "Fluid Catalytic Cracking II: concepts in catalysis design", Ed. M.L. Ocelli, ACS Washington D.C. (1991), 165-182

[3] M.A. Den Hollander, M. Makkee and J.A. Moulijn, Appl. Catal. A. 187 (1999), 3-12

[4] X. Dupain, L.J. Rogier, E.D. Gamas, M. Makkee and J.A. Moulijn, Appl. Catal. A. 238 (2003), 223-238
[5] X. Dupain, E.D. Gamas, R. Madon, C.P. Kelkar, M. Makkee and J.A. Moulijn, Fuel (2003), accepted for publication

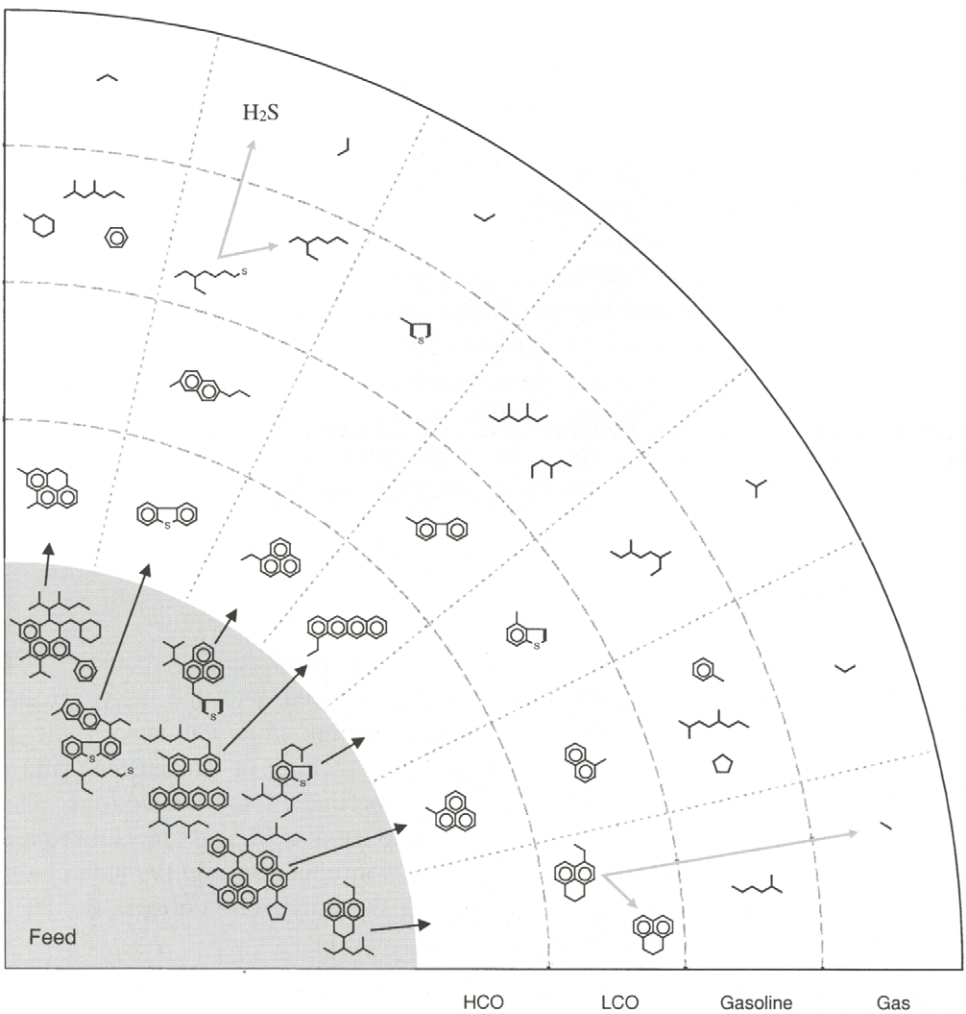

Fig. 11. Reaction scheme for the cracking of a FCC feed. Coke formation is not included.